Spatial and temporal patterns of localized thylakoid biogenesis in the chloroplast of *Chlamydomonas reinhardtii*

Melissa Valente Paterno

A Thesis
in
The Department
of
Biology

Presented in Partial Fulfillment of the Requirements
for the Degree of Masters of Science (Biology) at
Concordia University
Montreal, Quebec, Canada

August 2018

© Melissa Valente Paterno, 2018

CONCORDIA UNIVERSITY

School of Graduate Studies

This is to certify that the thesis prepared

By: Melissa Valente Paterno

Entitled: Spatial and temporal patterns of localized thylakoid biogenesis in the chloroplast of *Chlamydomonas reinhardtii*

and submitted in partial fulfillment of the requirements for the degree of

Masters of Science (Biology)

complies with the regulations of the University and meets the accepted standards with respect to originality and quality.

Signed by the final Examining Committee:

Dr. Vincent Martin	Chair
Dr. Alisa Piekny	Examiner
Dr. Madoka Gray Mitsumne	Examiner
Dr. Paul Joyce	External Examiner
Dr. William Zerges	Supervisor

Approved by _____
Chair of Department or Graduate Program Director

August 28th 2018 _____
Dean of Faculty

Abstract

Spatial and temporal patterns of localized thylakoid biogenesis in the chloroplast of *Chlamydomonas reinhardtii*

Melissa Valente Paterno

Eukaryotic cell compartmentalization concentrates the required substrates and reagents, preventing deleterious side-reactions. The sub-organellar spatial-temporal organization within many organelles is known, but not the chloroplast. Photosynthetic biochemical reactions are well studied, conversely the organization of photosynthetic thylakoid membrane biogenesis is lacking. We studied the spatial-temporal patterning of thylakoid biogenesis under two distinct developmental model systems using *Chlamydomonas reinhardtii*; 1) chloroplast differentiation using the *y-1* mutant and 2) mature chloroplast growth using diurnally-entrained cells. Immunoblot analysis uncovered the contrasting accumulation trends of photosynthetic electron transport chain complexes, correlating to their differing fluorescence microscopy *in situ* localizations. The chloroplastic T-zone region is now a privileged site for the synthesis and assembly of the chloroplast genome-encoded photosystem I and photosystem II subunits, as well as their chlorophyll pigment. Findings seen here also support the temporal regulation of the spatial T-zone region, which is related to thylakoid biogenesis within cells. A comparison of the two algal model systems has uncovered an increased capacity of chloroplast differentiation within mature algal cells. Finally, transmission electron microscopy results displayed candidate ultrastructures for the T-zone membrane platform. Therefore, using *C. reinhardtii*, we have expanded the spatial organization of thylakoid biogenesis, discovered temporal patterns, characterized potential T-zone related ultrastructures, and documented the T-zone within both differentiating and growing cultures.

Acknowledgements

I thank my colleague Dr. Sun who contributed equally to this research, his patience and expertise helped me advance. Dr. Sun conducted most of the biochemical work, which is clearly identified within the figure legends. The division of experimental tasks maximized our efficiency.

I would also like to thank the founders of this project, Dr. Uniacke and Dr. Zhan, for their pertinent results which directed us towards this avenue of investigation.

These results were not possible without the technical guidance of the CMCI managers Dr. Van Oostende and Dr. Law. All Fiji macros were written by Dr. Law, making the non-biased analysis of *in situ* microscopy patterns possible.

I thank Mr. Richard Allix for his extensive help with the design and completion of a synchronized cell system.

I thank all members of the Zerges' lab for their continual help and support.

I thank my committee members, Dr. Piekny and Dr. Madoka, for their helpful advice and constructive comments.

Lastly, I especially thank my supervisor Dr. Zerges for his guidance throughout my M.Sc. degree, and for all funding provided by his grant applications.

Contribution of Authors

The results featured in this thesis are part of a co-authored work, which has been submitted for publication to Plant Cell.

Dr. Yi Sun, Dr. William Zerges and Melissa Valente Paterno all contributed equally to the development of project ideas and project discussions.

Dr. Yi Sun and Dr. William Zerges initially supervised and trained Melissa Valente Paterno.

Dr Yi Sun and Dr. William Zerges obtained information regarding the synchronization of cells from experts in this field.

Dr. Yi Sun and Melissa Valente Paterno conducted all experiments. Please refer to individual figure legends for a detailed breakdown of contributions.

Dr. Yi Sun contributed almost all experimental work involving the Western blot analysis of both *y-1* cell samples and diurnally-entrained cell samples.

Melissa Valente Paterno and Mr. Richard Allix designed and built the synchronized cell system.

Melissa Valente Paterno assembled and tested the synchronized cell system.

Melissa Valente Paterno contributed at half of the work towards the *y-1* in situ experiments.

Melissa Valente Paterno contributed most of the work regarding diurnally-entrained cell characterization and *in situ* experiments.

Melissa Valente Paterno contributed almost all experimental work regarding the preparation, the acquisition, and the analysis of transmission electron microscopy results.

Dr. Christopher Law designed all automated Fiji based macro programming.

Melissa Valente Paterno conducted all Fiji macro-based work and analysis for both *y-1* and diurnally-entrained cells.

Melissa Valente Paterno carried out all the deconvolution for both *y-1* and diurnally-entrained cell acquisitions.

Melissa Valente Paterno carried out all statistical analysis, for this thesis, on both *y-1* and diurnally-entrained cells.

Melissa Valente Paterno created, assembled and finalized all figures presented in this thesis.

Melissa Valente Paterno was the only author of this thesis.

Table of Contents

List of Abbreviations

ADP	Adenosine Diphosphate
ATP	Adenosine Triphosphate
BF	Bright Field
βME	2-Mercaptoethanol
CCM	Carbon Concentrating Mechanism(s)
CH	Cell Harvester (an automated Fiji macro)
CMCI	Center for Microscopy and Cellular Imaging (Concordia University)
CO_2	Carbon Dioxide
cpSGs	Chloroplast Stress Granules
CTM	Chloroplast Translation Membrane
DEPC	Diethyl Pyrocarbonate
ER	Endoplasmic Reticulum
FEMR	Faculty for Electron Microscopy Research (McGill University)
FISH	Fluorescence *in situ* Hybridization
HSM	High Salt Medium
IF	Immunofluorescence Staining
LHC	Light Harvesting Complex
nm	Nanometer (unit of measurement for wavelength)
PBS	Phosphate Buffer Saline
PET	Photosynthetic Electron Transport (Chain)
pH	Potential of Hydrogen
PLB	Prolamellar Body
POR	Protochlorophyllide Oxidoreductase
PSI	Photosystem One
PSII	Photosystem Two
psi	Pounds per Square Inch

PSF	Point Spread Function (used in deconvolution)
NAD(P)H	Nicotinamide Adenine Dinucleotide (Phosphate) Hydrogen
PVD	Polyvinylidene Difluoride
ROI	Region of Interest (a tool provided in the Fiji software)
ROS	Reactive Oxygen Species
rpm	Rotations Per Minute
RuBisCo	Ribulose-1,5-bisphosphate carboxylase/oxygenase
SDS	Sodium Dodecyl Sulfate
SDS PAGE	Sodium Dodecyl Sulfate Polyacrylamide Gel Electrophoresis
TAP	Tris Acetate Phosphate (medium)
TEM	Transmission Electron Microscopy
T-zone	Translation Zone (localized areas around the pyrenoid)
ZT	Zeitgeber Time (unit of time based on the 24-hour light/dark cycle)

List of Figures

Main Figures

Supplemental Figures

Chapter 1 : Introduction

1.1 General Thesis Overview

This project investigates the spatial-temporal compartmentalization of thylakoid membrane biogenesis within two differing contexts of chloroplast development in *Chlamydomonas reinhardtii*. Building on previous findings, we hypothesized the biological significance of localized chloroplast thylakoid membrane biogenesis [1]–[3]. Chapter 1 reviews thylakoid membrane biogenesis. Chapter 2 documents the materials and methods and is supplemented by manuals as appendices. Chapter 3 comprises all *in situ* and biochemical discoveries regarding T-zone organized thylakoid membrane biogenesis. Lastly, Chapter 4 discusses the thesis findings, the current and future work stemming from them, and the implications of these discoveries.

1.2 Cellular Organization and Photosynthesis

Eukaryotic cells display intracellular compartmentalization using spatially distinct membrane-bound organelles. The mitochondrial and chloroplastic organelles originated through the endosymbiosis of ancestral prokaryotes [1]. Both these organelles have their own genome, which was reduced by gene loss or transfer to the nuclear genome [1]. Therefore, these semi-autonomous organelles organize the expression, targeting, and assembly of their proteins between these two distinct genomes. For example, the temporal coordination of nuclear and mitochondrial translation as well as the spatial localization of mitochondrial ribosome clusters nearby mitochondrial nucleoids, are current findings of intra-organellar localized spatial-temporal enrichment [4], [5]. Contrastingly, research into the intra-organellar organization of the photosynthetic chloroplast has been lacking.

The complexity of the chloroplast is due to the specialized photosynthetic thylakoid membranes, which are structurally organized [1], [6]. The correct assembly of thylakoid membrane components is imperative for photosynthesis and the growth of the organism. Photoautotrophic organisms harvest light energy and create chemical energy using photosynthetic reactions [1]. These photosynthetic reactions convert water and carbon dioxide into oxygen and carbohydrates, where the carbohydrates are utilized as an energy source and the oxygen contributes to our

ecosystem. Thus, the proper synthesis, assembly, and function of these specialized thylakoid membranes is essential.

These photosynthetic thylakoids partition the chloroplast into the stromal compartment and the luminal compartment. The stroma is used for the dark-reactions of photosynthesis while the lumen is a proton enriched compartment used within the light-dependent reactions. The photosynthetic electron transport chain (PET) uses these light-dependent reactions to photolyze water, conduct various forms of electron energy transfer, establish an electro-chemical proton gradient, and produce NAD(P)H and ATP. The splitting of water creates the oxygen (O_2) needed for aerobic respiration, while NAD(P)H and ATP are utilized by the Calvin-Benson dark reactions for carbon fixation. The PET chain is composed of; the photosystem II (PSII) complex, the cytochrome b_6f complex, the photosystem I (PSI) complex, and ATP synthase complex. These four major complexes work in concert with plastoquinone, one electron shuttle protein called plastocyanin, and the two final electron carriers ferredoxin and ferredoxin $NADP^+$ reductase. This PET chain and its four prominent complexes are required for the proper functioning of the thylakoids; therefore, we are investigating their potential organization.

These thylakoid bound PET chain complexes have a multi-component arrangement that must be assembled correctly to ensure their proper biochemical function. Given the known cellular compartmentalization by organelles, the importance of the chloroplast thylakoid membranes, and the molecular complexity of the photosynthetic machinery; we propose a specific spatial localization and temporal control for the biogenesis of these PET chain complexes.

1.3 The Algal Model Organism *C. reinhardtii*

The alga *C. reinhardtii* was used for all experimental work in this thesis. Evolutionary conservation of plant and animal characteristics, makes *C. reinhardtii* an ideal model organism for both photosynthesis and flagellar research [7]. Its sizable collection of mutants, modern genetic tools, published genome, and model organism characteristics has made this algal species popular for many decades [7]–[9]. Moreover, *C. reinhardtii* provides viable photosynthetic mutants, simple genetic crossing, and easily identifiable diurnal synchronization; offering an advantageous use of this algae when compared to typical plant models.

This unicellular algal displays a simple morphology, relative to the other photosynthetic organisms within the Plantae kingdom. *C. reinhardtii* has an oblong cellular shape ranging from 8-10 µm in length, which is surrounded by a plasma membrane and encased in a cell wall [6], [10]. The anterior pole of these algal cells is demarked by their whip-like flagella, while the posterior is denoted by their basally prominent chloroplast [6]. This chloroplast occupies approximately 41% of the cell while the remaining apical cellular space contains the cytosol and its associated organelles such as the nucleus, the ER and the Golgi apparatus [6], [10], [11].

This singular chloroplast has a cup-like shape which partially encloses the nucleus and other cytosolic structures using its multiple finger-like lobes [2]. The *C. reinhardtii* chloroplastic genome contains 99 genes which mostly encode photosynthetic machinery and its own gene expression system [12], [13]. Coordination of chloroplastic and nuclear gene expression is hypothesized to occur mostly at the translational level with the possibility of additional spatial-temporal regulation [14], [15]. The chloroplast genome-encoded proteins are translated by the chloroplastic bacterial-like 70S ribosomes while the nuclear genome-encoded chloroplast proteins are synthesized by the 80S cytosolic ribosomes and imported into the chloroplast where they are targeted to their destination [12], [14], [15]. Import of these cytosolic proteins occurs across the chloroplast envelope which is composed of two mostly concentric membranes [6], [16]. This envelope encloses chloroplastic compartments and structures such as the stroma, a primordial visual system called the eyespot, and the thylakoid membranes with their lumen [6], [10], [17]. Dispersed among these compartments are the chloroplastic starch granules and electron dense plastoglobuli. Algal plastoglobuli are thought to be similar to their plant counterparts, which contain components associated with thylakoid biogenesis [6], [16], [18]. Chloroplastic starch granules vary in size and quantity depending on growth conditions and only serve as a storage for future energetic consumption [19]–[21]. Arranged among these free floating plastoglobuli and starch granules are the photosynthetic thylakoid membranes.

Thylakoids resemble flattened vesicles and are often stacked in parallel ranging from 2-12 membranes per stack which form a highly connected network [6], [16], [19]. *C. reinhardtii* thylakoid membranes have demonstrated differences in electron density when undergoing biogenesis and sometimes display convergence zones, where multiple thylakoids congregate while becoming perpendicular to the chloroplast envelope and have direct and indirect contacts to the

inner envelope layer [16], [22]. These thylakoid convergence zones contain biogenesis-related proteins and can be associated with prolamellar body (PLB) like structures that are proposed to be similar to their plant counterparts, which are directly involved with *de-novo* thylakoid biogenesis [23]–[26]. These structures occasionally appeared close to the chloroplast pyrenoid.

The spherical chloroplast pyrenoid is a non-membrane-bound structure located within the basal chloroplast region, which serves as a biophysical algal carbon concentration mechanism (CCM) [27], [28]. This chloroplastic compartment is surrounded by starch plates and houses interconnected pyrenoid tubules dispersed within a matrix of packed ribulose-1,5-bisphosphate carboxylase and oxygenase (RuBisCo) [16]. These starch plates form a discontinuous biconcave shell around the pyrenoid and help increase CMM efficiency by preventing CO_2 leakage [6], [18], [27], [28]. The discontinuity of the starch plates provides fenestrations between the chloroplastic stroma and the pyrenoid matrix, which act as passages for pyrenoid tubules and mini-tubules [16], [18]. Pyrenoid tubules and their encased mini-tubules resemble a network within the pyrenoid center and become more cylindrical as they approach the pyrenoid periphery to connect with thylakoids [16], [28]. These tubules and mini-tubules are hypothesized to be a CCM trafficking highway by transporting required molecules such as CO_2, ATP, and the intermediate Calvin-Benson cycle sugars between the pyrenoid segregated RuBisCo and the chloroplast stroma or thylakoid lumen. Moreover, these pyrenoid tubules respond to multiple changing environmental conditions which provokes intrigue with regards to their CCM function and any other undiscovered functions [29].

C. reinhardtii is phylogenetically related to higher land plants and thus has similar photosynthetic machinery, identical biochemical reactions, and analogous environmental responses [30], [31]. Its scientific amenability and comparability to plants has made it attractive within the field of photosynthetic research [8], [32], [33]. Therefore, we used these advantages to characterize and investigate the spatial-temporal organization of PET chain complex biogenesis within two model systems. These algal models display rapid chloroplast thylakoid biogenesis while being analogous to the developmental process of chloroplast differentiation and chloroplast growth found within higher land plants [34]. Moreover, the resemblances between these algal models and their plant counterparts allow for parallels to be drawn between our findings and what

occurs within more complex photosynthetic organisms; providing an effective biological tool which helps further photosynthetic research.

1.4 Spatial and Temporal Evidence for the Localized Biogenesis of PET Chain Complexes

Although the thylakoid PET chain complexes are well understood, there is still no consensus regarding where and when these complexes are synthesized and assembled. This section discusses literature supporting the spatially and temporally organized biogenesis of this photosynthetic machinery.

Thylakoid biogenesis requires the synthesis and assembly of its photosynthetic machinery, where these PET chain complexes are composed of many proteins, pigments, and cofactors all inserted into their specific lipid membrane. The common model of thylakoid production and PET chain biogenesis proposes the even chloroplastic distribution of this process throughout the chloroplast. However, recent methodology detracts from this non-localized model within algal and cyanobacterial chloroplasts [2], [35].

The organization of thylakoid biogenesis was first proposed because of the prolamellar bodies (PLBs), found within the chloroplasts of plants. These PLBs were most often seen within partially differentiated plant etioplasts which contained very few membranes [23]. Subsequent studies uncovered the direct transformation of these tubular PLB membrane networks into flattened thylakoids upon light-exposure of plant etioplasts [24]. These plant PLB finings spurred the possibility of organized thylakoid biogenesis within other photosynthetic organisms, leading to the discovery of algal chloroplast organization. Transmission electron microscopy (TEM) images of a differentiating *C. reinhardtii* chloroplast revealed chloroplastic PLB-like structures, localized electron dense regions within growing thylakoids, and thylakoid connections with the chloroplast-envelope [25], [36]–[38]. The *'yellow in the dark 1'* mutant which resembled the etioplast-to-chloroplast differentiation seen in land plants, was the only model system that displayed these structurally organized membrane formations during thylakoid biogenesis [34]. Despite the similarity of these algal discoveries to the previous plant etioplast findings, the organization of the algal chloroplast became a debatable subject because of the lack of reproducibility for these algal thylakoid ultrastructures [39]. Alternatively, the transient observation of these thylakoid ultrastructures provided a fragile foundation for the spatial organization of the algal chloroplast specifically during thylakoid biogenesis, but additional

evidence directly connecting a preferential spatial chloroplastic location with the biogenesis of thylakoid complexes was required.

Decades later, evidence for the *in situ* localization of organized PSII subunit synthesis was uncovered using dark adapted and subsequently light-stimulated wild-type *C. reinhardtii*. This localized model depicted the specific spatial enrichment of PSII *de novo* biogenesis within defined thylakoid regions, alternatively PSII biogenesis for thylakoid repair was not localized [2]. These punctate regions lateral to the pyrenoid were called 'Translation-Zones' (T-zones) because they were specific to *de novo* PSII subunit translation and not a by-product of thylakoid distribution [2], [40]. Additionally, the T-zone was locally enriched in PSII messages, PSII translation factors, unassembled PSII core proteins, and both chloroplastic ribosomal subunits using an RNA mediated targeting mechanism that was independent of transcription and translation [2], [15], [40]. Biochemical characterization of the chloroplast thylakoid membranes yielded a heterogeneous membrane population, where the T-zone membrane platform was identified based on its heavier density and enrichment with known T-zone marking proteins [40]. This characterization of chloroplastic membranes also uncovered an import apparatus enriched envelope membrane fraction localized to the lobe-junctions [40]. These TIC-TOC import apparatus enriched lobe junctions displayed co-translationally localized LHCII subunits along their cytosolic border [2].

Taken together, these *in situ* localization findings and differing membrane varieties created the proposed *C. reinhardtii* model of T-zone organized *de novo* PSII biogenesis (Figure 1B). The chloroplastic T-zone is the site of early PSII complex synthesis and initial assembly as shown by its enrichment with chloroplastic ribosomes, PSII-specific translation factors, and unassembled PSII core proteins. Subsequently, these PSII subunits are partially assembled and re-located into the chloroplast lobe-junctions where they are combined with their TIC-TOC imported nuclear genome-encoded subunits [15]. Lastly, these fully assembled complexes continue their lateral posterior-to-anterior diffusion within the chloroplast lobes, where the migration along these compositionally different membranes is possible because they are continuous with one another [6], [40]. This T-zone organized biogenesis was confirmed for the PSII complex because the model system used only stimulated the biogenesis of this PET chain complex. Therefore, the *in situ* localization of other PET chain complexes and components during their biogenesis remains

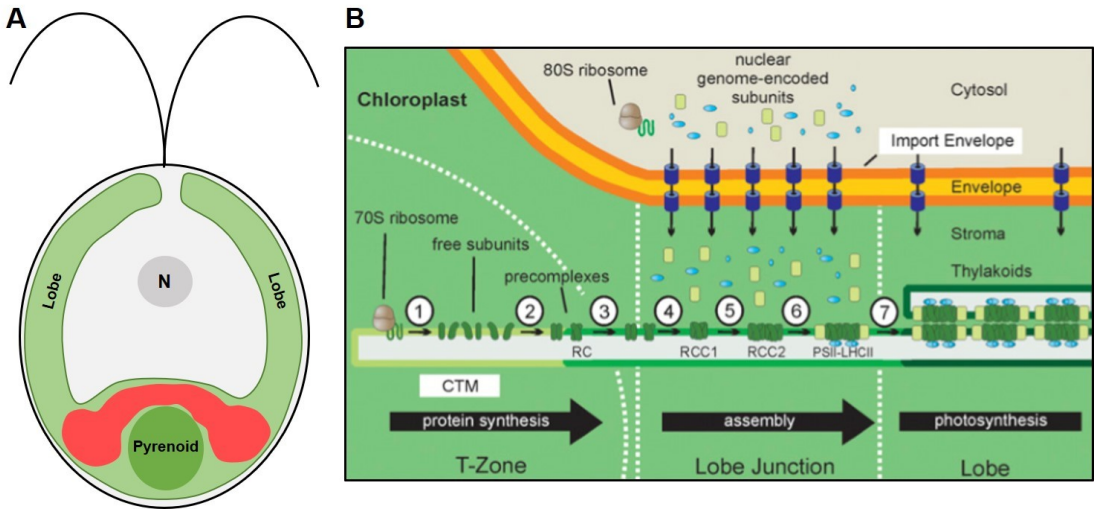

Figure 1. Translation-zone model in *C. reinhardtii*

(A) Cartoon cell depicting cellular features; the alga is encased by a cell wall and plasma membrane with two anterior flagella, the cytosol is in grey and the chloroplast is in light green. Nucleus = N and the T-zone is denoted in red.

(B) Schematic model for localized *de novo* PSII biogenesis within the T-zone.
Chloroplast Translation Membranes = CTM.

Schottkowski, M., Peters, M., Zhan, Y., Rifai, O., Zhang, Y., and Zerges, W. (2012). Biogenic membranes of the chloroplast in *Chlamydomonas reinhardtii*. Proc. Natl. Acad. Sci. U.S.A. *109*, 19286–19291.

* Cartoon cell created by Melissa V.P.

unknown, but uncovering their chloroplastic organization would help to further elucidate this localized model of spatially enriched photosynthetic machinery production.

The localization other PET chain complexes require an algal model system which strongly triggers their synthesis and assembly. Finding such an inducible model system for the ATP synthase complex and the cytochrome b_6f complex seems improbable because they have an established protein content even when grown in the dark and they only display minor amounts of synthesis during chloroplast differentiation [41], [42]. Therefore, if the biogenesis of these two chlorophyll-lacking PET chain complexes cannot be induced, then the *in situ* localization of this biogenic process is unlikely. Conversely, chloroplast differentiation causes the rapid synthesis of both photosystems which provides an ideal system for the localization of the PSI complex and its chlorophyll pigment. The spatial enrichment of PSI biogenesis within algae is unknown, however the evolutionarily related cyanobacterial chloroplast has PSI and PSII biogenesis localized together within specialized curved biogenic membranes centers along the cyanobacterial plasma membrane [35], [43]–[45]. Consequently, based on these cyanobacterial findings as well as kinetic and biochemical evidence the inner chloroplast envelope was proposed to be the site of organized PSI,

PSII, and chlorophyll biogenesis within algae [22], [36], [37]. However, PSII biogenesis was later spatially targeted to the T-zone using direct *in situ* localization and the quenching of newly assembled PSII complexes by neighboring PSI complexes indicated that the biogenesis of both photosystems should occur within the same or nearby spatial locations [2], [37]. Therefore, the organization of PSI biogenesis is likely but its spatial chloroplastic localization is debatable [46].

Correspondingly, other PET chain components also have a controversial spatial localization for their biogenesis. Synthesis enzymes for the major light harvesting pigment chlorophyll were initially shown to accumulate within plant etioplast PLBs but later appeared within the proteomes of both chloroplast envelope membranes and thylakoid membranes [47]. Similarly, newly synthesized chlorophyll within *C. reinhardtii* was initially suspected to be associated with PLB-like structures but these PLB-like structures were not reproducible and recently chlorophyll synthesis enzymes were found within the pyrenoid proteome [22], [48]. Thus, the *in situ* localization of chlorophyll biogenesis remains debatable but the photosystem-specific association of this pigment indicates that its biogenesis should be organized in a similar manner as PSI and PSII biogenesis [47].

The findings presented above favor the organized biogenesis of these various thylakoid PET chain complexes and components but their specific localized chloroplastic enrichment is controversial. A combination of biochemical and kinetic evidence has uncovered potential spatial chloroplastic locations of organized biogenesis, but this evidence isn't direct. The *in situ* localization of PSII subunits and components has provided direct evidence, leading to our proposed T-zone model of *de novo* PSII complex biogenesis which can reconcile most conflicts presented within the literature. The functional assembly of PSII requires the presence of its major light harvesting pigment, indicating that newly synthesized chlorophyll should be nearby. Similarly, PSI biogenesis also requires chlorophyll and occurs close enough to quench PSII fluorescence, thereby placing PSI biogenesis in or nearby the T-zone as well. Subsequently within the T-zone model, import and assembly of cytosolic proteins was localized within the lobe junctions which is an ideal region for the coordination of cytosolic and chloroplastic biogenic events. The proximity of the lobe junctions to both the T-zone and the Golgi or ER provides a spatial chloroplastic location which can aid the ER-to-Golgi-to-chloroplast trafficking of multiple thylakoid components including processed lipids. Recently, invaginations of the chloroplast

envelope containing encased cytosolic molecules were specifically localized to the lobe-junctions, validating the vesicular transport of cytosolic thylakoid components to the chloroplast thylakoid membranes [16]. Moreover, thylakoid convergence zones connecting with the inner envelope were localized to the lobe-junctions and lobe-tips which substantiates the involvement of the chloroplast envelope within thylakoid biogenesis and supports the proposed posterior-to-anterior movement of T-zone assembled PET chain complexes [16]. Therefore, as a function of their associations at least the two PET chain photosystems and their chlorophyll pigment should be T-zone enriched, requiring a coordinated and stimulating algal model system to characterize their experimental *in situ* spatial-temporal localization. Lastly, the existence of a chloroplastic spatial localization for PET chain complex biogenesis begs the possibility of a coexisting temporal organization, further co-ordinating these chloroplastic events.

The previous non-localized model of algal thylakoid biogenesis consequently negated the consideration of both a spatial and temporal chloroplastic organization. Thylakoid bound PET chain complexes were thought to be produced concurrently because of their similarly controlled post-transcriptional and translational regulation [10], [49]. However, algal model systems of increased thylakoid biogenesis displayed temporally organized transcription and translation of their PET chain complexes. Temporal organization of PET chain complex translation rates during algal chloroplast differentiation displayed ATP synthase complex synthesis before that of PSII [41]. Similarly, diurnally-entrained chloroplast growth demonstrated the temporally ordered peaks in transcript levels of the ATP synthase and cytochrome b_6f complex transcripts prior to PSI and PSII transcripts [3]. Moreover, chloroplasts employ co-translation or post-translational temporal organization to stabilize the intra-complex assembly of PET chain components in a stepwise manner [10], [49]. Thus, this chloroplastic temporal ordering of intra-complex assembly augments the plausibility of a similar temporal organization for inter-complex biogenesis. Therefore, the T-zone may contain a temporal aspect to help regulate the chloroplastic requirement for spatial organization of PET chain complex biogenesis and the temporal ordering of complex synthesis and assembly within the assembling thylakoids.

1.5 Algal Model Systems Displaying Increased Thylakoid Biogenesis

Optimized algal models were required to characterize the temporal organization of T-zone localized PSII biogenesis and to confirm the localization of other PET chain complexes and

components within this spatial-temporal model. These optimized algal model systems required increased thylakoid biogenesis triggering the synthesis and assembly of as many PET chain complexes and components as possible. Moreover, the model systems must coordinate their thylakoid biogenesis providing the possible temporal elucidation of the T-zone and they should also coordinate chloroplastic development ensuring that most cells display the same localization pattern. Lastly, these model systems should be analogous to plant biogenic processes allowing parallels between these eukaryotic algal findings and the organization of higher plant chloroplasts. Previous literature revealed model algal systems which satisfied all the requirements above, these models represented contexts of algal chloroplast differentiation using a mutant and algal chloroplast growth and division using the diurnal-entrainment of cultures.

Algal chloroplast differentiation was investigated using the *'yellow in the dark 1'* (*y-1)* mutant strain. When cultured in continuous light these *y-1* cells display wild-type growth, however when grown in the dark these mutant cells undergo partial chloroplast de-differentiation. A genetic mutation within one subunit of the light-independent protochlorophyllide oxidoreductase (POR) renders it non-functional thus halting the chlorophyll biosynthesis pathway of these mutants cells only when cultured in the dark [50]. This inability of dark-grown *y-1* cells to produce chlorophyll provokes the cessation of PET chain complex biogenesis, eventually leading to the disassembly and divisional dilution of the remaining thylakoid membranes. Thus, the partially de-differentiated *y-1* chloroplasts contain a vastly reduced thylakoid quantity and complexity, a distorted eyespot, and large quantities of stored starch if cultured in the dark for 5-to-7 generations [18]. When exposed to light, these dark-grown *y-1* chloroplasts undergo rapid differentiation or 'greening' into mature chloroplasts where greening is defined as light-induced thylakoid biogenesis without cellular division. Initial light-exposure of these dark-grown *y-1* cells triggers chlorophyll production, chloroplast ribosomes biogenesis, and starch degradation [38]. Subsequently, light-exposed *y-1* chloroplasts undergo a surge in thylakoid membrane biogenesis and fusion eventually displaying a thylakoid stacking complexity comparable to wild-type green chloroplasts after 9-10 hours greening [38]. This greening of *y-1* mimics the etioplast-to-chloroplast differentiation process, providing an algal model system which is analogous to higher land plants [34]. Furthermore, this algal model of chloroplast differentiation is biochemically well characterized providing the early ultrastructures of chloroplast organization and the expected stimulation of PSI, PSII, and chlorophyll biogenesis [6], [22], [25], [38]. Therefore, this *y-1* mutant algal model

system is ideal to confirm the spatial-temporal organization of T-zone localized PSII biogenesis and to localize the expected biogenesis of PSI in addition to the chlorophyll pigment.

Algal chloroplast growth and division was characterized using diurnally-entrained cells synchronized by multiple environmental cues including a 24-hour light/dark cycle [51]. Asynchronous algal cultures are frequently used for experimentation however diurnal-entrainment of cultures synchronizes cell growth and reflects natural algal populations [52]. These synchronized algal cells undergo an elongated growth cycle (G1) during the 12-hour light phase and a 12-hour dark phase where cells divide then idle [53]. Chloroplast and thylakoid biogenesis occurs during the light phase, resulting in a three-fold cell size increase or a ten-fold cell volume increase [52]. A division commitment point during mid-to-late light phase ensures that growing cells enter successive rounds of synthesis and mitosis (S/M) and divide during the subsequent dark phase [52]–[55]. The number of S/M rounds is dictated by the cell size where dividing cells can produce 2,4,8,16 or 32 daughter cells, once liberated these daughter cells reach an arrest point until the upcoming light phase [53], [54]. This model system coordinates 95% of algal cells within a culture and mimics plant chloroplast growth and division [34]. Previous diurnal findings provided evidence for the temporal organization of PET chain complex transcription and translation but the *in situ* spatial-temporal organization of their biogenesis is unknown [3], [41], [56]. Therefore, this diurnally-entrained algal model system provides a novel framework to investigate the spatial-temporal organization of PET chain complex biogenesis within mature growing chloroplasts.

1.6 Thesis Goals

The general aim of this thesis was to characterize the spatial-temporal organization of thylakoid biogenesis within the chloroplast of the green alga *C. reinhardtii*. Specifically, the goal was to further elucidate the spatial model of T-zone localized PET chain complex synthesis and assembly by using two model systems of increased thylakoid biogenesis.

The first objective of this study was to confirm the expected progression of *y-1* greening and PET chain complex biogenesis through immunoblot analysis and chlorophyll extractions. Secondly, we examined the temporal organization of T-zone localized PSII subunit translation during *y-1* chloroplast differentiation. The third and final *y-1* objective was to test the *in situ* use of complex-specific protein markers through the known spatial-temporal localization of PSII and

then employ this same protein marker strategy to localize the site(s) of synthesis and assembly for the PSI complex and the chlorophyll pigment during *y-1* chloroplast differentiation.

Like the previous model system, the fourth objective of this study was to characterize diurnal chloroplast growth and PET chain complex biogenesis through immunoblot analysis and chlorophyll extractions. Fifthly, during thylakoid biogenesis of the diurnal light phase we investigated the *in situ* spatial-temporal localization of PSII subunit translation. The sixth objective was to confirm the organization of PSII synthesis and accumulation by localizing a PSII-specific protein marker and its required light harvesting pigment chlorophyll during the diurnal light phase. The final objective of this thesis was to investigate the T-zone ultrastructure using TEM analysis and comparison between diurnally-entrained cell time points.

Therefore, the novel aspects of this thesis originated from these two algal models of increased thylakoid biogenesis, where the previous T-zone model was confirmed for PSII biogenesis and expanded to include PSI and chlorophyll biogenesis. Moreover, the physical ultrastructure of the T-zone was characterized and revealed several possible biogenesis related thylakoid membrane formations. Overall, the aim and various objectives of this thesis were fulfilled while also uncovering other intriguing avenues of investigation.

Chapter 2 : Materials and Methods

2.1 Culture Growth Conditions

2.11 *C. reinhardtii "Yellow in the Dark 1"* Mutant.

The *yellow in the dark 1* mutant *y-1* was obtained from the Chlamydomonas Resource Center (as strain CC-1168 mating type +). A *y-1* plate was routinely maintained by streaking every three days on fresh agar-solidified Tris Acetate Phosphate (TAP) medium. This plate was kept in an incubator at 24 ºC under continuous light (approximately 40-50 $\mu E \cdot m^{-2} \cdot s^{-1}$). Once a week cells from this plate were streaked on new agar-solidified TAP medium plate which was loosely wrapped twice in folded aluminum foil and kept in the dark for 7-10 days to "de-green" the cells.

Cultures of *y-1* were grown in liquid TAP medium because an external carbon source is needed for the growth of this dark-grown mutant strain. These cultures were subjected to continuous orbital shaking (40-50 rpm) and either light or dark conditions depending on the experiment. Liquid cultures were grown in Erlenmeyer flasks loosely topped with a cotton plug secured using labeled tape. Control cultures were inoculated with green *y-1* cells and then continuously exposed to 30-40 $\mu E \cdot m^{-2} \cdot s^{-1}$ of light for three days which yielded an exponential growth phase density of $1x\ 10^6$ to $3\ x\ 10^6$ cells/mL. Older control cultures undergoing less chloroplast biogenesis, were left to grow for approximately 5-6 days after inoculation until a log phase density of $4\ x\ 10^6$ to $6\ x\ 10^6$ cells/mL was achieved. Experimental cultures were inoculated with the de-greened yellow *y-1* cells and kept in the dark by wrapping the flask with two layers of aluminum foil in addition to a loose aluminum foil cap for the cotton plug. Dark-grown cultures were subsequently exposed to 30-40 $\mu E \cdot m^{-2} \cdot s^{-1}$ of light for the length of time indicated in each experiment. Light-induced chloroplast differentiation was possible if a dark-grown culture density of $1\ x\ 10^6$ to $2\ x\ 10^6$ cells/mL was achieved which was approximately 5-7 days of growth. Cultures with either lower then $9\ x\ 10^5$ cells/mL or higher then $2.5\ x\ 10^6$ cells/mL did not undergo efficient chloroplast differentiation.

Some experiments using *y-1* involved growth in different liquid media. These experiments required the above-mentioned control and experimental cultures, in addition to a nitrogen deficient culture. Nitrogen deficient liquid TAP medium was made and inoculated with green *y-1* cells

grown on agar-solidified TAP medium in the light. This culture was then subjected to the same conditions and growth time mentioned for the control cultures above.

2.12 Diurnally-Entrained *C. reinhardtii.*

The *C. reinhardtii* strain CC-125 (137c *wild-type mating-type* +) was obtained from the Chlamydomonas Resource Center and used for diurnal synchronization. A CC-125 plate was routinely maintained using the same growth conditions as previously stated for the green *y-1* plates.

Diurnal synchronization of liquid cultures was achieved through a system combining an incubator, a handmade light box, and an aeration delivery apparatus. For detailed methods on this synchronization system please refer to Appendix I: Technical Guide to Synchronized Culture Set Up. For a detailed description of the incubator set up refer to Appendix II: Programming 'Conviron TC-16' Growth Chamber for Synchronized Cells. A condensed version of the synchronized culture method is provided below.

The aeration system, consisting of a glass pipette and tubing connected to a bacterial air vent, was inserted into the flask via the cotton plug. Flasks were then filled specifically with liquid High Salt Minimal medium (HSM) to ensure only photoautotrophic growth and then sterilized by autoclaving. Starter cultures were inoculated using one loop-full of 1-week old CC-125 cells. Inoculated starter cultures were then connected to the aeration system, providing 0.5% to 1% CO_2 mixed air at a flow rate of approximately 300-400 mL/min for a 250mL flask. Growing cultures were placed in a red and blue LED light box providing approximately 250-280 $\mu E \cdot m^{-2} \cdot s^{-1}$ of light from each of the five sides. This light box is located within a programed growth chamber, which is regulated to 23 ºC during the 12-hour light phase and 27 ºC during the 12-hour dark phase. These growing starter cultures were entrained under a 24-hour light/dark cycle for three days without dilution. This growth time allowed cultures to reach a cell density of approximately 1 x 10^6 to 2 x 10^6 cells/mL which was suitable for subsequent dilution. For the following three days experimental cultures were diluted daily into fresh HSM medium between Zeitgeber Time (ZT) 1 and ZT3 to reduce the cell density to 1 x 10^5 - 2 x 10^5 cells/mL. Experimental cultures were subjected to the same conditions as starter cultures, except for the daily dilution over three consecutive days. On the fourth day, cultures were utilized for experiments. Prior to use, diurnally-entrained cultures were verified for known optimal synchronization markers; as described in the following method section 'Characterizing Diurnally-Entrained *C. reinhardtii* Cell Changes'.

Other strains capable of synchronization using our system are: CC-124 (137c *wild-type mating type* -), CC-1021 (or 2137 *mating type* -), and CC-4051 (4A+ *mating type* +). Some cell wall deficient strains display slight diurnal-entrainment by displaying coordinated cellular division and a minimal increase in cell size during the light cycle. Cell wall deficient strains cannot be diluted daily when synchronized due to their lower cell density increase between 24-hour cycles. Tested cell wall deficient strains which exhibit the above-mentioned traits were: CC-400 (*cw15* mating type +) and CC-503 (*cw92* mating type +).

2.2 Characterizing Diurnally-Entrained *C. reinhardtii* Cell Changes

2.21 Cell Density Measurement.

A 7-to-10-fold cell density increase is documented between 24-hour cycles. Fold change was determined by counting cell density with a hemocytometer during the early light phase prior to and after the daily dilution (described above). The average of two manual cell density counts was used unless one was significantly different; then an additional two to four counts were conducted to ensure accurate cell density recordings.

2.22 Measurement of Cell Size Changes and Mitotic Events.

Changes in cell size were observed visibly by using a Leitz Laborlux 12 light microscope with a 25x objective. These cell size changes were recorded and quantified using pictures taken with a digital camera programmed under the same exposure and color balance settings with a 4x zoom. Cell characteristics, such as length, width, area and roundness, were quantified over the 12-hour light phase of the 24-hour cycle as follows.

Length and width were manually measured using the image analysis software Fiji. Opened digital light microscope images were scaled using the known distance within a Hemocytometer versus its associated pixel number. These calibrated measurements determined the length and width of each cell for the different time points recorded. Using these length and width measurements, a length to width ratio was calculated by dividing length measurements with their corresponding width measurements for every cell imaged.

The remaining cell characteristics were determined using an automated Fiji macro written by Dr. Christopher Law. Images of the sampled diurnal cells were opened with Fiji and all oblong

objects within these images were outlined by the macro. Objects that were misidentified as cells were deleted by the user and the region of interest (ROI) manager was modified to include all correctly outlined cells. When a completed (ROI) manager was inputted, the macro then measured and displayed all chosen parameters such as area or roundness. Raw data for cell area was converted from pixel length into the appropriate measurement units (μm) using the previously determined scale for each image respectively.

2.23 Subjective Dark Phase Trial.

Diurnally-entrained cultures were also exposed to a subjective period of darkness. When diurnally-entrained cells were ready, after three dilutions as previously explained, the culture was maintained in darkness after ZT0 as a 'subjective dark' phase. After ZT5, the culture was exposed to light for two hours and 45 min (2.7 hours). During all these time points cell size characteristics were recorded and quantified as previously explained.

2.24 Coordinated Cell Death.

When diurnally-entrained cultures were not diluted on the fourth and fifth day, cells would undergo a form of coordinated rapid and dramatic death. Synchronized cultures were subjected to the same growth and maintenance conditions as explained previously except dilutions were stopped after the third day. On the fifth day, cells were visually inspected for signs of synchrony and viability (e.g. mobility, cell color, and brightness of the chloroplast), subsequently pictures were taken to record the rapid change in culture color. Continued experimental work on this form of synchronized cell death was partially conducted by M.Sc. student Zeyu Zhao and is not included in this thesis.

2.3 Extraction and Measurement of Chlorophyll and its Intermediates

2.31 Extraction of the Chlorophyll Pigment.

Chlorophyll extraction by either two methods provided comparable extraction efficiencies. Cell pellets were collected from *y-1* and diurnally-entrained cultures by centrifugation at 5000 x *g* for five minutes at 4 ºC using a MBI PrismR refrigerated table-top centrifuge. Pellets contained an equal cell number or equal culture volumes (for diurnally-entrained 24-hour cell samples only) and were stored at -80 ºC. Thawed pellets were subjected to extraction by 1 mL of cold (-20 ºC)

methanol or 80% (v/v) acetone. Resuspended pellets were mixed vigorously to extract pigments. Samples were subjected to centrifugation at 5000 x *g* for five minutes to remove cell debris.

For cold methanol extractions, all the supernatant was put into a clean cuvette and absorbance values were measured at 652 nm and 665 nm using the Labomed Inc. Specto UV-Vis RS Digital Spectrophotometer with a D2 Lamp power supply. The absorbance readings were then converted into µg amounts using the calculations: A_{652} x 22.12 and A_{665} x 2.71 for determination of Chl *a* and Chl *b*, respectively [57]. Alternatively, when using 80% (v/v) Acetone extraction, 200 µL of supernatant was aliquoted into a sterile transparent flat-bottomed 96 well plate. The plate was read by the Bio Tek Synergy H1 Hybrid Plate Reader, measuring absorbances at 663 nm and 645 nm using the Gen5 2.00 software. The absorbance readings were then converted into µg amounts using the calculations: (A_{663} x 212.72) – (A_{645} x 2.59) and (A_{645} x 22.88) – (A_{663} x 4.67) for determination of Chl *a* and Chl *b* respectively [58]. The µg amount of chlorophyll was calculated for $1x10^7$ cells in *y-1* greening experiments and for 1 mL of culture in diurnally-entrained cultures.

2.32 Extractions of the Intermediates in Chlorophyll Biosynthesis.

Cell pellets were collected from *y-1* and diurnally-entrained cultures as previously described. Pellets contained an equal cell number and were stored at -80 ºC. Thawed pellets were subjected to pigment extraction using 1 mL of fresh 80% (v/v) acetone; where samples were mixed vigorously to extract all pigments. Centrifugation at 5000 x *g* for five minutes removed all cell debris. Equal volume (750 µL) of supernatant and pre-combined hexanes were mixed and subjected to centrifugation at 5000 x *g* for five minutes; which separated the organic and inorganic layers. The top layer was carefully removed, and the bottom layer was washed two more times with equal volumes of pre-combined hexanes. A 200 µL aliquot of the bottom layer was transferred to a black round bottomed 96 well plate. The plate was read by the Bio Tek Synergy H1 Hybrid Plate Reader and fluorescence was measured of several chlorophyll precursors: protoporphyrin IX 400 nm excitation : 632 nm emission, Mg-protoporphyrin IX 420 nm excitation : 595 nm emission, Protochlorophyllide 440 nm excitation : 633 nm emission, chlorophyllide 440 nm excitation : 672 nm emission using the Gen5 2.00 software [58].

2.4 Western Blots (Protein Immunoblots)

Cell pellets were collected from *y-1* and diurnally-entrained cultures as previously described. Pellets contained an equal cell number or equal culture volume (for diurnally-entrained 24-hour samples) and were stored at -80 ºC until needed. Thawed pellets were then resuspended in an appropriate volume of 1x denaturation buffer; composed of 5x SDS-loading dye with 4% (v/v) βME diluted with TKM buffer (20 mM potassium chloride, 25 mM magnesium chloride, 10 mM Tricine [pH 7.5] made with DEPC-treated water). Samples were then subjected to denaturation at room temperature for 1h utilized for the protein A1 (PSI – *psaA*), or 65 ºC for 1h with intermittent mixing utilized for all other proteins tested. The gel casting apparatus was washed, and then used to make a 12% (v/v) poly-acrylamide resolving gel and a typical stacking gel. SDS-PAGE gels were loaded with equal volumes of sample and electrophoresis was performed in 1x Tris-Glycine running buffer. A voltage of 70 volts was used until samples cleared the stacking gel, and then was increased to 110 volts for approximately 1.5 hours or until the loading dye front reached the bottom of the gel.

Proteins in the polyacrylamide gels were transferred in transfer buffer (1x Tris Glycine and 18% (v/v) methanol diluted in deionized Nano Pure water) overnight to PVDF membrane (Bio Rad) at 4 ºC and a 25-volt or 100 mA current with constant magnetic stirring. Post transfer membranes were removed and washed in PBS and 0.1% (v/v) Tween (PBS-T). Membranes were then blocked with 5% (wt/v) skim milk in PBS-T for 1h with orbital shaking at 40 rpm. Blocked membranes were cut into strips for probing and heat sealed in plastic pockets with their respective primary antibodies diluted in the 5% (wt/v) skim milk and PBS-T mixture. Primary antibody probing was conducted for 1h at room temperature with rotation.

Primary antibodies used for main body figures were:

- αD1 (PSII – *psbA*) dilution 1:4000 purchased from Agrisera (Product #AS111786)
- αPsaAp (PSI) dilution 1:60 000 supplied by Dr. Kevin Redding
- αCytf (b_6f – *petA*) dilution 1:100 000 supplied by Dr. Yves Choquet
- αAtpB (ATP Synthase) dilution 1:5000 supplied by Dr. André Jagendorf
- αS-21 (30S chloroplast ribosomal) dilution 1:4000 supplied by Dr. Elizabeth Harris

Primary antibodies used for supplemental figures were:

- αD2 (PSII – *psbD*) dilution 1:5000 supplied by Dr. Jörg Nickelsen

Primary antibody probed membranes were washed three times in PBS-T for 5 minutes, and subsequently reacted with secondary antibody at a 1: 10 000 dilution of horseradish peroxidase-conjugated goat anti-rabbit IgG antibody (KPL) for 1h at room temperature with orbital shaking at 50 rpm. Stained membranes were washed three times in PBS-T for five minutes, drained well and then detected using ECL (Thermo-Fisher Scientific). Chemiluminescent bands were visualized using an Amersham Imager 600 (GE). Cut membrane strips from the same original membrane were reassembled and exposed using the same parameters.

2.5 Immunofluorescence Staining and Fluorescence *in situ* Hybridization

The procedure for both IF and FISH were previously documented, and the mRNA *psbA* FISH probe used here was also previously designed and labeled by Dr. J. Uniacke [2], [59]. An empirically determined amount of probe; 18-20ng per sample, was hybridized overnight at 37 ºC in the InSlideOut slide hybridization oven (Boekel Scientific). Slide desiccation was avoided by the incorporation of wet paper towels under the slide rack.

IF primary antibodies used are described above in the 'Western Blots (Protein Immunoblots)' section. Primary antibody dilutions for IF staining were as follows:

- αS-21 (30S chloroplast ribosomal) dilution 1:1,000
- αAtpB (ATP Synthase) dilution 1:1,000
- αD1 (PSII – *psbA*) dilution 1:1,000
- αPsaAp (PSI) dilution 1:2,000
- αCytf (b_6f – *petA*) dilution 1:1,000

The secondary antibody used was Alexa Fluor 568 conjugated goat anti-rabbit IgG (Molecular Probes-Thermo-Fisher Scientific). Images were acquired using the inverted epifluorescence microscope Leica DMI6000B with a Leica controller CTR6500, an XY inverted Piezo Stage MLC MS-2000, halogen lamp lights source for bright field (BF), a Leica EL6000 mercury short arc reflector lamp, and a Hamamatsu ORCA R2 C10600-10B digital CCD camera. The objective lens employed was a HCX PL APO 63x 1.40-0.6 under oil immersion, with an added 1.6x magnification which yielded an overall pixel size of 0.064. Images were captured and stored using the Volocity Acquisition System (Improvision). Filters used were: Texas Red 4040B 562/40 nm excitation : 624/40 nm emission for protein labeling, and GFP 3035B 472/30 nm excitation : 520/35 nm emission for probed mRNA message *psbA*. Images were acquired with Z plane stacks

of 0.2 μm spacing, and all other velocity settings were default or recommended by the program. Acquisition parameters for fluorescent channels and the bright field channel, remained the same for all time points used within a data set.

Deconvolution of all acquired images was performed using AutoQuant X3 software (Bitplane). Settings for image recognition were chosen according to the optics recorded in the meta data, and the utilized glycerol-based sample medium; Prolong Gold Antifade (Molecular Probes). An adaptive PSF was applied for deconvolution of 15 iterations, using low background removal for the IF signals and medium background removal for the FISH signal from the *psbA* mRNA.

Control cells were subjected to the same growth conditions and processing steps used within the experiment. Control experimental conditions used for slide preparation were: primary antibody probing with no secondary staining, secondary antibody staining with no primary probing, and the FISH protocol with a mock probe.

2.6 Live Cell Chlorophyll Autofluorescence

Growing *y-1* and diurnally-entrained cultures were sampled at various time points to characterize their *in vivo* distribution(s) of chlorophyll autofluorescence. Prior to cell sampling, 3% (wt/v) low-melting point agarose (Bethesda Research Laboratories) was prepared in the appropriate media: TAP for *y-1* cells and HSM for diurnally-entrained cells. This melted mixture was maintained liquid at 37 ºC. Aliquoted cells were carefully immobilized on a clean slide using an equal volume of 3% (wt/v) low-melting point agarose and sampled cells [60]. This 1.5% (wt/v) low-melting point agarose cell mixture was quickly swirled and then secured gently by lightly pressing a clean coverslip on the sample.

Live cells were imaged using the same epifluorescence microscope, velocity settings, and acquisition settings stated previously. The filter cube used was: CY5 4040A 628/40 nm excitation : 692/40 nm emission. Acquisition parameters for the CY5 channel and the bright field channel, remained the same for all time points used within a data set. Deconvolution of all acquired images was performed as previously explained, while using low background removal for *in vivo* chlorophyll autofluorescence.

Acquired *y-1* cell images, for all time points, were alternatively subjected to normalization. Normalization was achieved using an automated Fiji macro written by Dr. Christopher Law.

Representative cell images were reduced to the most focused z slice and saved in the same folder. The macro then read this folder, consisting of all time points, and allowed the user to select a 16-bit minimum and maximum displayed value for the highest intensity image within the folder. This pixel intensity range was then propagated to all images, normalizing them. Normalized 16-bit images were converted into 8-bits, and then modified for contrast using the same parameter values within all images.

2.7 Transmission Electron Microscopy

All TEM samples were prepared by the McGill Faculty for Electron Microscopy Research (FEMR) staff as described previously [61]. Samples were fixed in 2.5% (v/v) glutaraldehyde in 0.1M sodium cacodylate buffer containing 4% (wt/v) sucrose and 0.1% (wt/v) $CaCl_2$ pH 7.4 (fixed samples were kept consistently at 4 ºC until delivered to the FEMR) then were washed three times with 0.1M sodium cacodylate for up to 1h, and were post-fixed with 1% (v/v) aqueous osmium tetroxide + 1.5% (wt/v) aqueous potassium ferrocyanide for 2h at 4 ºC. Once stained, the osmium tetroxide mixture was removed by pipetting and discarded. Samples were then washed three times with distilled water for five minutes in the fume hood. Washed samples were dehydrated for 8-to-15 minutes using increasing concentrations of acetone: 30%, 50%, 70%, 80%, 90%, and finally three times using 100% acetone dehydration. Dehydrated samples were then infiltrated with an Epon:Acetone mixture using three successive ratios: in a 1:1 ratio for overnight treatment, followed by treatment with a 2:1 ratio the entirety of the next day, and lastly treatment with a 3:1 ratio overnight on the second day. These Epon:Acetone infiltration treatments were always performed on the rotator for agitation. The following day, samples are subjected to pure Epon for 4h with the caps of the tubes open, the next 2h on a rotator, and the final 2h under a vacuum. They were then embedded with the proper labels in the appropriate molds and left to sit for 1h under the fume hood. Finally, samples were embedded with Epon and polymerized in a 68 ºC oven for 48 hours. The final grids contained slices of cells that are on average 90-100 nm thin and stained with uranyl acetate and Reynold's lead.

Images were acquired on the FEMR's transmission electron microscope the FEI Tecnai 12, operating at an accelerating voltage of 102kV and using the Tecnai User Interface software and an AMTv601 CCD Camera. Settings used were an aperture of three, a spot size of two, and variable

magnifications ranging from 2900x to 68 000x. Images were adjusted for contrast and gamma units using the Tecnai User Interface.

2.8 Quantification of *in situ* Distribution Patterns

2.81 Visual analysis of *in situ* distribution patterns.

Various results required quantification of *in situ* fluorescent signal distribution from IF and FISH, to establish the frequency with which different patterns were presented. Objectivity was maintained by setting a series of criteria tailored to the specific data set prior to tallying patterns by manual counting. The data set in question was reviewed quickly to assess the pattern(s) seen then excel files were created to record the patterns that were scored.

The first example of this quantification was the localization of marker proteins specifically to the T-zone. Where the T-zone was revealed by the localized FISH signal from the *psbA* mRNA (Uniacke and Zerges, 2007). Cells that were scored positive showed significant overlap of the first appearing and highest intensity signal for both channels in the T-zone area. Cells that were scored negative either did not display this criterion or were questionable. This quantification of T-zone localization was used for both *y-1* and diurnally-entrained cells. Diurnally-entrained cells tallied during the dark phase contained a mixed population; those not yet divided, those in the process of division, and newly released daughter cells. Dividing cells were excluded due to their multiple daughter cells (2-to-32) which caused overlapping diffracted signal. For applicable measured time points, the population of large not divided cells and small newly divided cells were tallied and recorded separately.

The sub-patterns, within the greater T-zone pattern, were classified and recorded. Positive T-zone scoring cells were classified into one of four documented sub-patterns; localization of the signal to one or both lobe junctions, a band-like pattern including both lobe junctions and extending between them into the chloroplastic area anterior to the pyrenoid, a necklace-like pattern highlighting the top of the pyrenoid only, or a discontinuous ring-like pattern coupled with strings of signal entering the pyrenoid. This analysis was conducted using only the diurnally-entrained data set for the localization of the 30S chloroplastic ribosomes coupled with the *psbA* mRNA message. This same data set was also used to monitor the appearance of stress granules.

Another pattern quantified, was the *in vivo* live cell localization preference of chlorophyll and it precursors. The data set was superficially reviewed to identify patterns and a set of objective criteria were designed for scoring. For *y-1* this criterion looked for the *in situ* location of the chlorophyll autofluorescence. Positive scoring cells showed the first appearing and most intense chlorophyll autofluorescence in the T-zone area. Negative scoring cells showed the autofluorescence everywhere along the chloroplast. For diurnally-entrained cells this criterion required a chlorophyll autofluorescence intensity difference between the lobes and T-zone area. Positive scoring diurnally-entrained cells displayed a chlorophyll autofluorescence difference of 300 arbitrary fluorescent units or more between these two areas. The Fiji image analysis software was used to measure the average chlorophyll autofluorescence intensity along the T-zone versus along the lobes, by using a 10-pixel thick freehand line. The averages and differences between the T-zone and the lobes were calculated, and this analysis was conducted for all diurnally-entrained times points tested.

Lastly, the *in-situ* presence or absence of cytochrome f staining foci was quantified. Cells stained for cytochrome f were categorized as either containing foci (positive) or not (negative). This analysis was conducted for various *y-1* greening time points, a *y-1* green culture, and a nitrogen deficient culture.

Tallying *in situ* patterns by eye was a tedious and error-prone process. The use of criteria makes this process more objective, but the possibility of person-to-person subjectivity and error is always an issue. The above-mentioned patterns were independently visually scored by both Dr. Zerges and myself, similar numbers were achieved.

2.82 Visual analysis of ultrastructures in TEM images.

TEM images revealed several ultrastructure characteristics that could be quantified. Thylakoid convergence zones, a meeting point for 3 or more thylakoids, were tallied for: quantity, location, envelope association, and if they ended in a ball-like structure. This tally was conducted for the time points which displayed *in situ* T-zone localization ZT2 and ZT3, versus the time points which did not display *in situ* T-zone localization ZT10 and ZT11. Convergence zone quantity per cell was tallied based on the criteria of presence or absence, while also recording their location and other structural characteristics stated above. Chloroplastic location was broken down into five

groups; posterior to the pyrenoid, on lateral sides of the pyrenoid, lobe junctions, the chloroplastic region anterior to the pyrenoid, and anywhere in the lobes.

The disappearance of the pyrenoid tubules was also tallied within the same diurnal time points stated above. The amount of pyrenoid tubules within the pyrenoid was analyzed based on a qualitative scale using a symbolic plus and minus system where each symbolic score represented a degree to which pyrenoid tubules were present.

2.83 Nonbiased Cell Harvester image analysis of *in situ* patterns.

Visual analysis and manual scoring of *in situ* intra-organellar localization patterns can introduce human error and subjectivity. To simplify this process and reduce these issues, Dr. Christopher Law created an automated Fiji macro for the analysis of *in situ* patterns within fluorescent microscopy images. This macro named "Cell Harvester" (CH), helps researchers avoid potential biases for the scoring of cells with multiple intra-organellar localization patterns.

Deconvolution of all images was necessary because diffracted light from labeled molecules causes a reduction in subcellular resolution. All images were deconvolved as previously explained where low background removal was used for the protein signal and medium background removal was used for the mRNA *psbA* signal. The CH has three steps; the first is a 'preprocessing' step, followed by an cell isolation step, and completed by the generation of an average compiled cell based on the initial data.

The preprocessing step compiles acquisitions into their respective maximum z projections, for both channels analyzed. Where the TexRed channel imaged the IF signal from our protein(s) of interest and the GFP channel imaged the *psbA* mRNA probe. Part one of the macro identifies the cells, based on a typical ellipse shape, within the first maximum projection channel. Identified cells are outlined and inputted into an ROI manager. This ROI manager can be modified by the user, which allows incorrectly identified objects to be removed, and for the addition of non-identified cells. User approved completion of the ROI manager triggers the cutting out of all outlined cells within the given acquisition. These cut cells are oriented along their long axis, have their pyrenoid towards the right, and are subsequently saved in an output folder along with the ROI.

All cells within a data set were subjected to these first two steps and compiled into a general folder. This library of cells to be analyzed was verified for pyrenoid orientation and manually curated removing cells that were squished, unstained, or oriented in an unclear manner (e.g.: top-view or rear-view). The curated cell libraries were then inputted into the second part of the CH protocol where the different data sets for different proteins were kept separate from each other. This second part of the CH compiled all given cells into an 'average representative cell' where the average cell size was determined based on the largest cell in the data set and all other cells were then scale in X and Y accordingly. Meanwhile, the average signal intensity was generated by the normalization of each cell in the data set, which ensured that all cells contributed equally. The final output of the CH macro is a variety of z projections saved under their respective type; average, maximum, minimum, and sum. For our purposes the average z projection is the best representation of the signal distribution(s) because it is not skewed by the weakest or most intense pixels like the other z projections. Thus, every average compiled cell image is an average z projection derived from the compilation of maximum z projections from multiple cells.

These average compiled cell images were then used to generate distance plots for each channel independently. Distance plots were derived from a drawn freehand line from the tip of one chloroplast lobe through the lobe junctions and pyrenoid all the way to the tip of the other lobe. Numerical data of distance versus intensity points was generated from these plots, and then used to derive correlation coefficients which were put on a colorimetric scale in excel. These coefficients range from 1 to -1; delineating a perfectly correlated data set to a perfectly anti correlated data set respectively. Distance plots and correlation coefficients were generated for all time points tested.

An additional third part to the CH macro has yet to be completed. This third instalment would allow one to draw freehand lines for all the cells independently by converting them to the same size, and then propagating the line of interest to all cells within the data set. This would give a distance versus intensity plot which is 'shaded' where the 'shade' denotes the individual deviation for every data point. This third part of the Cell harvester would display the time point specific standard deviation for the predominant *in situ* pattern and could be complimented with additional co-localization analysis using Mander's overlap coefficients.

Chapter 3 : Results and Discussion

3.1 Chloroplast Differentiation: The Translation Zone is the Primary Location for Chlorophyll Accumulation, PSI and PSII subunit Biogenesis

3.11 Characterization of the *y-1* mutant model system for chloroplast differentiation:

Previously, PSII biogenesis was localized to the T-zone but was limited by the algal model system employed [2], [40]. Alternatively, use of the *y-1* mutant provided increased thylakoid biogenesis triggered by chloroplast differentiation which is an optimized system to elucidate the spatial and temporal localization of other PET chain complexes and components.

The efficient greening of this *y-1* mutant was achieved in our laboratory. Expected markers of *y-1* chloroplast differentiation were the change in culture color from yellow to green prior to cell division, the rapid accumulation of the pigment chlorophyll, and the progressive synthesis of the PSI and PSII complexes [38], [41]. Therefore, these anticipated behaviours were identified within our greening *y-1* cultures.

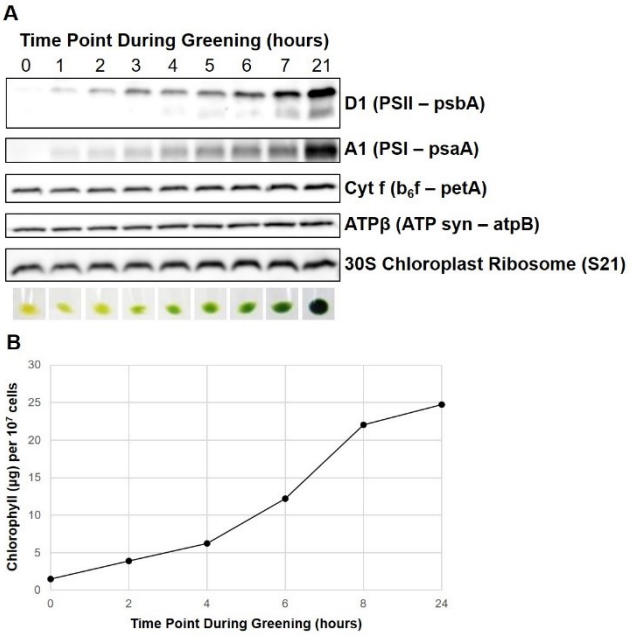

Figure 2. Characterization of protein and chlorophyll content during *y-1* greening
(A) Immunoblot analysis of marker proteins for: the PSI complex (D1), the PSII complex (A1 or PsaA), the cytochrome b_6f complex (Cyt f), the ATP synthase complex, and the small chloroplastic ribosome subunit. Cell pellet images demonstrate color change.
(B) Chlorophyll accumulation in µg for 1 x 10^7 *y-1* cells versus greening time points in hours.
* Dr. Yi Sun contributed most to the data presented in this figure. Pellet collection and figure making were conducted 50% by Melissa V.P.

A change in cell pellet color from yellow to green was seen after 1-2 hours of *y-1* dark-grown culture illumination (Figure 2A). Differentiating *y-1* does not divide within the first 6 to 9 hours of greening because of insufficient chlorophyll accumulation causing inadequate thylakoid production which halts chloroplastic division and associated nuclear division [38]. The 1-2-hour initiation of greening within our *y-1* cultures was to short a time for cell division. Thus, this change in color was not due to a new generation of cells but instead caused by the chloroplastic differentiation of the same generation. This resulting phenotypic greening enabled the verification of other expected biochemical changes throughout *y-1* chloroplast differentiation.

Pigment extraction during *y-1* greening revealed the rapid accumulation of chlorophyll with dark-grown cells containing less than 2 μg/10^7 cells versus 8-hours greening cells which contained approximately 22 μg/10^7 cells (Figure 2B). Past 8 hours of greening, chlorophyll displayed a reduced accumulation trend reaching a plateau of 25 μg/10^7 cells when chloroplasts were mature (Figure 2B). The rapid accumulation of this pigment during greening is known to have an initial lag phase followed by an increase in synthesis and accumulation until an eventual equivalence to the maximal chlorophyll synthesis rate expected of differentiated green chloroplasts [38]. Therefore, this rapid chlorophyll accumulation trend supports the proper differentiation of our *y-1* cultures, requiring only the verification of protein accumulation prior to experimentation.

Immunoblot levels for the photosynthetic complexes during *y-1* chloroplast differentiation revealed the expected rapid increase of PSI and PSII which are accumulating similarly to their associated chlorophyll pigment (Figure 2A). This PSI and PSII protein accumulation trend correlates with the increased synthesis rates of these complexes which is hypothesized to be controlled by a combination of light, the prevention of ROS, and the potential localized organization of their molecular components [41], [47]. Moreover, this rapid protein accumulation trend was only documented for PSI and PSII during *y-1* greening and was not seen for the ATP synthase complex, the cytochrome b_6f complex, or the ribosomal protein marker (Figure 2A). These contrasting protein accumulation patterns have been previously documented, what has yet to be explored is the potential for differing *in situ* localization patterns between these PET chain complexes when studying this *y-1* model of algal chloroplast differentiation [41].

3.12 Temporal changes in T-zone localized PSII subunit translation markers during *y-1* chloroplast differentiation:

Protein accumulation trends between the thylakoid membrane-bound PET chain complexes differ based on their association with the chlorophyll pigment. PSI and PSII are undergoing biogenesis while the non-chlorophyll-containing ATP synthase and cytochrome b_6f complexes denote the distribution of all chloroplast thylakoids (Figure 2). *In situ* fluorescence microscopy was used in combination with temporal analysis of *y-1* chloroplast differentiation to compare the PSII complex undergoing biogenesis versus the ATP synthase complex representing thylakoid membrane placement. We hypothesized that the organization of PSII subunit translation will be temporally localized to the T-zone when using chloroplast differentiation and that this organizational phenomenon will not be present for our thylakoid marker. However, the proper *in situ* fluorescent controls were necessary.

Algal *in situ* fluorescent microscopy controls were reported in previous publications [2], [15], [59]. Some controls were repeated and the same non-patterned *in situ* results were documented for all control conditions used (Supplemental Figure 1). Additional IF antibody specificity verifications were conducted through immunoblot analysis where cross-reactivity was detected for the antisera against ATP synthase β subunit and cytochrome f of the cytochrome b_6f complex (results not shown). The antibody against the ATP synthase β subunit was shown to also detect another thylakoid membrane protein, which does not interfere with our experimental strategy [62]. In contrast the cytochrome f antibody strongly cross-reacted with an unknown protein and demonstrated potential artifacts *in situ* (discussed below). Procedural controls for FISH, autofluorescence, and secondary antibody retention controls all exhibited no artefactual

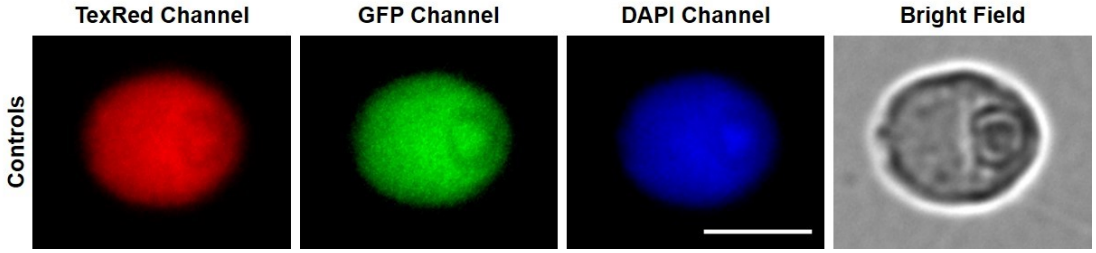

Supplemental Figure 1. *In situ* localization control cells

y-1 greening and diurnally-entrained control cells were exposed to various procedural and staining controls. Bright field provides cellular orientation. Scale bar is 5 μm.

*Dr. Yi Sun contributed 50% towards making these multiple control slides and imaging them. The other 50% contribution towards slide making and imaging, and figure making provided by Melissa V.P.

signals or patterns (Supplemental Figure 1). All control samples visualized regardless of the algal model system or time point used had an evenly dispersed internal cellular background fluorescence level that amounted to no more than 300 arbitrary fluorescence units (Supplemental Figure 1). Thus, we confidently began documenting the *in situ* spatial and temporal localizations of these differing PET chain complexes throughout the process of *y-1* chloroplast differentiation.

Dark-grown *y-1* cells exhibited localization of both the chloroplastic ribosomes and the *psbA* message within the basal region of the chloroplast (Figure 3). The chloroplast of dark-grown *y-1* cells appears larger, rounder, and distorted due to the accumulation of starch. The presence of starch granules often distorts *in situ* signals causing a bubble-like appearance, these starch granules are identifiable as dense rounded structures within the bright field channel of dark *y-1* time points (e.g. Figure 3). Despite the physical displacement of signal caused by these starch granules, 77% of cells imaged displayed T-zone localized overlap of the chloroplastic ribosomes and the *psbA* message. Confirmation of T-zone localized PSII subunit translation markers within dark-grown *y-1* cells was conducted by an unbiased automated macro called 'Cell Harvester' (CH). The CH can isolate, orient, normalize, and size cells accordingly to overlay their maximum intensity

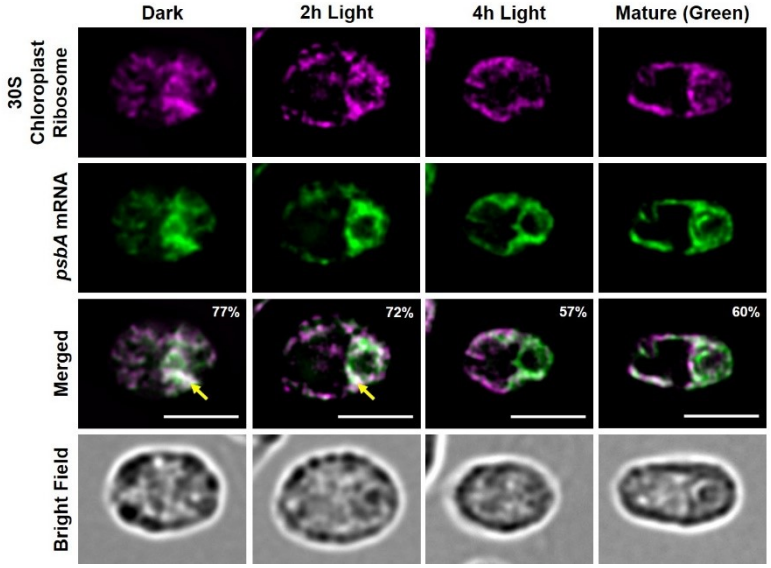

Figure 3. *In situ* localization of markers for PSII subunit translation during *y-1* greening
Immunofluorescence staining of the chloroplastic small (30S) ribosomal subunit coupled with fluorescence *in situ* hybridization of the PSII-specific *psbA* message. Merged channels indicate overlapping areas between both markers (white) and T zone is indicated by yellow arrows. Bright field provides the cellular orientation. Percentages of the given pattern are displayed. The scale bar is 5 µm. Sample sizes of cells: Dark (n=51), 2h Light (n=113), 4h Light (n=79), Mature (n=91).
*Dr. Yi Sun contributed 50% towards making the slides and imaged all the slides. The other 50% of making the slides, deconvolution, analysis, and figure making conducted by Melissa V.P.

projections yielding an average compiled cell for all cells imaged in each time point. Subsequently, the user can draw a thick line across the chloroplast and determine the average fluorescent intensity along this line (Figure 4A or D).

CH analysis resulted in an average compiled dark-grown cell and its corresponding graphical representation which agreed with the visually counted percentage of dark-grown *y-1* cells containing T-zone localized PSII subunit translation markers (Figure 4A and B). An average cell image denoting the IF chloroplastic ribosome marker signal in red and the FISH *psbA* message signal in green, displayed enriched yellow coloration within the T-zone revealing the presence of

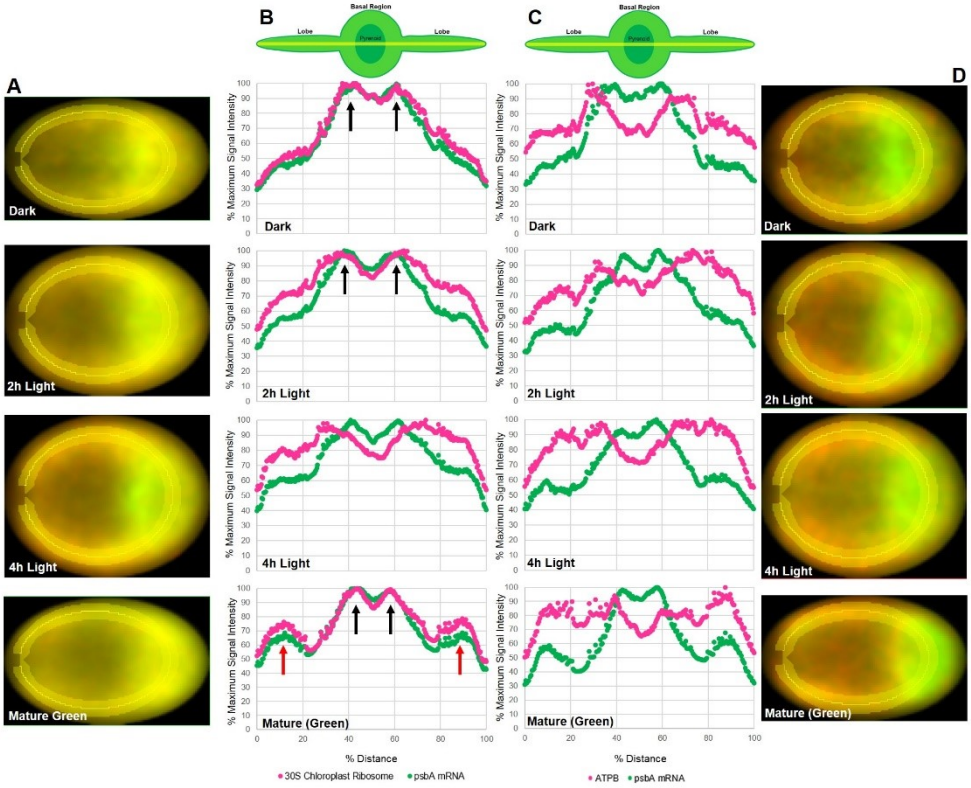

Figure 4. Cell harvester analysis for PSII subunit translation markers and the thylakoid marking ATP synthase complex during *y-1* greening

(A) Average compiled cells for the chloroplastic small (30S) ribosomal subunit and PSII-specific *psbA* message. Sample sizes of cells: Dark (n=52), 2h Light (n=95), 4h Light (n=79), Mature (n=77)

(B) Graphs of 'percent of maximum intensity vs percent of distance' for panel A cell images. T-zone foci are denoted by the black arrows and the lobe-tip maxima are denoted by red arrows. Straightened chloroplast denoted above graphs for positioning reference (pyrenoid center = 50%)

(C) Average compiled cells for the ATP Synthase β subunit and PSII-specific *psbA* message. Sample sizes of cells: Dark (n=35), 2h Light (n=54), 4h Light (n=46), Mature (n=47)

(D) Graphs of 'percent of maximum intensity vs percent of distance' for panel C cell images. Straightened chloroplast denoted above graphs for positioning reference (pyrenoid center = 50%)

*All work conducted by Melissa V.P.

both markers (Figure 4A). This yellow overlap is further defined by plotting a 'percent of maximal intensity versus percent distance' plot for each channel where an straightened chloroplast cartoon relates the graphed intensity percentage to the spatial location of these differing markers (Figure 4B black arrows). Therefore, this majority of dark-grown *y-1* cells showing T-zone localized PSII subunit translation markers is supported by the unbiased quantification of *in situ* fluorescent patterns using the CH. To confirm that this documented *y-1* T-zone is similar to the previously discovered T-zone we categorized its pattern in greater detail.

The chloroplastic T-zone area contained signal localized in four differing sub-patterns the majority of which resembled the previously documented PSII Translation-zone (Supplemental Figure 2). When T-zone sub-patterns were examined within diurnally-entrained cells (discussed below), lobe-junctions were included in half of the sub-patterns described and represented a majority the T-zone localized cells regardless of the time point analyzed (Supplemental Figure 2A

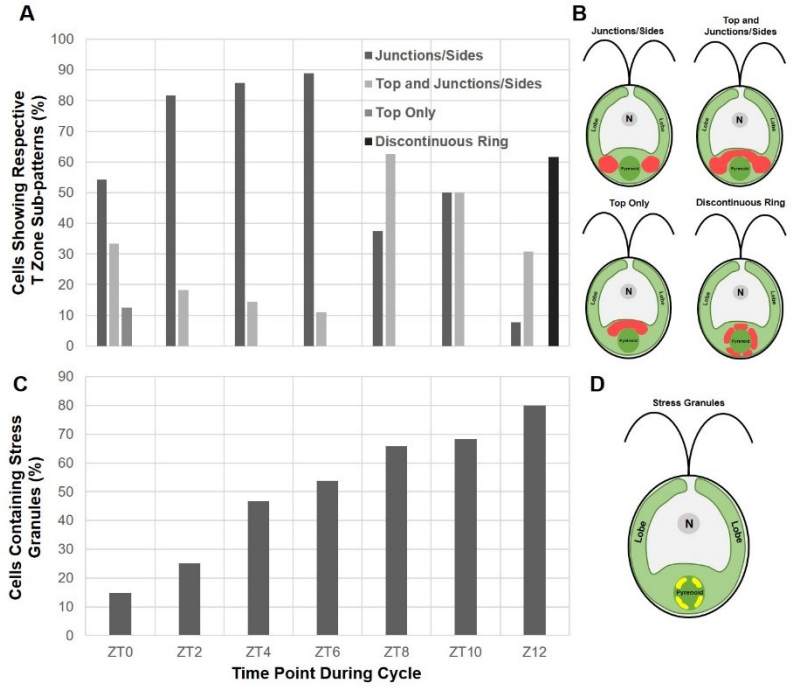

Supplemental Figure 2. Quantified T-zone sub-patterns and stress granules for the localization of PSII subunit translation markers during the light phase of diurnally-entrained cells
(A) Percent of each T-zone sub-pattern per 2-hour ZT light phase time points. Sample sizes of cells: ZT0 (n=24), ZT2 (n=22), ZT4 (n=21), ZT6 (n=18), ZT8 (n=8), ZT10 (n=4), ZT12 (n= 14).
(B) Cartoons of algal cells depicting the quantified T-zone sub-patterns.
(C) Percent of stress granule positive cells per 2-hour ZT light phase time points. Sample sizes of cells: ZT0 (n=27), ZT2 (n=28), ZT4 (n=55), ZT6 (n=78), ZT8 (n=44), ZT10 (n=41), ZT12 (n= 20).
(D) Algal cartoon depicting the location of stress granules within *Chlamydomonas reinhardtii.*
*All work conducted by Melissa V.P.

and 2B). Similarly, Uniacke and Zerges (2007) chose algal cells displaying a chloroplast morphology where the lobe-junctions extended to the lateral sides of the pyrenoid. Therefore, previously documented PSII T-zones and our T-zone analysis describe the same sub-organellar localization. The most frequent T-zone sub-pattern displayed one or both lobe junction foci often coupled with a chloroplastic band anterior to the pyrenoid and was easier to identify at later time points throughout y-*1* chloroplast differentiation (Figure 1A and 3).

T-zone specific localization of the chloroplastic ribosomes and the *psbA* message persisted for at least 2-hours of greening as displayed in 72% of cells (Figure 3). When comparing dark-grown and 2-hour greening cells, the *psbA* message displayed slight dispersal into the chloroplast lobes. Conversely, the chloroplastic ribosomes exhibited a more prominent spreading into the lobes. Despite these changes in distribution, the T-zone remained spatially enriched in PSII subunit translation markers for the first 2-hours of *y-1* greening (Figure 3).

This 2-hour T-zone localization of PSII subunit translation markers is corroborated by the results of the CH (Figure 4A and B). The average compiled 2-hour greening cell image displays yellow coloration specifically within the lobe-junction areas (Figure 4A). Furthermore, the graphical representation of this image shows the strongest fluorescence of both markers spatially enriched within the T-zone (Figure 4B black arrows). Moreover, this graph supports the visual *in situ* analysis above by demonstrating the dispersal of these markers; where the chloroplastic ribosomes displayed a larger increase in signal intensity within the chloroplast lobes then the *psbA* message (Figure 4B 'Dark' vs. '2h Light'). Therefore, these CH findings support the 2-hour greening enrichment of PSII subunit translation markers within the T-zone while also documenting the temporally regulated chloroplastic ribosome dispersion out of the T-zone and into the chloroplast lobes.

After 4-hours of *y-1* greening, the PSII subunit translation markers were no longer enriched together within the T-zone as displayed by 57% of cells (Figure 3). This 4-hour greening shift from T-zone localized to non-localized marker distribution was reinforced by the predominantly green cell pellet color which could indicate a light-triggered dispersion of T-zone localized *de novo* PSII subunit synthesis (Figure 2A). *In situ*, the chloroplastic ribosomes appeared to strongly disperse out of the T-zone and into the chloroplast lobes which supports this transitional state (Figure 3). Similarly, the *psbA* message also demonstrated increased dispersal into the lobes but is still slightly

basally enriched as demonstrated by its strong intensity T-zone signal (Figure 3). These *in situ* marker localization patterns demonstrate that PSII subunit translation has now shifted from being T-zone enriched towards being evenly distributed throughout the chloroplast. This shift in localization of PSII subunit translation markers potentially associates with the change from rapid PSII biogenesis utilized for thylakoid assembly into decreased PSII subunit synthesis utilized for PSII repair coupled with the chloroplastic translation of other non-localized chloroplast proteins.

CH analysis of 4-hour greening cells also displayed this loss of localized PSII subunit translation markers (Figure 4A and B). This was demonstrated by the less prominent yellow T-zone coloration within the average compiled cell image and by the absence of high intensity marker overlap within the T-zone of the CH generated graph (Figure 4A and B). Moreover, the chloroplastic ribosomes show an additional 15% signal intensity increase within the chloroplast lobes while the *psbA* message only displays a 5% increase (Figure 4B '2h Light' vs. '4h Light'). Therefore, this unbiased analysis reinforces the dispersal of chloroplastic ribosomes into the lobes and supports the 4-hour greening loss of T-zone localized PSII subunit translation markers. Combined, these *y-1* greening results provide the first evidence for a spatial-temporal shift of PSII subunit translation markers within differentiating algal chloroplasts. Investigation into the *in situ* localization of PSII subunit translation markers within mature green *y-1* cells not undergoing thylakoid biogenesis, was subsequently compared.

Green *y-1* cultures had a mixed population of cells, where a 60% majority showed the even distribution of PSII subunit translation markers throughout the chloroplast (Figure 3). These green cells displayed the *psbA* message along the chloroplast with a slight T-zone localized intensity bias, and the even distribution of the chloroplastic ribosomes (Figure 3). Therefore, these green *y-1* chloroplasts that are not in a state of massive biogenesis display non-localized PSII subunit translation markers as was seen within 4-hour *y-1* greening cells. This finding supports the potential connection between the temporal regulation of T-zone PSII subunit translation marker enrichment and the corresponding change in thylakoid biogenesis required within the cell. Verification of green *y-1* cell findings was conducted by the unbiased CH.

CH analysis for *y-1* green cells indicated subtle localization patterns of PSII subunit translation markers which were not identified during visual analysis (Figure 4A and B). Both the average compiled green cell image and its respective graph displayed T-zone localization of PSII

subunit translation markers (Figure 4A and B black arrows). *In situ* visual analysis revealed the presence of T-zone localized chloroplastic ribosomes and *psbA* message but also displayed strong intensity signal patches elsewhere within the chloroplast (Figure 3). Therefore, these cells were not consistent with the defined criteria for T-zone specific enrichment of PSII subunit translation markers. These green *y-1* cells lack the coordination of chloroplastic development seen within their greening counterparts. This asynchronous cell population gives rise to chloroplasts at different stages of development producing the mixed spatial localization findings denoted by the CH analysis (Figure 3 and Figure 4B). Additionally, this green *y-1* CH analysis uncovered local maxima at the tips of the chloroplast lobes (Figure 5B). These chloroplast lobe-tip maxima could potentially be another area for PSII subunit translation marker enrichment, possibly used for PSII repair within differentiated green cells. Therefore, this average compiled green *y-1* cell image contained a mixed *in situ* PSII subunit translation marker distribution which was explainable and local maxima at the chloroplast lobes containing PSII subunit translation markers. Furthermore,

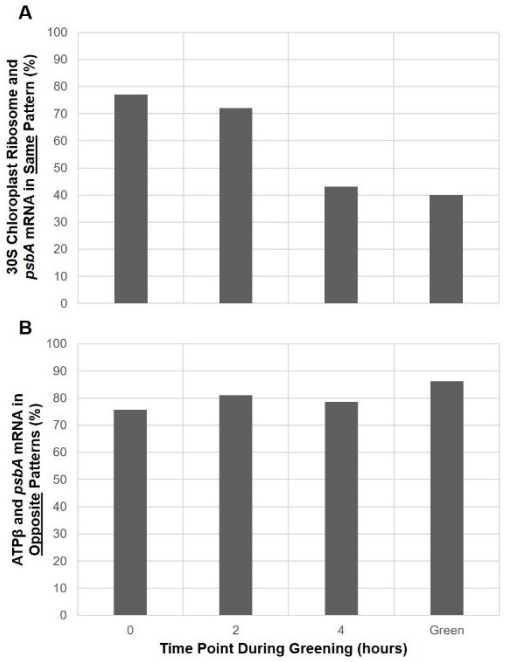

Supplemental Figure 3. Graphs for the visual analysis of *in situ* localization patterns for PSII subunit translation markers and a thylakoid marker during *y-1* greening

(A) Percentages of visually scored cells that display T-zone localized of both the small (30S) ribosomal subunit and the PSII-specific *psbA* message.

Sample sizes of cells: Dark (n=51), 2h Light (n=113), 4h Light (n=79), Mature (n=91)

(B) Percentages of visually scored cells that do NOT display T-zone localization of both the ATP synthase β subunit and the PSII-specific *psbA* message.

Sample sizes of cells: Dark (n=37), 2h Light (n=74), 4h Light (n=47), Mature (n=51).

*All work conducted by Melissa V.P.

CH detection of these lobe-tip maxima shows that this automated macro can help identify intra-organellar patterns that are not visually apparent within most cells.

Despite the slight discrepancies both visual and automated analysis support the temporal regulation of T-zone localized PSII subunit translation markers during *y-1* greening (Supplemental Figure 3A). To determine whether this localization of PSII translation markers reflects a sub-organellar spatial enrichment or an alternative distribution of thylakoid membranes, we characterized the *in situ* localization of the thylakoid marking ATP synthase complex.

The cytochrome b_6f and ATP synthase complexes denote thylakoid membrane distribution because these complexes do not display coordinated rapid protein biogenesis during *y-1* chloroplast differentiation (Figure 2A). Since the protein accumulation trends of these PET chain thylakoid markers differed from the photosystems we predict that so would their *in situ* localization during the greening process of *y-1*.

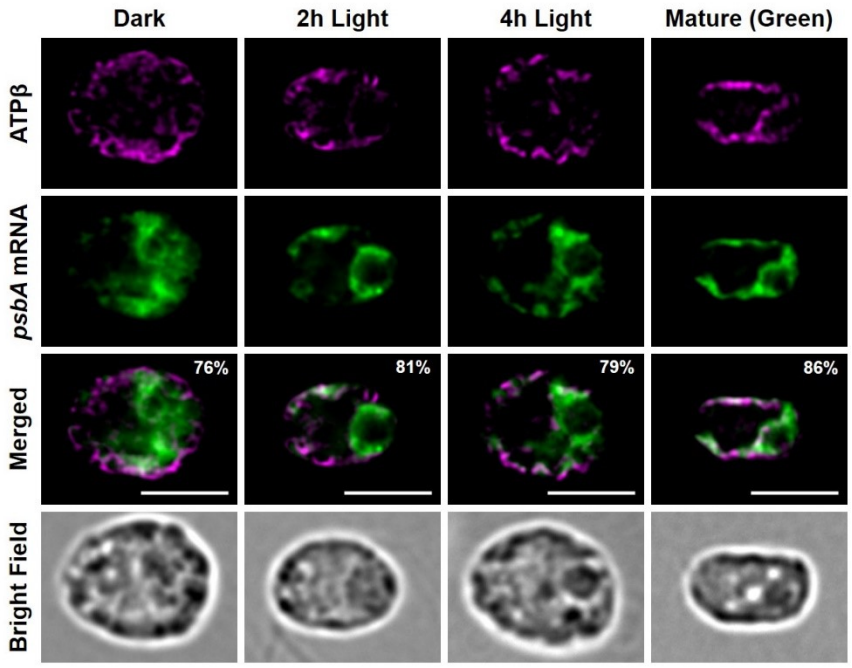

Figure 5. *In situ* localization of an ATP synthase marker versus the PSII-specific *psbA* message during *y-1* greening

Immunofluorescence staining of the ATP synthase β subunit coupled with fluorescence *in situ* hybridization of the PSII-specific *psbA* message. Merged channels indicate lack of overlapping white areas between both markers. Bright field provides the cellular orientation. Percentages of the given pattern are displayed. The scale bar is 5 μm. Sample sizes of cells: Dark (n=37), 2h Light (n=74), 4h Light (n=47), Mature (n=51).

*Dr. Yi Sun contributed 50% towards making the slides and imaged all the slides. The other 50% of making the slides, deconvolution, analysis, and figure making conducted by Melissa V.P.

As predicted, the even chloroplastic distribution of the ATP synthase marker was maintained throughout *y-1* greening and within green *y-1* cells (Figure 5). This PET chain complex is not T-zone localized and is instead mostly within the chloroplast lobes. Conversely, the *psbA* message remained basally enriched and displayed the same partial lobe dispersal as described above. Therefore, regardless of the greening time point or *y-1* chloroplast development the ATP synthase marker and the *psbA* message show partial non-localized overlap within the chloroplast lobes. This non-localized distribution is seen in a consistent majority of cells: 76%, 81%, 79%, and 86% in dark-grown, 2-hour greening, 4-hour greening, and in green *y-1* cells respectively.

The persistence of this non-localized pattern for the ATP synthase thylakoid marker was supported by the CH results. All compiled average cell images show the separated distribution of the ATP synthase marker and the *psbA* message by the presence of distinct red and green coloration (Figure 4D). Moreover, the graphs of these compiled cell images also displayed this non-localized distribution as denoted by the absence of high-intensity overlapping signal within the T-zone (Figures 4B vs. 4C). The constancy of this non-localized ATP synthase marker distribution throughout *y-1* greening and within green *y-1* cells can be seen in Supplemental Figure 3B.

The difference between the *in situ* spatial-temporal localization of PSII subunit translation markers and the ATP synthase marker is striking (Supplemental Figure 3A vs B). PSII showed a coordinated increase in protein accumulation during *y-1* greening and was localized for its early translation within the T-zone. Moreover, this spatial-temporal T-zone localization was not a by-product of chloroplastic thylakoid arrangement because of the even distribution seen for another PET chain complex. This thylakoid marking ATP synthase complex did not rapidly increase in protein content during *y-1* greening and was consequently not localized to the T-zone within this model system, instead displaying an even distribution along all thylakoids. The cytochrome b_6f complex is the other thylakoid PET chain complex which did not rapidly accumulate in protein content but its *in situ* localization was complicated by other factors (Figure 2A).

The cytochrome b_6f complex marker displayed a similar *in situ* even chloroplastic distribution as the ATP synthase complex marker (data not shown). Given the similar protein accumulation rates of these two chlorophyll-lacking complexes it was not surprising that their *in situ* localization patterns would also be comparable. The cytochrome b_6f complex was not used as a thylakoid marker nor displayed in the data because the antibody cross-reacted strongly with an

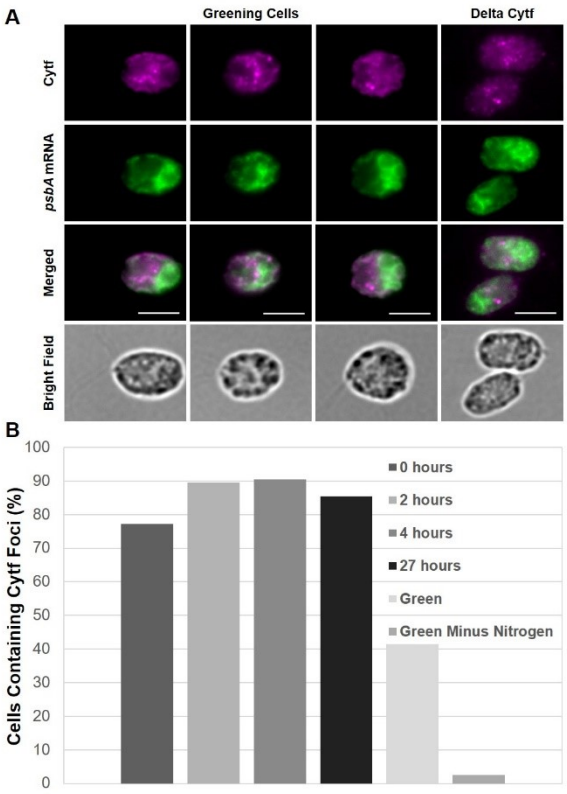

Supplemental Figure 4. *In situ* localization of a cytochrome b_6f marker into responsive foci
(A) Examples of fluorescence microscopy cell images depicting various foci arrangements throughout *y-1* greening and within the *petA* null mutant (foci are less organized and have a lower intensity)
(B) Graph for the visually score percentage foci positive cells within various conditions.
Sample sizes of cells: Dark (n=35), 2h Light (n=57), 4h Light (n=42), 27h Light (n=41), Mature (n=70), Mature minus nitrogen (n=41).
* Dr. Yi Sun contributed 50% to the making of the slides, and imaged these slides, the other 50% of slide making, deconvolution, analysis, and figure making conducted by Melissa V.P.

unknown protein causing brightly stained foci which were arranged and localized in a variable manner (Supplemental Figure 4A). Furthermore, these foci were not confirmed to be within the chloroplast and were also present to a certain degree in the Δ Cytf (*petA*) mutant (Supplemental Figure 4A). Taken together, these concerns led to the eventual exclusion of these data.

3.13 Spatial-temporal T-zone localization of chlorophyll autofluorescence during *y-1* chloroplast differentiation:

Using the model system of *y-1* chloroplast differentiation, the spatial-temporal T-zone enrichment of PSII subunit translation markers was discovered (Figure 3,4 and Supplemental Figure 3A). Alternatively, this spatial-temporal organization was not seen for the ATP synthase and cytochrome b_6f complexes (Figure 4C, 4D and 5). Moreover, this *in situ* spatial-temporal T-

zone organization was correlated with photosystem-specific rapid protein accumulation during *y-1* chloroplast differentiation. This increased protein accumulation and *in situ* spatial-temporal T-zone enrichment correlated with chlorophyll pigment association, while the chlorophyll-lacking complexes ATP synthase and cytochrome b_6f did not display this sub-organellar organization. Therefore, we hypothesized that chlorophyll would behave like PSII subunit translation markers, displaying an *in situ* spatial-temporal T-zone organization.

Autofluorescence is an energy dissipation process exhibited by the pigment chlorophyll which is often an inconvenience to fluorescence microscopy because it can obscure the detection of fluorescent signals. Alternatively, this naturally occurring autofluorescence can be used as an indicator of where chlorophyll begins to accumulate. The chlorophyll content within dark-grown *y-1* cultures is minimal, showing less than 8% of the amount measured within green cells (Figure 2B). Therefore, monitoring the *in situ* appearance of chlorophyll autofluorescence during greening of these dark-grown *y-1* cells can determine if chlorophyll accumulation occurs within the T-zone for *de novo* PSII biogenesis. These autofluorescence signals were initially bubble-like due to the presence of large starch granules, and later became more continuous as the starch was degraded (e.g. Figure 6). Chlorophyll accumulation findings during *y-1* greening are subsequently explained.

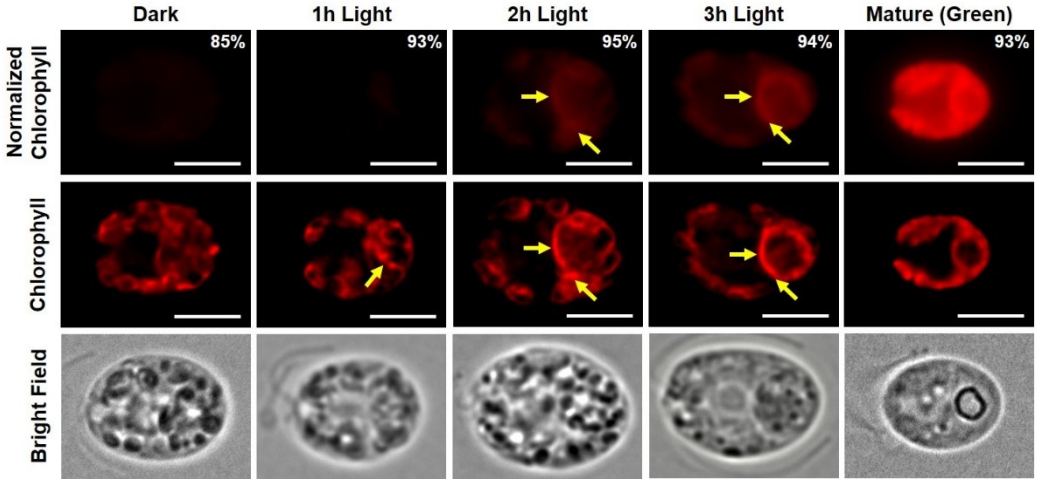

Figure 6. *In situ* localization of Chlorophyll autofluorescence during *y-1* greening
Live immobilized *y-1* cells of various greening time points were visualized for their naturally fluorescent chlorophyll pigment. Chlorophyll autofluorescence within the same cells is displayed using both normalized intensity images (row one) and non-normalized images (row two). T-zone localized enrichment is denoted by the yellow arrows. Bright field provides the cellular orientation. Percentages of the given pattern are displayed. The scale bar is 5 μm. Sample sizes of cells: Dark (n=13), 1h Light (n=14), 2h Light (n=22), 4h Light (n=18), Mature (n=14)
*Dr. Yi Sun contributed 50% towards making the slides and 50% towards imaging them. The other 50% of making the slides and imaging, deconvolution, analysis, and figure making conducted by Melissa V.P.

Dark-grown *y-1* cells displayed a relatively even chloroplastic distribution of chlorophyll autofluorescence with some stronger intensity T-zone patches (Figure 6). The 8% of chlorophyll after *y-1* de-greening is dispersed almost evenly across the thylakoid remnants present within this partially differentiated chloroplast [18]. These lower levels of chlorophyll autofluorescence within the dark-grown chloroplasts can be seen by comparing the 'Dark' and 'Green' normalized images (Figure 6). Additionally, higher intensity chlorophyll autofluorescence patches were enriched within the T-zone but did not contain any distinct patterns. These less distinct T-zone localized patches were depicted in 85% of cells. Thus, the remaining chlorophyll within dark-grown *y-1* cells showed some T-zone enrichment, a finding which supports the localization of chlorophyll autofluorescence during subsequent *y-1* greening.

1-hour greening *y-1* cells displayed a similar chlorophyll autofluorescence pattern as the previous time point, except for the distinct patches of higher intensity chlorophyll localized into two predominant T-zone patterns (Figure 6). These T-zone patterns were either necklace-like or band-like; highlighting the chloroplastic area anterior to the pyrenoid only or also extending into one or both lobe-junctions, respectively. This T-zone localization of chlorophyll autofluorescence was documented for 93% of cells where these higher intensity patches are slightly visible within the normalized 1-hour image (Figure 6). This initial accumulation of chlorophyll within the T-zone supports a coordinated spatial enrichment for the rapid assembly of the chlorophyll-requiring PSII complex. This T-zone specific enrichment of chlorophyll autofluorescence and its migration were documented throughout the *y-1* greening process.

Cells differentiated for 2-hours contained a substantially higher amount of chlorophyll throughout the chloroplast as well as increased chlorophyll autofluorescence localized to the T-zone (Figure 6). Having surpassed the known lag in chlorophyll synthesis, these greening *y-1* cells accumulated more of the chlorophyll pigment which is denoted by the increased autofluorescence seen throughout the entire chloroplast [18], [38]. This overall increase in chlorophyll can be visualized through the comparison of the normalized images (Figure 6). Moreover, the highest intensity chlorophyll autofluorescence signal was localized within the band-like T-zone pattern as seen for 95% of cells. Progressive migration of the chlorophyll pigment was temporally regulated and continued throughout the differentiation process.

Similarly, the 3-hour differentiated *y-1* cells continued to accumulate chlorophyll throughout the chloroplast while still maintaining stronger intensity chlorophyll autofluorescence localized to the T-zone (Figure 6). The increase in chlorophyll throughout the chloroplast is consistent with the pigment accumulation trend described previously and the expected constant chlorophyll synthesis rate being maintained until the chloroplast is differentiated (Figure 2B) [38]. Once again, this increase is noticeable when comparing the normalized images (Figure 6). Despite this overall chlorophyll increase, T-zone areas maintained a higher chlorophyll autofluorescence as depicted in 94% of cells. Moreover, these 3-hours greening *y-1* cells displayed migration of the T-zone localized stronger chlorophyll autofluorescence; where some cells changed T-zone pattern from the band-like pattern into a ring-like pattern encircling the pyrenoid (Figure 6). This T-zone accumulation of chlorophyll, its migration within the T-zone, and its subsequent temporal increase along all chloroplast thylakoids supports the model for T-zone PET chain complex biogenesis and migration as described earlier (Figure 1B). This T-zone directed model for thylakoid biogenesis was further investigated by comparing greening and green *y-1* cells.

Green *y-1* cells contained the highest amount the chlorophyll pigment but did not display any distinguishable localization of chlorophyll autofluorescence within the chloroplast (Figure 6). Chlorophyll autofluorescence within green *y-1* cells was present at a relatively higher intensity and in a more even distribution throughout the chloroplast, as seen when comparing the normalized images (Figure 6). This significant increase in non-localized chlorophyll autofluorescence relative to *y-1* greening cells was anticipated because the amount of chlorophyll pigment during early greening was not comparable to the 25μg seen within these green cells (Figure 2B). When tallied, 93% of green *y-1* cells contained a non-localized even distribution of chlorophyll autofluorescence. However, when quantifying the chlorophyll autofluorescence signal intensity along the chloroplast some green cells contained slightly stronger patches of chlorophyll autofluorescence localized to the T-zone in the band-like pattern. This slight T-zone intensity bias might reflect the presence of unquenched chlorophyll, where unassembled chlorophyll pigments display a higher autofluorescence when compared to their LHC bound counterparts [22].

In summary, T-zone localized chlorophyll accumulation during *y-1* greening and the slight chlorophyll intensity bias within the T-zone of green cells is consistent with the incorporation of chlorophyll into the assembling PSII complexes also found within T-zone localized thylakoids.

Newly synthesized PSII subunits need to be incorporated quickly into their respective complex assembly before they get rapidly degraded [63]. Chlorophyll is an essential component of the LHCII therefore it is required for the functional assembly of the PSII complex. Thus, the T-zone localization of multiple PSII proteins and components supports the spatial-temporal organization of PSII assembly during thylakoid biogenesis. The spatial localization for the initial accumulation of chlorophyll mirrors the T-zone localized translation of PSII subunits, with some differences. The predominant sub-patterns seen for PSII subunit translation initially was the lobe-junction localized pattern which transitioned into the band-like pattern (Figure 3 and Supplemental Figure 2A, 2B). In contrast, T-zone localized chlorophyll autofluorescence contained these same T-zone sub-patterns but in the opposite order (Figure 6). Potentially, this complementary T-zone sub-patterning for PSII biogenesis and chlorophyll accumulation has a biological significance. Furthermore, unlike PSII subunit translation the chlorophyll pigment accumulation prior to light exposure is not discretely localized to the T-zone but is instead more dispersed (Figure 3 vs 6). When monitoring chlorophyll, the final pigment product is localized after the process of synthesis which is not the same as localizing translation markers that place the process of synthesis itself. The T-zone localization of PSII translating components is known to be translationally independent or RNA mediated, therefore the sequestration of these translation components prior to PSII synthesis is possible [15], [41]. What is hypothesized but remains unanswered is if proteins translated from their T-zone localized RNA messages can mark their own site of synthesis via their initial localized accumulation. In other words, if PSII subunit translation is localized to the T-zone will the accumulated proteins also be localized there?

3.14 Spatial-temporal T-zone localization of PSII-specific and PSI-specific protein marker accumulation during *y-1* chloroplast differentiation:

The concurrent spatial-temporal localization of chloroplastic ribosomes and the PSII-specific *psbA* FISH probe was utilized to support T-zone localized PSII translation. However, the only functional FISH probe obtained was for PSII therefore this experimental design was not possible for the other PET chain complexes. Thus, we determined if complex-specific proteins could mark their own synthesis and assembly sites. Confirmation of this hypothesis was conducted using the *in situ* localization of the known T-zone localized *psbA* message coupled with the localization of its encoded PSII core protein D1. We hypothesized that the D1 protein will initially

accumulate in a T-zone localized manner because its message and the translation of it are both specifically localized to the T-zone. These subsequent *in situ* localization patterns were analyzed using our reliable CH which provided the representative compiled average cell images.

The dark-grown *y-1* average cell displayed a spotty D1 protein signal which appeared to be slightly T-zone localized (Figure 7A and B). This observed spotty signal reflects the low amount of the D1 protein present within dark-grown *y-1* cells which was supported by the *y-1* immunoblot demonstrating little if any D1 protein (Figure 2A). The lack of chlorophyll within these dark-grown *y-1* cells prohibits the correct assembly of the photosystems therefore these unassembled D1 proteins are degraded quickly [18], [63]. Upon visual analysis, no predominant D1 protein

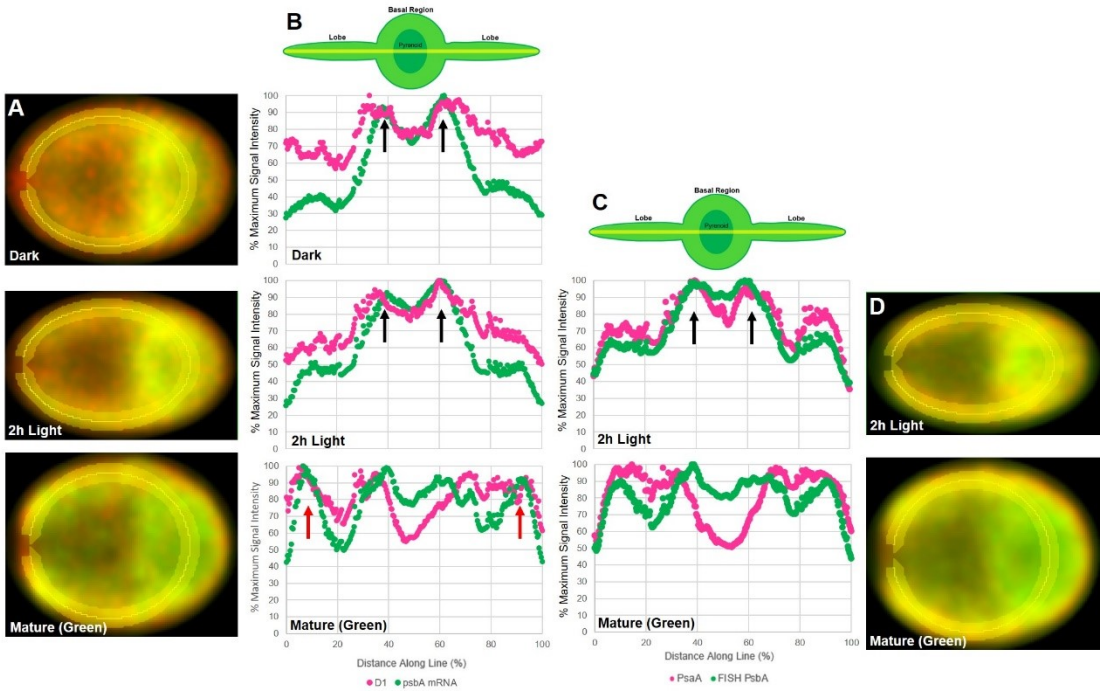

Figure 7. Cell harvester analysis for PSII-specific and PSI-specific protein markers during *y-1* greening

(A) Average compiled cells for the PSII core protein D1 and the PSII *psbA* message.
Sample sizes of cells: Dark (n=75), 2h Light (n=89), Mature (n=34)
(B) Graphs of 'percent of maximum intensity vs percent of distance' for panel A cell images.
T-zone foci are denoted by the black arrows and the lobe-tip maxima are denoted by red arrows.
Straightened chloroplast denoted above graphs for positioning reference (pyrenoid center = 50%)
(C) Average compiled cells for the PSI core protein PsaA and the PSII *psbA* message.
Sample sizes of cells: 2h Light (n=89), Mature (n=43)
(D) Graphs of 'percent of maximum intensity vs percent of distance' for panel C cell images.
T-zone foci are denoted by the black arrows. Straightened chloroplast denoted above graphs for positioning reference (pyrenoid center = 50%)
*All work conducted by Melissa V.P.

localization was seen within dark-grown cells, however CH analysis revealed a subtle T-zone preference. Within this CH dark graph, T-zone localization is denoted by the *psbA* message which was overlapping with some localized D1 protein foci (Figure 7B black arrows). The subtlety of this T-zone localized PSII-specific protein marker was reinforced by the low difference between the T-zone localized signal intensity and the signal intensity within the chloroplast lobes (Figure 7B). Therefore, the decreased D1 protein level within these dark grown *y-1* cells gave a spotty signal which did show some subtle T-zone localization. These results begin to support the hypothesis of T-zone organized protein accumulation for the PSII complex during *y-1* greening.

After 2-hours of greening *y-1* cells demonstrated a smoother D1 signal coupled with a more evident T-zone localization (Figure 7A and B). The 2-hour average compiled cell displays an obvious yellow coloration within the T-zone which denotes overlap of the D1 protein with its message (Figure 7A). This prominent T-zone localized D1 protein accumulation is also seen within the graph of the compiled cell image (Figure 7B black arrows). The increase in D1 protein accumulation after 2-hours of greening is supported by the *y-1* immunoblot (Figure 2A). Thus, as the *psbA* message is translated within the T-zone its encoded D1 protein is also accumulated there as denoted by the prominent T-zone localization of this PSII-specific marker. This 2-hour T-zone specific accumulation of the D1 protein is reinforced by the 10% increase in intensity difference between the T-zone localized signal and the chloroplast lobes signal (Figure 7B 'Dark' vs. '2h Light'). Subsequently, these unassembled D1 proteins must be either degraded or assembled into their PSII complex which is later distributed within all thylakoid membranes [63]. Therefore, these D1 proteins are expected to be assembled then migrated out of the T-zone specific thylakoids and into the remaining chloroplast, as *y-1* greening progresses.

Green *y-1* cells show no predominant T-zone localization of the D1 protein which correlates well with the non-localized PSII translation results explained previously (Figure 7A and B). As previously stated the localization of PSII subunit translation markers within green *y-1* cells was variable, with only 40% of these asynchronous cells showing T-zone localization however this variability was not observed for the localized PSII-specific protein marker under this same condition (Figure 4B vs 7B). Being the product of translation, accumulated proteins may initially mark their site of synthesis when using specific conditions however they will not indefinitely remain in that location. While recently divided green *y-1* cells may still require T-zone localized

PSII translation for chloroplast growth, the highly accumulated D1 protein no longer marks its site of synthesis and has now migrated to its final intended destination assembled within PSII complexes which are found along all chloroplast thylakoids (Figure 2A and 7B). Moreover, CH analysis of these green *y-1* cells also showed chloroplast lobe-tip maxima (Figure 4B and 7B red arrows). These lobe-tip foci are enriched with the *psbA* message and its encoded D1 protein which supports the hypothesis that these local maxima potentially act as a PSII repair site, specifically synthesizing and turning over the D1 protein because of its frequent damage [64]–[66].

In summary, these results support the use of complex-specific proteins markers to localize their site of translation when using early *y-1* chloroplast differentiation. The remaining D1 protein within dark-grown *y-1* cells displayed less pronounced T-zone enrichment which mirrored the distribution of the remaining chlorophyll, this suggests the slight localization of PSII components prior to light exposure. Greening cells undergoing increased thylakoid biogenesis displayed T-zone localized accumulation of the D1 protein which temporally corresponded with an increase in protein content. Moreover, green *y-1* cells that are not experiencing a burst of thylakoid biogenesis no longer displayed T-zone localized D1 protein accumulation. This *in situ* localization within greening versus green *y-1* cells support the proposed migration of newly assembled PSII complexes out of the T-zone and into the chloroplast lobes (Figure 1B). Therefore, the use of *in situ* complex-specific protein markers provides spatial evidence of their localized translation during early greening time points and temporal evidence of their migration from this synthesis area into their final thylakoid destination within differentiated chloroplasts. Therefore, the localized biogenesis of other PET chain complexes can also be conducted using protein markers.

Previous *in situ* studies attempted to localize the PSI complex but were inconclusive due to the lack of PSI biogenesis within the algal model system used [2]. When utilizing *y-1* chloroplast differentiation there is rapid protein subunit accumulation for both the PSII and PSI complexes (Figure 2A). The previous results depicted that these photosystem proteins accumulate in accordance with chlorophyll and this rapid complex biogenesis for PSII was spatially localized within the T-zone which was also temporally regulated. Given these photosystem-specific findings, we hypothesized that the PSI core marker protein PsaA (or A1) will also be T-zone localized. Using our CH, the *in situ* PsaA-specific protein marker localization was analysed and compared for 2-hour greening and green *y-1* cells.

The PsaA-specific protein marker exhibited T-zone accumulation during early *y-1* greening and subsequent loss of this specific localization within green *y-1* cells (Figure 7C and D). 2-hour greening cells displayed T-zone accumulated PsaA protein marker as denoted by the strong intensity overlapping regions between this protein marker and the *psbA* message (Figure 7D black arrows). T-zone accumulation of the PSI-specific protein marker was less evident than that of the PSII-specific protein marker, represented by the intensity difference between T-zone enriched signal and signal within the lobes (Figure 7B vs. 7C '2h Light'). Like other T-zone localized components, the PSI-specific protein marker displayed temporal regulation as denoted by loss of T-zone localization within green *y-1* cells (Figure 7C). Moreover, CH analysis of green *y-1* cells demonstrated the lack of PSI-specific protein markers within the chloroplast lobe-tip maxima which further supports this spatial enrichment as being a PSII-specific subunit repair region employed during conditions of decreased thylakoid biogenesis [64].

In summary, we have demonstrated that *y-1* chloroplast differentiation is an ideal model system to identify the spatial-temporal *in situ* chloroplast localization changes of several PET chain complexes and their associated components. PET chain complexes undergoing biogenesis are T-zone localized as supported by the T-zone enrichment of PSII, PSI, and chlorophyll biogenesis (Figure 2,3,4,6,7 and Supplemental Figure 3A). Alternatively, the ATP synthase and the cytochrome b_6f complexes are undergoing little-to-no biogenesis thus did not display localized protein-marker accumulation and instead denoted the overall distribution of thylakoids within the chloroplast (Figure 4,5 and Supplemental Figure 4A). Taken together these novel spatial-temporal findings support the T-zone specific organization of photosystem complex synthesis, assembly and subsequent migration into the remaining chloroplast thylakoid membranes (Figure 1B).

3.2 Chloroplast Growth and Division: Diurnally-Entrained Mature Cells Display Increased Chloroplast Differentiation and T-Zone Localization Reminiscent of the *y-1* Mutant

3.21 Verification of the diurnally-entrained model system for chloroplast growth and division:

T-zone localized PSII biogenesis was shown to occur during *y-1* chloroplast differentiation (Chapter 3.1) and within light-stimulated dark-adapted mature cells [2]. The previous mature cell model system had two critical issues: PSI biogenesis was not stimulated and the percentage of cells displaying T-zone localization were limited due to asynchronous algal growth. Therefore, it

was advantageous to use another mature algal model system which is undergoing coordinated thylakoid biogenesis and thus can still stimulate both photosystems in a temporal manner.

The use of diurnally-entrained cultures provided both a synchronized cell cycle and the coordination of thylakoid membrane biogenesis for mature chloroplast growth. Synchronization of algal cultures was achieved using a home-made system in substitute of a bioreactor. Through the control of environmental parameters, this system provided us with reproducible 24-hour diurnally-entrained cells which were verified for markers of synchrony and then subsequently used for experimentation. An acceptable level of synchrony was achieved if the following markers were observed: a visible cell size increase throughout the light cycle, coordinated division during mid-dark phase, and a 10 fold increase in cell density between 24-hour cycles [3], [52], [67]. Light microscope images qualitatively assessed synchrony throughout the 24-hour cycle (Figure 8).

Diurnally-entrained cells displayed the expected qualitative changes in cellular morphology and cell-cycle events (Figure 8). Zeitgeber Time 0 cells (ZT0) the first time point of the 24-hour cycle, displayed morphology typical of newly released progeny after division: pale green color, actively swimming, a small size, and oblong in shape. Cells at the end of that same 12-hour light phase (ZT12) exhibited the expected morphology of grown chloroplasts ready to

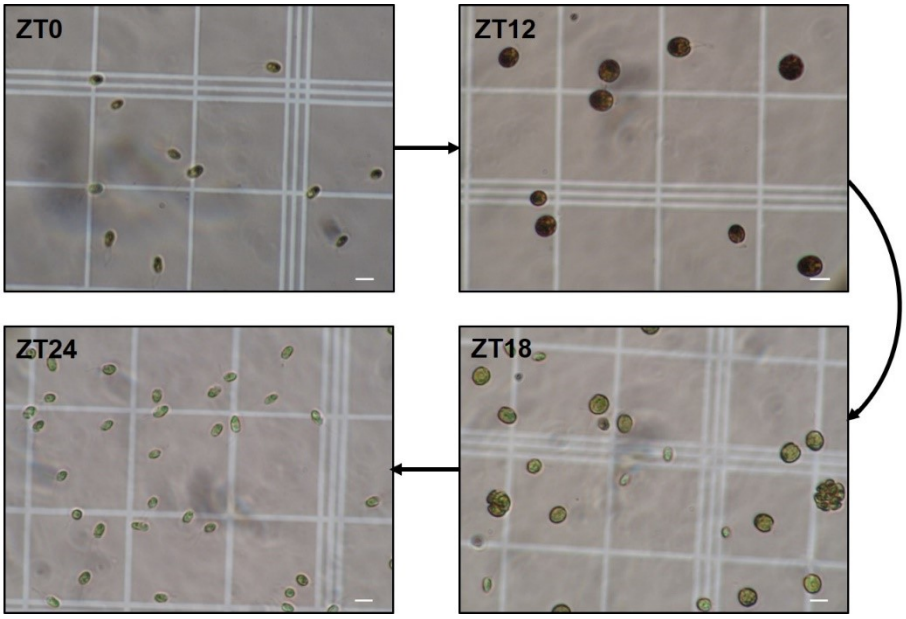

Figure 8. Qualitative verification of diurnally-entrained cells
Light microscope images of synchronized cells entrained under a 24-hour light/dark cycle. Scale bar is 10 µm, indicating comparative change in cell size.
*All work conducted by Melissa V.P.

begin division: darker green color, relatively immobile, a larger size, and a rounded shape. This change in cell shape and size is one diurnally-entrained marker of synchrony. Another hallmark of synchrony is denoted by the characteristics of cells preparing for division, where the noticeable qualitative cellular changes were; the re-absorption of the two flagella resulting in limited cellular movement, and the less-clear internal chloroplast morphology (Figure 8) [3]. These light phase changes in chloroplast morphology are accompanied by the intra-chloroplastic accumulation of starch for use as an energy source during the dark phase [20]. Upon entering the dark phase these diurnally-entrained cells begin dividing by multiple fission which must be completed before the beginning of the next 24-hour cycle [3], [55].

Another marker of synchrony is the timing of division, where the expected mid-dark phase divisional timing was confirmed within our diurnally-entrained cultures (Figure 8). The presence of dividing cells and newly released progeny at ZT18 denotes that cells began this divisional process during the early-to-mid dark phase (Figure 8). Moreover, by the end of this dark phase (ZT24) a large majority of cells had completed division and thus were newly released progeny (Figure 8). Therefore, our diurnally-entrained cells displayed the expected dark phase coordination of division and the required completion of this process before the subsequent light phase. Lastly, the final marker of synchrony was the rapid and large increase in culture density.

The increase in culture density was qualitatively suggested by the light microscope images and was quantitatively confirmed through counting (Figure 8 and 9A). Comparison of the ZT0 and the ZT24 light microscope images revealed a visible augmentation in cell number and hence cell density during the 24-hour light/dark cycle (Figure 8). This cell density increase began after ZT16 which supports the commencement of division during early-to-mid dark phase (Figure 9A). Moreover, the surge in diurnal cell density between ZT16 and ZT24 temporally coincided with the previously observed cell division within the ZT18 cell population image (Figure 8 and 9A). Therefore, this rapid 7-fold dark-phase increase in cell density confirms the final marker of synchrony within our diurnally-entrained cells. Having numerically supported this hallmark of synchrony we sought to do the same for the other qualitative observations covered previously.

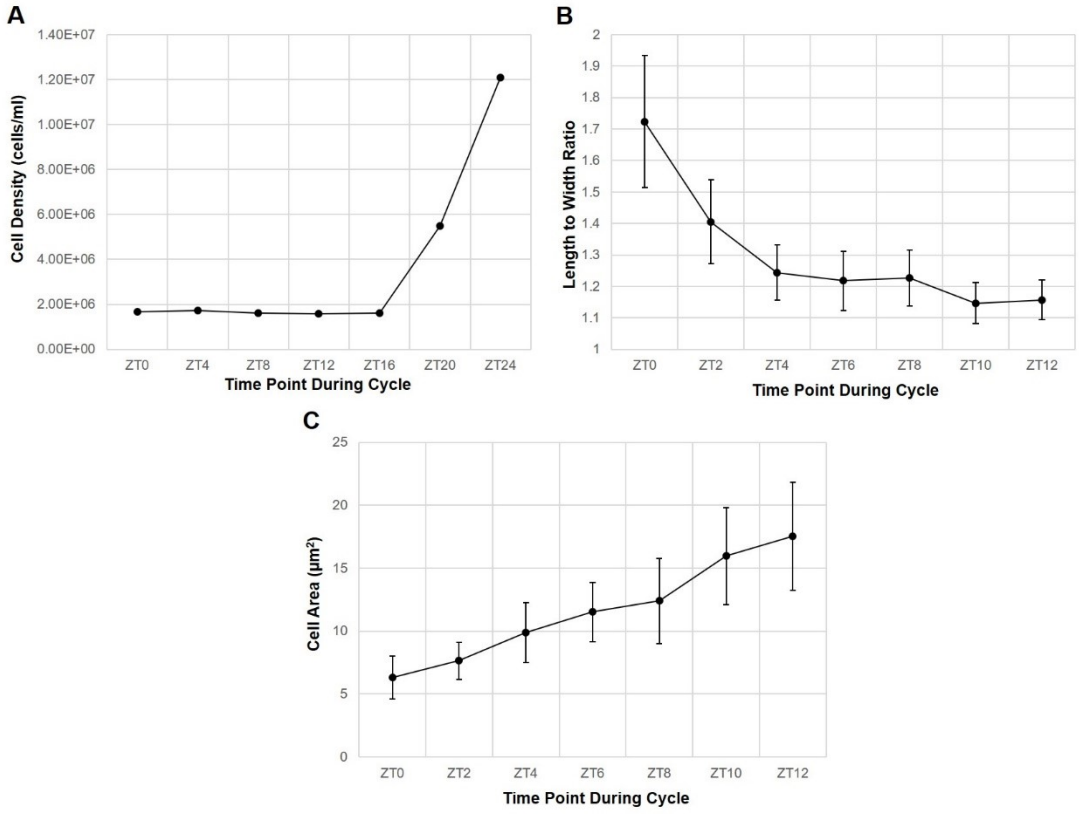

Figure 9. Quantitative verification of diurnally-entrained cells

(A) Cell density (cells/mL) counted over the 24-hour cycle.

(B) Calculated length to width ratio based on manual measurements of light microscope images. Sample sizes of cells: ZT0 (n=58), ZT2 (n=52), ZT4 (n=50), ZT6 (n=68), ZT8 (n=69), ZT10 (n=59), ZT12 (n=63).

(C) Cell area, calculated through use of a Fiji macro and light microscope images. Sample sizes of cells: ZT0 (n=60), ZT2 (n=51), ZT4 (n=50), ZT6 (n=67), ZT8 (n=68), ZT10 (n=58), ZT12 (n=65).

* All work conducted by Melissa V.P.

Imaged cells were electronically measured thus their cell size increase throughout the 12-hour light phase was numerically quantified (Figure 9B, 9C and Supplemental Figure 5). Previous qualitative analysis during the 12-hour light phase reveled a change in cell size and shape, where cells became larger and rounder (Figure 8). Comparison between ZT0 cells and ZT12 cells displayed an increase of average cell length from 7 μm to 10 μm while the average cell width increased from 4 μm to 9 μm (Supplemental Figure 5A). This numerical cell size increase supports the growth of cells from the beginning to the end of the light phase and indicates a change in cell shape as suggested by the 1.4-fold increase in cell length as compared to the 2.25-fold increase in cell width. This change in cell shape was supported by the calculated decline in length-to-width ratio and by the increase of an arbitrary Fiji parameter called ‘roundness’ (Figure 9B and

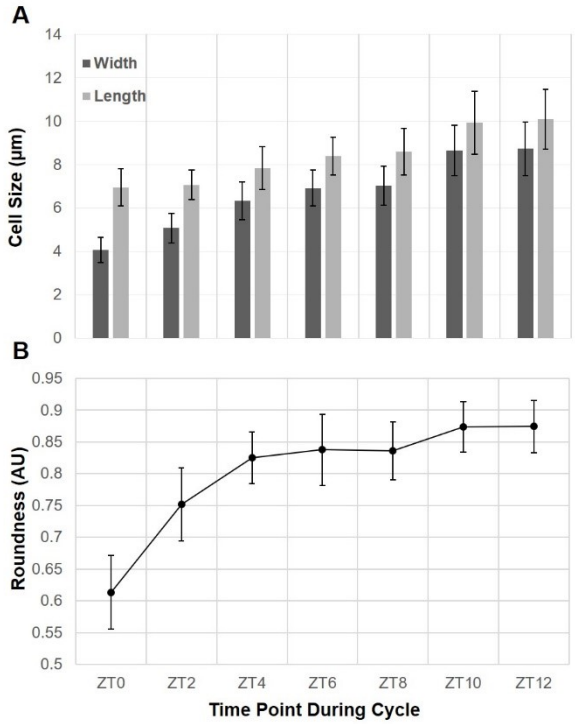

Supplemental Figure 5. Additional quantitative verification of diurnally-entrained cells
(A) Average length and width of cells per 2-hour ZT time point, derived through manual measurements of light microscope images. Sample sizes of cells: ZT0 (n=58), ZT2 (n=52), ZT4 (n=50), ZT6 (n=68), ZT8 (n=69), ZT10 (n=59), ZT12 (n=63).
(B) Fiji calculated roundness of cells per 2-hour ZT time point, derived through light microscope images. Sample sizes of cells: ZT0 (n=60), ZT2 (n=51), ZT4 (n=50), ZT6 (n=67), ZT8 (n=68), ZT10 (n=58), ZT12 (n=65).
* All work conducted by Melissa V.P.

Supplemental Figure 5B). Lastly, cell size increase was further confirmed using calculated cell area. The comparison of the cell area between ZT0 and ZT12 cells denoted an increase from 7 μm^2 to 18 μm^2 (Figure 9C). These quantitative analyses confirm that our diurnally-entrained cells are changing in cell size, cell shape, and cell area satisfying more markers of culture synchrony.

In summary, our synchronized cell system reproducibly generates diurnally-entrained algal cultures which demonstrate all expected markers of synchrony. Qualitative visual analyses supported these known hallmarks of diurnally-entrained cells and quantitative measurements confirmed these observed changes in cell size, cell shape, and divisional timing. Most importantly, these results have shown that our diurnally-entrained cultures are equivalent to those grown within more sophisticated apparatuses and thus they are suitable for subsequent experimental use.

3.22 Characterization of the diurnally-entrained model system for chloroplast growth and division:

Diurnally-entrained cells eliminate all previous issues seen within the asynchronous mature cultures of Uniacke and Zerges, 2007. The use synchronized cultures temporally coordinates cell-cycle events leading to a more homogenous *in situ* localization. Moreover, these diurnally-entrained cultures provide coordinated growth and thylakoid membrane biogenesis during the light phase which was supported by an increase in mRNA expression for PET chain related components and a simultaneous surge in thylakoid ribosome loading [3], [68]. Having verified the synchrony of this model system for mature cell growth and division we subsequently characterized the protein accumulation trends as was done previously for *y-1* chloroplast differentiation.

Diurnally-entrained cells displayed a temporal patterning of protein accumulation for the PET chain complex markers and chloroplastic ribosomes (Figure 10A). The temporal

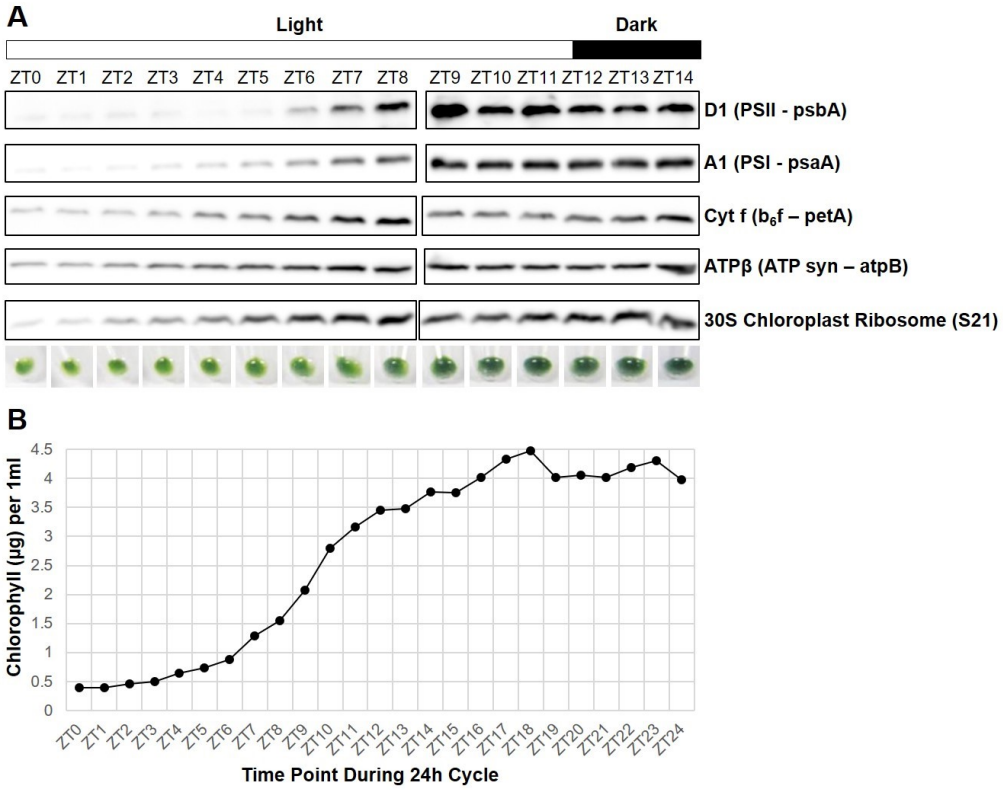

Figure 10. Characterization of protein and chlorophyll content of diurnally-entrained cells
(A) Immunoblot analysis of marker proteins for: the PSI complex (D1), the PSII complex (A1 or PsaA), the cytochrome b_6f complex (Cyt f), the ATP synthase complex, and the small chloroplastic ribosome subunit. Cell pellet images under the immunoblot demonstrate color and size change.
(B) Chlorophyll accumulation in µg for 1ml of culture versus time points in ZT hours
*Dr. Yi Sun contributed to this figure by producing the protein blot analysis and 50% to the pellet collection.
The other 50% of pellet collection, chlorophyll extraction and most of the figure making were conducted by Melissa V.P.

accumulation of these protein markers was classified into two groups: those beginning at the start of the light phase or those displaying a variable time lag with later light phase accumulation.

Protein markers displaying a steady accumulation represented the cytochrome b_6f complex, the ATP synthase complex, and the chloroplastic ribosomes (Figure 10A). The two PET chain complexes had clearly detectable amounts of protein at the start of the light phase and built-up steadily in quantity throughout much of the light phase. From these three protein markers, the ATP synthase complex marker displayed the most rapid protein increase which appeared to peak at ZT9 then stay relatively constant. Alternatively, the cytochrome b_6f complex marker displayed a slower protein accumulation trend which seemed to be staggered by 1-2 hours as best displayed within the early light phase time points where the ATP synthase complex marker begins to rapidly accumulate as of ZT2/ZT3 while the cytochrome b_6f complex marker only starts its rapid accumulation as of ZT3/ZT4 (Figure 10A). Meanwhile, the chloroplastic ribosomal marker had a lower initial protein quantity at the beginning of the light phase but exhibited a more consistent and non-staggered protein accumulation. Lastly, the cytochrome b_6f complex marker and the chloroplastic ribosomal marker decreased in protein quantity prior to the dark phase at ZT9-ZT1, indicating potential light-independent oscillations which will be discussed later (Section 3.4). Therefore, a temporal regulation and ordering of these different protein markers appears to exist.

The remaining PET chain photosystems markers accumulated after a time-dependent lag (Figure 10A). The PSI and PSII protein markers exhibited a much lower protein content at the beginning of the light phase and displayed a 4-to-6-hour lag in protein accumulation. PSI protein marker accumulation began at ZT4 while the PSII protein marker accumulation only commenced at ZT6. However, once this lag in protein accumulation was overcome both photosystems underwent a much more dramatic and rapid protein build-up then any of the other PET chain complexes. Additionally, these photosystem protein markers also exhibited more subtle indications of protein content oscillations at ZT12 – ZT13.

When combined, these data reveal the temporal ordering of PET chain protein build-up. The ATP synthesizing complex of photosynthesis is accumulated first which is followed by the cytochrome b_6f complex that serves as an intermediate between both photosystems. The final complexes to be accumulated are the photosystems with PSI being built-up first followed by PSII. This temporal protein accumulation ensures that PET chain complexes are assembled in a certain

order where this sequence of complex assembly hints at a protective roll against ROS production because potential ROS producing complexes are made last while ROS protecting complexes are made first. This temporal staggering of PET chain complex biogenesis was previously seen for the RNA abundance peaks of the PET chain related genes, which were ordered in the same manner as the accumulation of protein markers above [3], [56]. This temporal patterning of protein accumulation is not due to mRNA expression because most genes are fully expressed by late dark phase or early light phase [3], [56]. Nor was this temporal ordering caused by protein synthesis rates because the translation rates of these PET chain complexes do not reflect the protein accumulation patterns denoted above (data not shown). The results discussed above and previous findings indicate a potential role for post-translational PET chain complex management in the form of assembly, stabilization or degradation of unassembled subunits [47], [63], [69].

Similarly, chlorophyll build-up coincided with the temporal accumulation of PSI and PSII protein markers (Figure 10B). This photosystem-associated light-harvesting pigment did not rapidly increase in quantity prior to ZT4 which is also displayed by the consistent light-green pellet color and coincided with the lag phase of the PSI protein marker (Figure 10A). The rate of chlorophyll accumulation from ZT6-to-ZT12 increased when compared to the rate from ZT4-to-ZT6 which temporally corresponded to the accumulation of the PSII protein marker in addition to the already accumulating PSI protein marker. This increase in chlorophyll accumulation rate was also indicated by the greener pellet coloration and by the larger size of the pellet, implying chloroplastic growth thus thylakoid membrane production. Moreover, chlorophyll quantity also displayed temporal oscillations during the late dark phase which temporally coincided with dark phase protein marker accumulation findings discussed later (Section 3.4). The correlation of photosystem protein accumulation and chlorophyll accumulation supports the concept of cellular ROS protection through the use of temporally delayed photosystem and LHC assembly until other PET chain complexes are made [3], [47]. This temporally regulated accumulation of chlorophyll provoked the investigation into the potential temporal ordering of chlorophyll intermediates.

The extraction of chlorophyll intermediates displayed some temporal organization potentially for the prevention of deleterious ROS side-reactions (Supplemental Figure 6). Fluorescence of ZT0 chlorophyll intermediates displayed low quantities of all molecules which could be a strategy to avoid the known photodynamic damage caused by these unbound

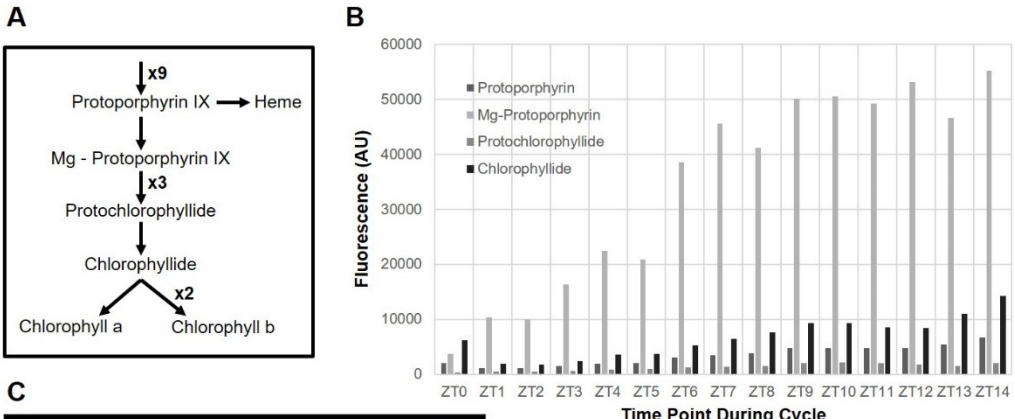

C

Precursor Molecule	Excitation (nm)	Emission (nm)
Protoporphyrin IX	400	632
Mg – Protoporphyrin IX	420	595
Protochlorophyllide	440	633
Chlorophyllide	440	672

Supplemental Figure 6. Fluorescence of chlorophyll precursors for diurnally-entrained cells
(A) Chlorophyll biosynthesis pathway denoting the order chlorophyll precursors measured in B.
(B) Relative fluorescence of chlorophyll precursors measured during the ZT0 to ZT14 time points.
(C) Emission and excitation wavelengths for each chlorophyll precursor measured.
*Dr. Yi Sun contributed 50% towards pellet collection.
The other 50% of pellet collection, extraction, measurement, analysis, and figure making provided by Melissa V.P.

intermediates upon light exposure [47]. During the remining light phase these chlorophyll intermediates accumulated at differing degrees (Supplemental Figure 6B). Lower accumulation of certain precursors could be caused by their various roles such as directly triggering toxic ROS formation or acting as signaling molecules which modulate upstream transcriptional and translational events [70]. Alternatively, the rapid accumulation of the Mg-protoporphyrin intermediate might be connected to its dual utilization within the chlorophyll synthesis pathway and the Heme production pathway [70]. Moreover, most chlorophyll intermediates displayed slight oscillations throughout the light phase.

These observed oscillations within PET protein accumulation trends, chlorophyll quantity, and relative chlorophyll precursors fluorescence reveals the potential control of these events by an 'internally regulated clock' or circadian rhythm. Oscillations were documented during the light phase despite the provided light energy and during the dark phase in anticipation of the subsequent light phase. The control of cellular molecules and events by a master clock is a controversial subject which continues to be investigated, therefore it will be discussed in Section 3.4 [52].

When summarized, this characterization of diurnally-entrained cells uncovered novel temporally regulated protein and chlorophyll accumulation patterns. These accumulation trends coupled with recent findings support the temporal ordering of PET chain biogenesis as a biological organization strategy to avoid the toxicity and damage caused by ROS [3], [47]. Moreover, these findings displayed light phase and dark phase oscillations which warrant the potential investigation of circadian clock control. Furthermore, these diurnal findings revealed the unexpected rapid accumulation of both PSI and PSII protein markers as well as an 86% increase in chlorophyll content during the diurnal light phase. This photosystem-specific rapid increase in protein content coupled with the rapid accumulation of chlorophyll, is reminiscent of the previously documented *y-1* chloroplast differentiation findings. Therefore, diurnally-entrained cells revealed a novel chloroplast differentiation-like behavior which indicates their potential *in situ* T-zone enrichment.

3.23 Temporal changes in T-zone localized PSII subunit translation markers during diurnally-entrained chloroplast growth and division

Surprisingly, characterization of the algal model system for mature chloroplast growth and division displayed PET chain complex accumulation trends reminiscent of *y-1* greening. These similarities in characterization indicate that the photosystems are undergoing biogenesis and are probably T-zone enriched, while the ATP synthase complex is undergoing much less biogenesis and is probably in a non-localized pattern representing the overall mature chloroplast thylakoid membrane arrangement. *In situ* fluorescence microscopy localization studies were conducted as previously presented for *y-1* greening. We hypothesized that this differentiation-like behaviour of diurnally-entrained chloroplasts would cause a spatial-temporal regulation for T-zone enrichment of PSII subunit translation markers, PSII subunit accumulation, and chlorophyll accumulation.

A majority of ZT0 cells displayed T-zone localized PSII subunit translation markers (Figure 11). Due to their mature chloroplasts and when compared to *y-1* greening time points, diurnally-entrained cells appeared to display increased distribution of the chloroplastic ribosomes and the *psbA* message into the chloroplast lobes (Figure 11 vs. Figure 3). Despite this chloroplastic dispersal, these PSII subunit translation markers showed T-zone enrichment in 89% of ZT0 cells (Figure 11 yellow arrow). Most ZT0 cells displayed a T-zone sub-pattern which had one or both lobe-junction foci often connected to the chloroplastic region anterior to the pyrenoid

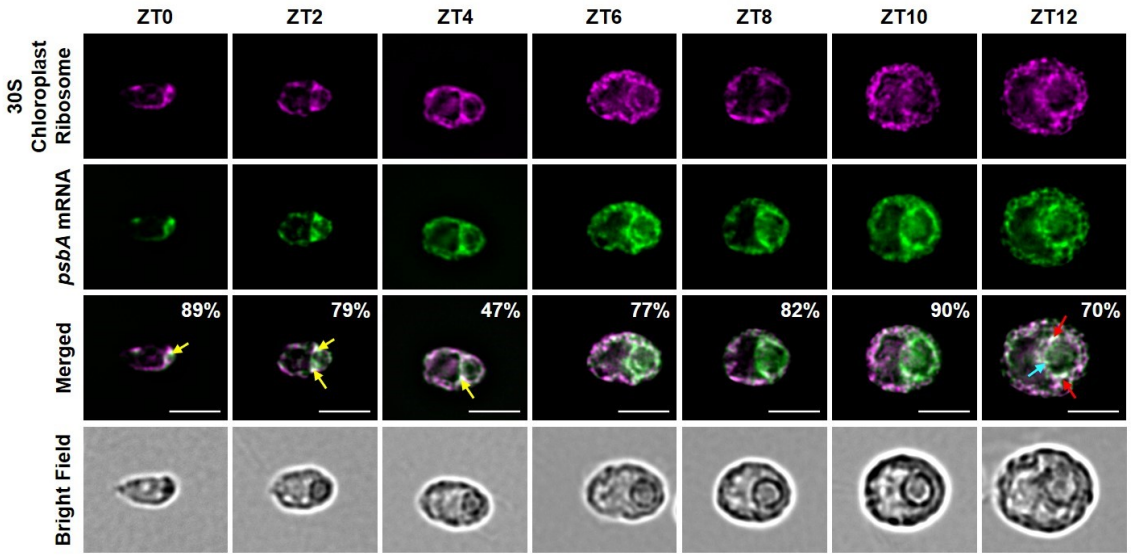

Figure 11. *In situ* localization of markers for PSII subunit translation during the light phase of diurnally-entrained cells

Immunofluorescence staining of the chloroplastic small (30S) ribosomal subunit coupled with fluorescence *in situ* hybridization of the PSII-specific *psbA* message. Merged channels indicate overlapping areas between both markers (white), T zone = yellow arrows, discontinuous ring-like pattern = red arrows, pyrenoid infiltrating strings = blue arrow. Bright field provides the cellular orientation. Percentages of the given pattern are displayed. The scale bar is 5 µm. Sample sizes of cells: ZT0 (n=27), ZT2 (n=28), ZT4 (n=45), ZT6 (n=78), ZT8 (n=44), ZT10 (n=41), ZT12 (n=20).
*All work conducted by Melissa V.P.

(Supplemental Figure 2A and 2B). However, the T-zone subcellular resolution appeared condensed within these ZT0 cells due to their small and oblong cellular morphology as indicated by the barely visible chloroplastic pyrenoid within the bright field channel (e.g. Figure 11). Therefore, this T-zone localization within ZT0 cells was verified using the unbiased CH analysis.

CH analysis of ZT0 diurnally-entrained cells confirmed the T-zone enrichment of PSII subunit translation markers (Figure 12A and B). Despite the small morphology of ZT0 cells PSII subunit translation markers had prominent T-zone overlap as displayed by the yellow coloration within the average compiled cell (Figure 12A). Moreover, the graphical analysis of this compiled cell image clearly demonstrates the T-zone enrichment of chloroplastic ribosomes and the *psbA* message within this average ZT0 chloroplast (Figure 12B black arrows). Therefore, this unbiased cell analysis supported the T-zone enrichment of PSII subunit translation markers within these small ZT0 chloroplasts, indicating the requirement of localized PSII biogenesis during the dark-to-light transition of these diurnally-entrained cells. Temporal regulation of these T-zone localized PSII subunit translation markers was subsequently investigated throughout the light phase.

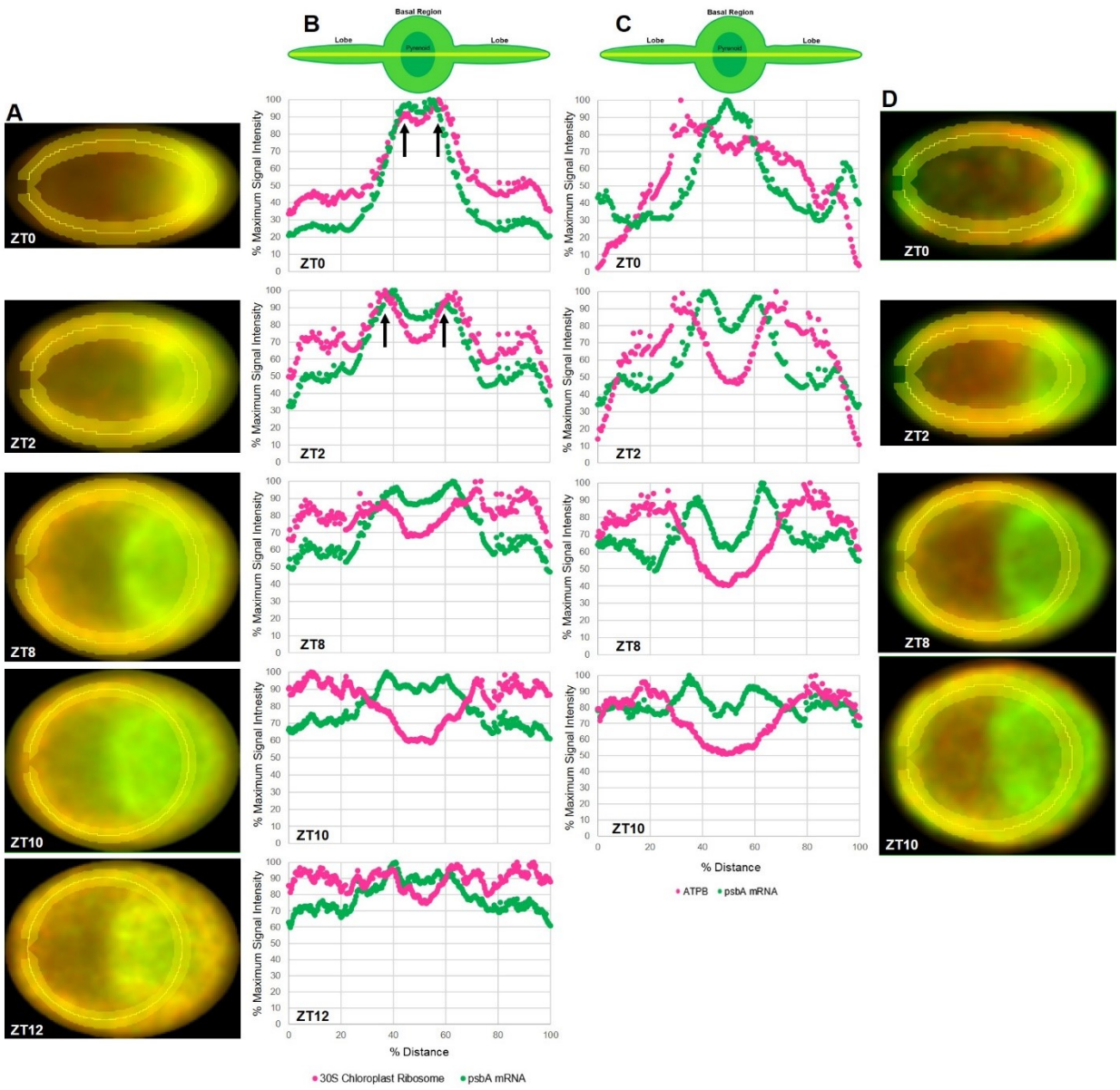

Figure 12. Cell harvester analysis for PSII subunit translation markers and the thylakoid marking ATP synthase complex during the light phase of diurnally-entrained cells

(A) Average compiled cells for the chloroplastic small (30S) ribosomal subunit and PSII-specific *psbA* message. Sample sizes of cells: ZT0 (n=27), ZT2 (n=28), ZT8 (n=44), ZT10 (n=41), ZT12 (n=20).

(B) Percent of Maximum Intensity vs Percent of Distance graphs for the images displayed in panel A. T-zone foci are denoted by the black arrows. Straightened chloroplast denoted above graphs for positioning reference (pyrenoid center = 50%)

(C) Average compiled cells for the ATP Synthase β subunit and PSII-specific *psbA* message. Sample sizes of cells: ZT0 (n=22), ZT2 (n=65), ZT8 (n=52), ZT10 (n=59).

(D) Percent of Maximum Intensity vs Percent of Distance graphs for the images displayed in panel C Straightened chloroplast denoted above graphs for positioning reference (pyrenoid center = 50%)

*All work conducted by Melissa V.P.

Similarly, ZT2 cells also depicted T-zone enriched PSII subunit translation markers within 79% of cells (Figure 11). The subcellular resolution this T-zone band-like sub-pattern was improved within these ZT2 cells because of the increase in cell size when compared to the ZT0 cells (Figure 11 ZT0 vs. ZT2). Moreover, these *in situ* ZT2 images exhibited the dispersal of the chloroplastic ribosomes and *psbA* message further into the chloroplast lobes of these growing diurnally-entrained cells. Additionally, chloroplast stress granules (cpSGs) were seen within 25% of ZT2 cells; where cpSG's are localized to stromal pockets along pyrenoid perimeter and contain the oxidative stress targeted *psbA* message coupled with the small chloroplastic ribosomal subunit (Figure 11 and Supplemental Figure 2C, 2D) [71]. Therefore, ZT2 cells exhibited the dispersion of both markers into the chloroplast lobes but still required T-zone enriched PSII subunit translation markers during this early diurnal chloroplast growth.

The unbiased ZT2 analysis supported T-zone enriched PSII subunit translation markers and displayed the dispersal of these markers further into the chloroplast lobes (Figure 12A and B). T-zone specific enrichment of PSII subunit translation markers was represented by the yellow coloration within the average ZT2 compiled cell and by the overlap of strong intensity signal for both markers within the representative graph (Figure 12A and 12B black arrows). Moreover, the temporal dispersion of both markers was denoted by the increase in signal intensity within the chloroplast lobes when compared to the previous ZT0 cells (Figure 12B ZT0 vs. ZT2). Therefore, CH analysis of ZT2 diurnally-entrained cells supports the T-zone enrichment of PSII subunit translation markers and confirms the spreading of these markers further into the chloroplast lobes.

In situ analysis of ZT4 cells revealed that less than half of cells displayed T-zone enriched PSII subunit translation markers (Figure 11 yellow arrows). The continued dispersal of the chloroplastic ribosomes into the lobes caused a non-localized distribution as seen within 53% of cells. Similarly, the *psbA* message also displayed a slight dispersal into the lobes but remained basally enriched (Figure 11). Furthermore, approximately 50% of ZT4 cells displayed the presence of cpSGs (Supplemental Figure 2C). This dissipation of T-zone localized PSII subunit translation markers into a non-localized distribution is reminiscent of the *y-1* greening findings where this temporal *in situ* localization shift corresponded with a switch from PSII biogenesis for thylakoid assembly into PSII biogenesis for repair of the complex coupled with the chloroplastic translation of other proteins (Figure 3). This diurnal temporal shift into PSII complex repair which is triggered

by light induced oxidative stress, was supported by the frequent cpSGs within these ZT4 diurnally-entrained cells (Supplemental Figure 2C) [71], [72].

Similarly, subsequent diurnal time points ZT6, ZT8, and ZT10 also displayed non-localized PSII subunit translation markers (Figure 11). During these later light phase time points diurnal cells exhibited the progressive dispersal of the chloroplastic ribosomes into the lobes which depleted the basal chloroplastic regions by ZT8 (Figure 11). This non-localized distribution of PSII subunit translation markers was seen in 77%, 82% and 90% of cells for the ZT6, the ZT8 and the ZT10 time points, respectively. Moreover, cpSGs were observed within 55%, 65%, and approximately 70% of diurnally-entrained cells for the ZT6, the ZT8 and the ZT10 time points, respectively (Supplemental Figure 2C). Additionally, synthesis of the PSII core protein D1 increased at ZT8 while the other PSII core proteins did not display this synthesis increase (data not shown). Therefore, this late light phase temporal loss of T-zone enriched PSII subunit translation markers coupled with frequent cpSGs and the ZT8 surge in D1 translation all support a chloroplastic shift from rapid coordinated thylakoid biogenesis into PSII repair united with the translation of other non-localized chloroplast proteins [2], [65], [71].

Using the CH, this non-localized distribution for the PSII subunit translation markers was confirmed for ZT8 and ZT10 cells (Figure 12A and B). The average compiled cells for these time points displayed separated red and green respective marker colors, thus they did not overlap within the T-zone (Figure 12A). This non-enriched distribution of PSII subunit translation markers was also exhibited within the graph, where the *psbA* message remained slightly T-zone localized but the chloroplastic ribosomes were evenly dispersed (Figure 12B). Moreover, these graphs also displayed decreasing chloroplastic ribosomal signal intensity within the lobe junction regions which supported the basal chloroplastic depletion seen within the *in situ* findings (Figure 12B). Therefore, most later light phase time points displayed the non-localized distribution of PSII subunit translation markers as seen *in situ* and verified using the unbiased CH analysis.

Contrastingly, ZT12 diurnally-entrained cells displayed PSII subunit translation markers re-localized within the chloroplastic basal region as a discontinuous ring-like pattern (Figure 11 red arrows). This discontinuous ring-like overlap of the chloroplastic ribosomes and *psbA* message was found within 70% of cells and was not equivalent to the T-zone pattern because it did not discreetly localize into lobe-junction foci, instead it appeared as dispersed patches around the

pyrenoid coupled with strings of signal entering the pyrenoid (Figure 11 red and blue arrows). These pyrenoid infiltrating strings of overlapped chloroplastic ribosomes and the *psbA* message were often nearby cpSGs, where 80% of ZT12 cells displayed cpSGs (Figure 11 and Supplemental Figure 2C). This ZT12 localization likely does not represent PSII subunit translation for thylakoid biogenesis as denoted by the non-localized distribution of these markers for 7-8 hours before ZT12, the string-like signal entering the pyrenoid, the frequent stress granules, and the appearance of this pattern only at the end of the diurnal light phase (Figure 11 and Supplemental Figure 2C). Alternatively, this differing ZT12 overlapping localization for the small chloroplastic ribosomal subunit and the *psbA* message could be related to cpSG formation because of its proximity to cpSGs within the pyrenoid, as discussed later in section 3.4 [71].

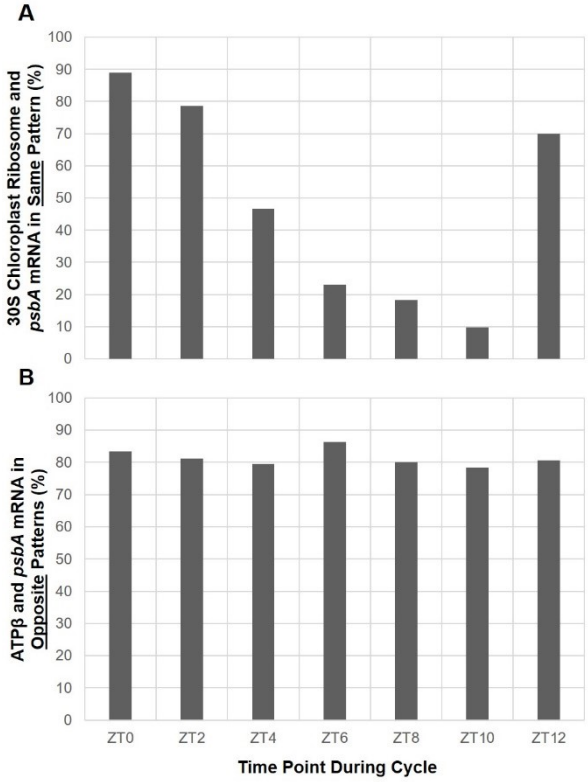

Supplemental Figure 7. Graphs for the visual analysis of *in situ* localization patterns for PSII subunit translation markers and a thylakoid marker during the light phase of diurnally-entrained cells

(A) Percentages of visually scored cells that display T-zone localized of both the small (30S) ribosomal subunit and the PSII-specific *psbA* message. Sample sizes of cells: ZT0 (n=27), ZT2 (n=28), ZT4 (n=45), ZT6 (n=78), ZT8 (n=44), ZT10 (n=41), ZT12 (n= 20).

(B) Percentages of visually scored cells that do NOT display T-zone localization of both the ATP synthase β subunit and the PSII-specific *psbA* message. Sample sizes of cells: ZT0 (n=18), ZT2 (n=64), ZT4 (n=83), ZT6 (n=81), ZT8 (n=55), ZT10 (n=60), ZT12 (n= 36).

*All work conducted by Melissa V.P.

In summary, these diurnal *in situ* findings resemble the results seen during *y-1* greening and together they suggest increased chloroplastic differentiation within diurnally-entrained cells, which is unexpected within these green mature chloroplasts. Moreover, the temporally regulated dispersion of PSII subunit translation markers during the diurnal light phase supports the *in situ y-1* greening results, where the temporal loss of chloroplastic T-zone enrichment was associated with a switch from thylakoid biogenesis to thylakoid repair. This change in localization of PSII subunit translation markers was graphically displayed during the diurnal light phase (Supplemental Figure 2A, 2B and 7A). As done previously, T-zone localization was verified to be a form of sub-organellar spatial enrichment and not an alternative distribution of thylakoid membranes by localizing the thylakoid marking ATP synthase complex during the diurnal light phase.

The ATP synthase complex previously represented the *in situ* thylakoid membrane arrangement within greening *y-1* chloroplasts (Figure 5). This non-localized distribution was associated with the non-rapid protein accumulation of this complex, which differed from the accumulation of the photosystem complexes during both *y-1* chloroplast differentiation and diurnally-entrained growth (Figure 2A and 10A). Therefore, we hypothesize that the ATP synthase complex will also have a non-localized distribution within diurnally-entrained chloroplasts.

During the diurnal light phase, the ATP synthase marker displayed a non-localized chloroplastic pattern (Figure 13). The temporally indiscriminate even chloroplastic distribution for this thylakoid marker contrasts the T-zone localized *psbA* message and resembled the non-localized distribution of the chloroplastic ribosomes during the mid-to-late light phase (Figure 13 vs. Figure 11). This differing marker localization was documented within most diurnally-entrained cells which resembles the previous *y-1* greening findings (Figure 5 and 13). This *in situ* distribution of the ATP synthase marker was then verified using the unbiased CH.

CH analysis for this thylakoid marking complex confirmed its temporally unchanging non-localized distribution (Figure 12). The average compiled cells for all diurnal times points displayed no yellow T-zone coloration denoting the lack of T-zone overlap between markers (Figure 12D). Similarly, the graphical representation of these compiled cells also exhibited this lack of T-zone overlap, where the *psbA* message denoted the T-zone and the ATP synthase marker was not

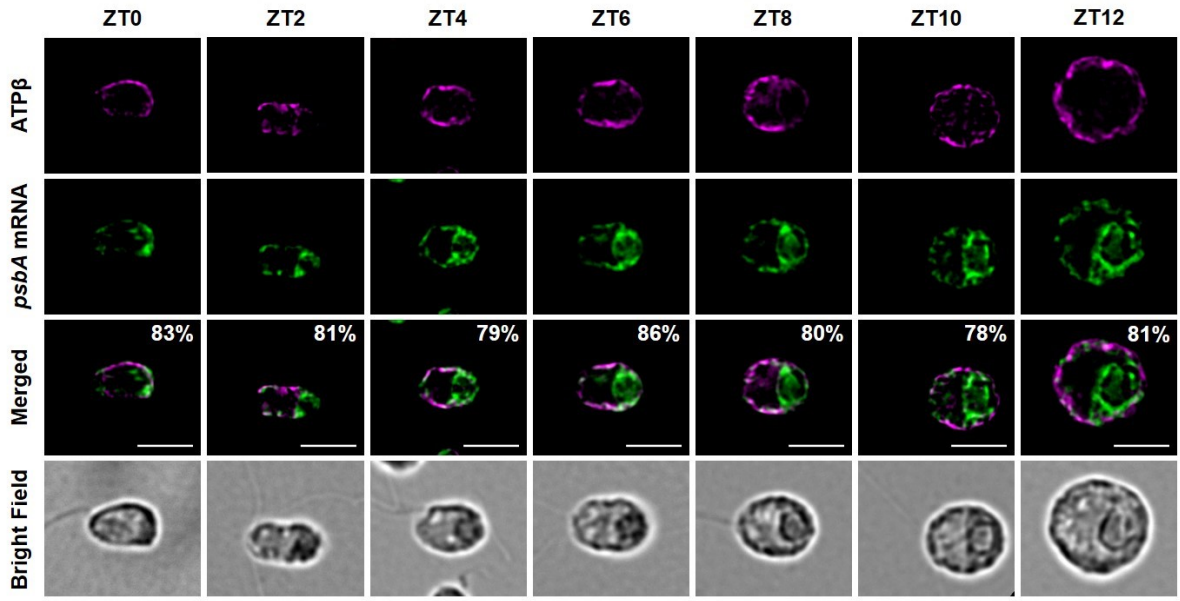

Figure 13. *In situ* localization of an ATP synthase marker versus the PSII-specific *psbA* message during the light phase of diurnally-entrained cells

Immunofluorescence staining of the ATP synthase β subunit coupled with fluorescence *in situ* hybridization of the PSII-specific *psbA* message. Merged channels indicate lack of overlapping white areas between both markers. Bright field provides the cellular orientation. Percentages of the given pattern are displayed. The scale bar is 5 μm. Sample sizes of cells: ZT0 (n=18), ZT2 (n=64), ZT4 (n=83), ZT6 (n=81), ZT8 (n=55), ZT10 (n=60), ZT12 (n=36).

* Dr. Yi Sun contributed 50% towards making the slides. Imaging, analysis, deconvolution, and figure making conducted by Melissa V.P.

spatially enriched within the chloroplast of diurnally-entrained cells (Figure 12C). This unbiased analysis supports the spatially and temporally consistent even chloroplastic distribution of this thylakoid marking complex, which was also represented graphically (Supplemental Figure 7B).

In summary, the unchanging spatial-temporal distribution of the ATP synthase marker within diurnally-entrained cells reflects the previous *y-1* greening findings, supporting the uniform chloroplastic distribution of thylakoid membranes within both model systems. Additionally, the correlation between protein accumulation trends and their *in situ* localization has revealed T-zone-specific enrichment only for PET chain complexes undergoing rapid biogenesis. These diurnal *in situ* findings reinforce the proposed T-zone model denoting the chloroplastic organization of *de novo* photosystem biogenesis and thylakoid membrane assembly (Figure 1B). Moreover, the spatial-temporal resemblance between these diurnally-entrained cell findings and the previous *y-1* chloroplast differentiation results supports the increased chloroplast differentiation capacity of growing diurnal chloroplasts. Indicating that even mature chloroplasts display T-zone localized enrichment for the biogenesis of PET chain complexes, needed to produce thylakoid membranes.

3.24 Spatial-temporal T-zone localization of chlorophyll autofluorescence during diurnally-entrained chloroplast growth and division

During *y-1* greening the novel T-zone specific accumulation of chlorophyll and the bias of chlorophyll autofluorescence within the T-zone of green *y-1* cells supported the model of T-zone organized photosystem biogenesis and assembly (Figure 1B and Figure 6). Thus far the characterization and the *in situ* localization of PET chain complexes within diurnally-entrained cells has mirrored the findings obtained during *y-1* greening. Therefore, we hypothesize that chlorophyll accumulation throughout the diurnal light phase will also be T-zone enriched.

ZT0 diurnally-entrained cells contained 14% of chlorophyll quantity when compared to the grown ZT12 cells and double the percentage found within dark-grown *y-1* cells (Figure 10B vs. 2B). Due to this larger chlorophyll quantity ZT0 chloroplast thylakoids should display a relatively higher chlorophyll autofluorescence than the dark-grown *y-1* cells. However, the rapid 86% increase in chlorophyll throughout the diurnal light phase indicates that this pigment is undergoing biogenesis and thus should accumulate *in situ* (Figure 10B). These newly produced unassembled chlorophyll pigments display a stronger autofluorescence when compared to their LHC assembled counterparts which are fluorescently quenched [22], [47]. Therefore, newly synthesized and accumulated unassembled chlorophyll will display stronger intensity autofluorescence throughout the light phase, helping to localize its *in situ* spatial enrichment within these growing diurnal cells.

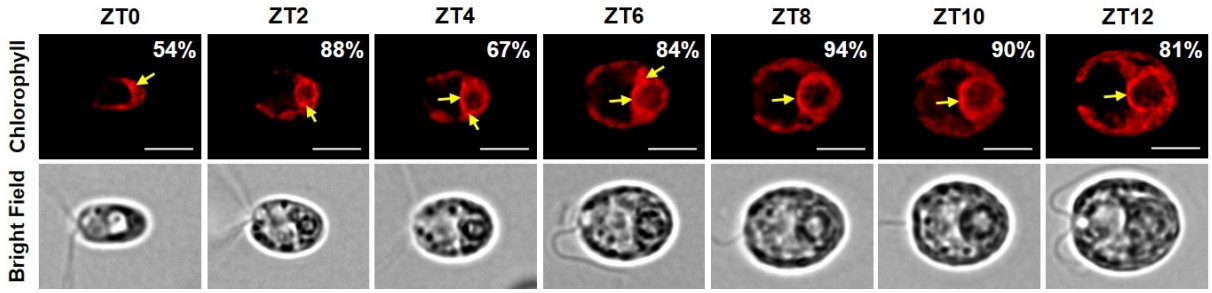

Figure 14. *In situ* localization of Chlorophyll autofluorescence during the light phase of diurnally-entrained cells

Live immobilized synchronized cells of various diurnal light phase time points were visualized for their naturally fluorescent chlorophyll pigment. Chlorophyll autofluorescence is displayed using non-normalized images. T-zone localized enrichment is denoted by the yellow arrows. Bright field provides the cellular orientation. Percentages of the given pattern are displayed. The scale bar is 5 µm. Sample sizes of cells: ZT0 (n=13), ZT2 (n=16), ZT4 (n=15), ZT6 (n=19), ZT8 (n=18), ZT10 (n=19), ZT12 (n=21).

*All work conducted by Melissa V.P.

Chlorophyll throughout the diurnal light phase consistently exhibited a higher autofluorescence specifically within the T-zone (Figure 14). Higher chlorophyll autofluorescence was seen in the band-like T-zone pattern for 54% of ZT0 cells and 88% of ZT2 cells. Additionally, most of these early diurnal light phase cells exhibited little-to-no chlorophyll autofluorescence within one or both chloroplast lobes (Figure 14). Contrastingly, ZT4 cells no longer lacked chlorophyll autofluorescence within the lobes but did display a transient decrease in T-zone enriched chlorophyll autofluorescence as seen within 67% of cells. Moreover, ZT4 cells and all subsequent diurnal light phase time points displayed a stronger chlorophyll autofluorescence within the chloroplastic area anterior to the pyrenoid (Figure 14). This necklace-like T-zone pattern was documented within 84%, 94%, 90%, and 81% of diurnally-entrained cells for the ZT6, the ZT8, the ZT10, and the ZT12 time points, respectively. Quantification of this stronger T-zone localized chlorophyll autofluorescence when compared to other chloroplastic regions was conducted during the light phase, as verification of this T-zone enriched chlorophyll accumulation.

Even when quantified, the average chlorophyll autofluorescence intensity was stronger within the T-zone for all light phase time points (Supplemental Figure 8). The production and accumulation of chlorophyll was displayed by the increase in chlorophyll quantity and autofluorescence within the chloroplasts of diurnal light phase cells (Figure 10B, 14 and Supplemental Figure 8A). Despite the overall increase in chlorophyll, diurnally-entrained cells maintained a quantifiably stronger difference in chlorophyll autofluorescence between the T-zone and the chloroplast lobes during the light phase (Supplemental Figure 8A). Most diurnal light phase time points displayed a numerically consistent chlorophyll autofluorescence difference between the T-zone and the lobes except for ZT2 which displayed a 27% higher T-zone difference (Supplemental Figure 8B). This diurnal time point temporally coincided with the clearest T-zone enrichment of PSII subunit translation markers (Figure 11).

In summary, these quantifiable *in situ* chlorophyll autofluorescence findings support the accumulation of newly synthesized un-quenched chlorophyll within the T-zone of growing diurnally-entrained cells. This stronger intensity chlorophyll autofluorescence within the T-zone was displayed throughout the diurnal light phase but also exhibited temporal fluctuations that corresponded within T-zone localized PSII biogenesis. These temporally coordinated multi-

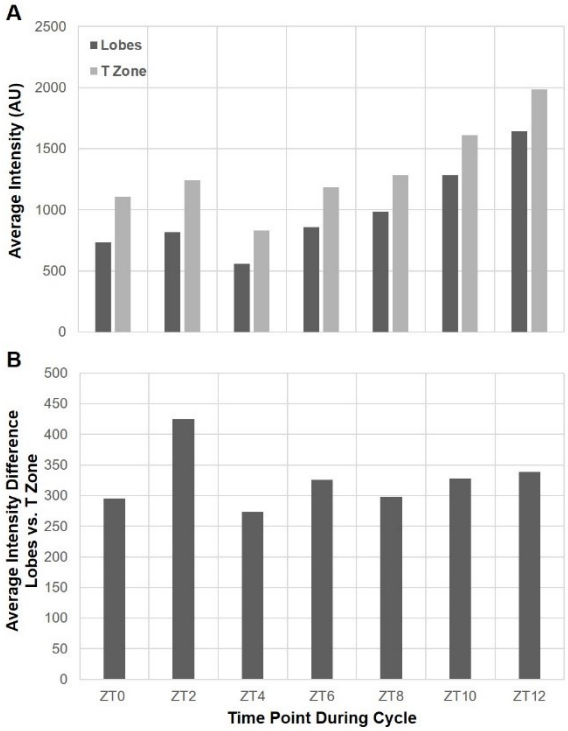

Supplemental Figure 8. Graphs for the quantified *in situ* T-zone enrichment of chlorophyll autofluorescence during the light phase of diurnally-entrained cell

Average *in situ* chlorophyll autofluorescence intensity was Fiji quantified within different regions of the algal chloroplast during the diurnal light phase.

(A) Average chlorophyll autofluorescence intensity within both chloroplast lobes and the T-zone independently. Sample sizes of cells: ZT0 (n=13), ZT2 (n=16), ZT4 (n=15), ZT6 (n=19), ZT8 (n=18), ZT10 (n=19), ZT12 (n= 21).

(B) Average chlorophyll autofluorescence intensity difference between the chloroplast lobes and the T-zone. Sample sizes of cells: ZT0 (n=13), ZT2 (n=16), ZT4 (n=15), ZT6 (n=19), ZT8 (n=18), ZT10 (n=19), ZT12 (n= 21).

*All work conducted by Melissa V.P.

component T-zone localized events further support the T-zone model and demonstrate the occurrence of chloroplast differentiation within these growing mature chloroplasts (Figure 1B).

3.25 Spatial-temporal T-zone localization of PSII-specific protein marker accumulation during diurnally-entrained chloroplast growth and division

The use core subunits as *in situ* markers for their respective complex is possible due to the strong post-translational control of PET chain complex regulation, assembly, and degradation [63], [69]. The spatial-temporal localization of these complex-specific protein markers was tested during *y-1* greening, where they were initially accumulated at their synthesis site and later migrated into their final chloroplastic destination. Given the similar findings between the *y-1* chloroplast

differentiation model and the diurnal model for mature chloroplast growth, we predict the T-zone accumulation of the PSII-specific D1 protein marker during the early diurnal light phase. Moreover, un-assembled and thus highly immunogenic D1 proteins were shown to be T-zone localized within asynchronously growing mature mutant cells [2]. Therefore, PSII-specific protein marker localization within the light phase of diurnally-entrained cells was verified by comparison to the T-zone marking *psbA* message. *In situ* D1 localization results were analyzed using the CH, thus the average compiled cells and their respective graphical representations are displayed.

CH analysis of ZT0 cells displayed T-zone enriched D1 protein marker (Figure 15). The quantity of D1 protein within diurnally-entrained cells is higher then dark-grown *y-1* cells because

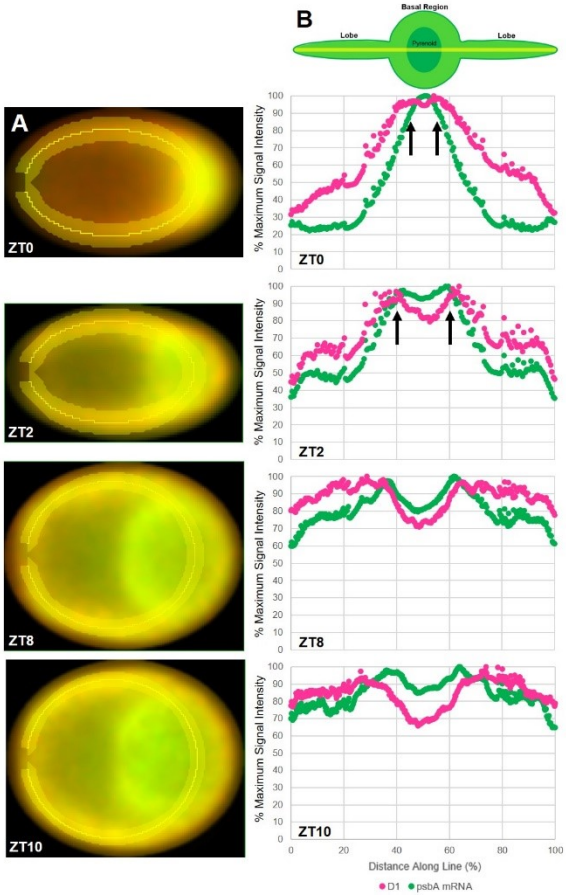

Figure 15. Cell harvester analysis for PSII-specific protein markers during the light phase of diurnally-entrained cells

(A) Average compiled cells for the PSII core protein D1 and the PSII *psbA* message.
Sample sizes of cells: ZT0 (n=153), ZT2 (n=141), ZT8 (n=142), ZT10 (n=103)
(B) Percent of Maximum Intensity vs Percent of Distance graphs for the images displayed in panel A. T-zone foci are denoted by the black arrows and the lobe-tip maxima are denoted by red arrows. Straightened chloroplast denoted above graphs for positioning reference (pyrenoid center = 50%)
*All work conducted by Melissa V.P.

of their green and mature chloroplasts, however this ZT0 quantity of the D1 protein-marker is relatively low when compared to the grown ZT12 cells at the end of the light phase (Figure 10A). Therefore, during the diurnal light phase this PSII protein marker is undergoing biogenesis hence its enrichment within the T-zone as displayed by the yellow coloration within the ZT0 average compiled cell (Figure 15A). Similarly, the graphical representation of this ZT0 average compiled cell also displayed T-zone enriched D1 protein-marker, where the strongest intensity D1 signal was overlapped with the *psbA* message which marks the T-zone (Figure 15B black arrows). This T-zone enrichment could represent the localized accumulation of this PSII-specific marker in the same spatial area of its synthesis or the stronger immunogenic nature of the unassembled D1 proteins. In either of these scenarios, the T-zone is a preferential site for D1 protein accumulation and the additional presence of PSII subunit synthesis within this same spatial region supports the T-zone model of photosystem biogenesis for thylakoid membrane production (Figure 1B).

The unbiased analysis of ZT2 cells displayed somewhat T-zone enriched D1 protein marker accumulation (Figure 15). This T-zone accumulation of the D1 protein marker was denoted by the yellow coloration within the average ZT2 compiled cell and within its representative graph which displayed the strongest intensity signals of both markers overlapping within the T-zone (Figure 15A and 15B black arrows). Moreover, the ZT2 graph also exhibited the increased dispersion of the D1 protein marker into the chloroplast lobes (Figure 15B ZT0 vs. ZT2). This migration of the D1 protein marker reflects the final chloroplastic distribution of the assembled PSII complex which is found within all thylakoids. Therefore, this ZT2 CH analysis revealed the T-zone enriched D1 protein marker while also displaying the temporally regulated migration of assembled PSII complexes. These diurnal findings resemble the spatial-temporal localization of the D1 protein marker during *y-1* greening and support the model for T-zone organized photosystem biogenesis (Figure 1B).

As a consequence of its progressive migration the D1 protein marker was not localized within the ZT8 and ZT10 time points (Figure 15). This non-localized distribution of the PSII protein marker temporally correlated with non-localized distribution of PSII subunit translation markers and with the peak of D1 protein accumulation during the diurnal light phase (Figure 10A and 11). The loss of T-zone localized D1 protein marker was displayed by the separated green colored *psbA* message and the red colored D1 protein within both average compiled cell images

(Figure 15A). Similarly, the graphical representation of the ZT8 and ZT10 average compiled cells displayed the even intensity distribution of the D1 protein marker across the chloroplast (Figure 15B). Furthermore, this diurnal migration of the D1 protein marker mirrors the temporal dispersion of this same PSII-specific marker during early and later *y-1* greening.

In summary, the use of core proteins to initially mark their complex-specific synthesis site was supported using two differing model systems that display increased thylakoid biogenesis. CH analyses highlighted the similarities between *y-1* chloroplast differentiation and synchronized chloroplast growth during the diurnal light phase. Furthermore, this unbiased analysis has shown the temporal chloroplastic migration of photosystem-specific protein markers from their initial synthesis site towards their known destination among all thylakoids. Therefore, diurnally-entrained cells have demonstrated T-zone enriched PSII subunit translation which was correlated with the rapid protein accumulation of the PSII complex. Moreover, higher intensity T-zone localized chlorophyll autofluorescence was observed throughout the diurnal light phase which could represent the non-quenched and un-assembled state of this pigment specifically within the T-zone. Similarly, despite the mature chloroplasts of diurnally-entrained cells the D1 protein marker still displayed T-zone enrichment during the early light phase which could represent a larger D1 protein quantity or the highly immunogenic state of this protein when un-assembled [2]. Thus, these spatially and temporally coordinated events within the chloroplastic T-zone area support and further elucidate the proposed T-zone model of PET chain complex biogenesis as well as the migration of assembled complexes within the chloroplast thylakoid membranes (Figure 1B). Lastly, investigation into the organization of PSI-specific protein markers and other complex-specific assembly or translation factors is currently underway (Supplemental Figure 9).

Synchronized CC-125	*y-1*	
Cytf	AtpE	L7/L12
D1-N Terminal	Cytf	Rbp40
PsaA	D1-N Terminal	AOX1
YCF4/YCF3	D2	Cyl4
Rbp40	PsaA	Hsp70
POR	CP43	Vipp1
HSP70	YCF4/YCF3	POR
	NDA2	Mitotracker

Supplemental Figure 9. List of protein markers completed for both algal model systems used
First column: completed fluorescence microscopy protein markers for diurnally-entrained cells
Second column: completed fluorescence microscopy protein markers for *y-1* greening and green cells
*Dr. Yi Sun contributed 50% towards the making and imaging of these slides, the other 50% was conducted by Melissa V.P.

3.26 Transmission electron microscopy of the T-zone ultrastructure during diurnally-entrained chloroplast growth and division

Multifaceted evidence presented above supports the model for T-zone localized PET chain complex biogenesis but lacks the ultrastructural characterization of this sub-organellar organization. TEM ultrastructure characterization of *y-1* revealed the evenly distributed thylakoid remnants within dark-grown cells whereas greening cells displayed electron dense globular ends of elongating thylakoids and chloroplast envelope-connected heavy membrane structures containing newly synthesized chlorophyll [18], [22], [38]. The known even dispersal of thylakoid remnants within dark-grown *y-1* cells was supported by the non-localized even chloroplastic distribution of the thylakoid marking ATP synthase marker (Figure 5). Despite this even thylakoid distribution, PSII biogenesis was preferentially localized within defined regions known as the T-zone thereby validating this sub-organellar spatial enrichment (Figure 3, 4A/B, 7A/B, 11, 12A/B, 15, and Supplemental Figure 2, 3A, 7A) [2]. Similarly, the previously discovered *y-1* greening electron dense membrane structures which contain newly synthesized chlorophyll could be spatially located within the T-zone as supported by the initial *in situ* chlorophyll autoflorescence accumulation (Figure 6). Considering the parallels between these previously uncovered *y-1* ultrastructures and the current *y-1* greening T-zone findings, we decided to characterize diurnally-entrained cells while using a comparable TEM ultrastructure analysis. Given the similarities between chloroplast differentiation and diurnal chloroplast growth, we first hypothesize that thylakoids will be evenly distributed within the diurnally-entrained chloroplasts which would confirm preferential T-zone localized biogenesis as opposed to basally aggregated thylakoid membranes. Furthermore, we hypothesized that the T-zone would have a corresponding physical ultrastructure potentially involving electron dense thylakoid membrane regions and thylakoid membrane formations supporting the proposed T-zone model (Figure 1B).

TEM ultrastructural analysis of ZT0 diurnally-entrained cells revealed the even distribution of thylakoid membranes within the chloroplast (Figure 16). Thylakoid membranes of ZT0 cells displayed the stacking complexity and homogenous posterior-to-anterior arrangement expected of mature green chloroplasts. This TEM confirmation of even thylakoid distribution within a T-zone displaying diurnal light phase time point was documented for 100% of ZT0 cells imaged (Figure 11 and 16). Therefore, this even arrangement of thylakoid membranes within diurnally-entrained

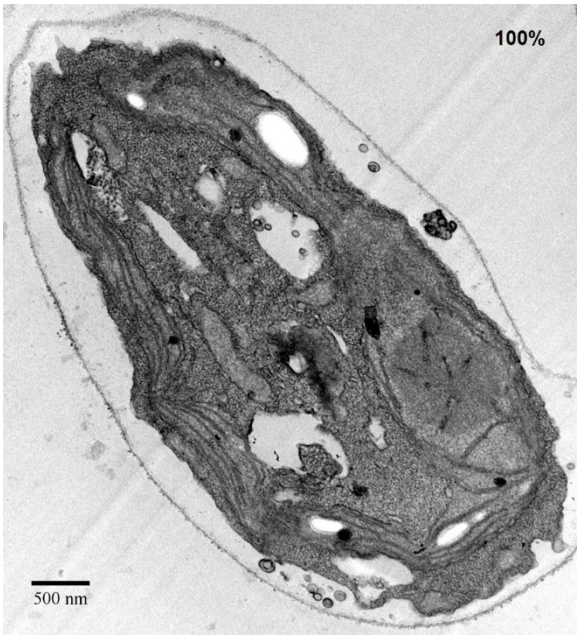

Figure 16. TEM ultrastructure of ZT0 diurnally-entrained cells
Image of ZT0 cell showing typical thylakoid membrane arrangement throughout the chloroplast. Scale bar is 500 nm. Percentages of the given thylakoid arrangement among ZT0 cells is displayed. Sample size of cells (n=13)
*All work conducted by Melissa V.P.

cells confirmed the *y-1* thylakoid distribution findings, which supports that T-zone localized biogenesis is not a by-product of thylakoid membrane aggregation (Figure 5 and 4C/D) [2].

Comparison of TEM images between a T-zone containing light phase time point (ZT3) and a non-localized time point (ZT10) showed several ultrastructural differences as candidates for further analysis. These ultrastructural differences included the presence, location, and characterization of thylakoid membrane convergence zones, the amount and complexity of thylakoid-pyrenoid tubule connections, the presence of electron dense thylakoids, and the existence of PLB-like structures in the T-zone.

Thylakoid membrane convergence zones are areas where three or more thylakoid membranes curve sharply to become perpendicular with the chloroplast envelope. The comparative analysis between ZT3 and ZT10 time points could reveal quantitative and spatial localization difference for convergence zones which might associate with the *in situ* T-zone area and its proposed role in photosystem biogenesis. Association of thylakoid convergence zones with the T-zone was supported by the localization of asynchronous mature cell convergence zones mostly within the lobe tips and lobe-junctions, where the lobe-junctions also displayed chloroplast

envelope invagination potentially for the import of nuclear encoded chloroplast proteins [16]. Given this association of convergence zones with the spatial lobe-junction T-zone area and nuclear-chloroplast import, we hypothesized that convergence zones would be more numerous and

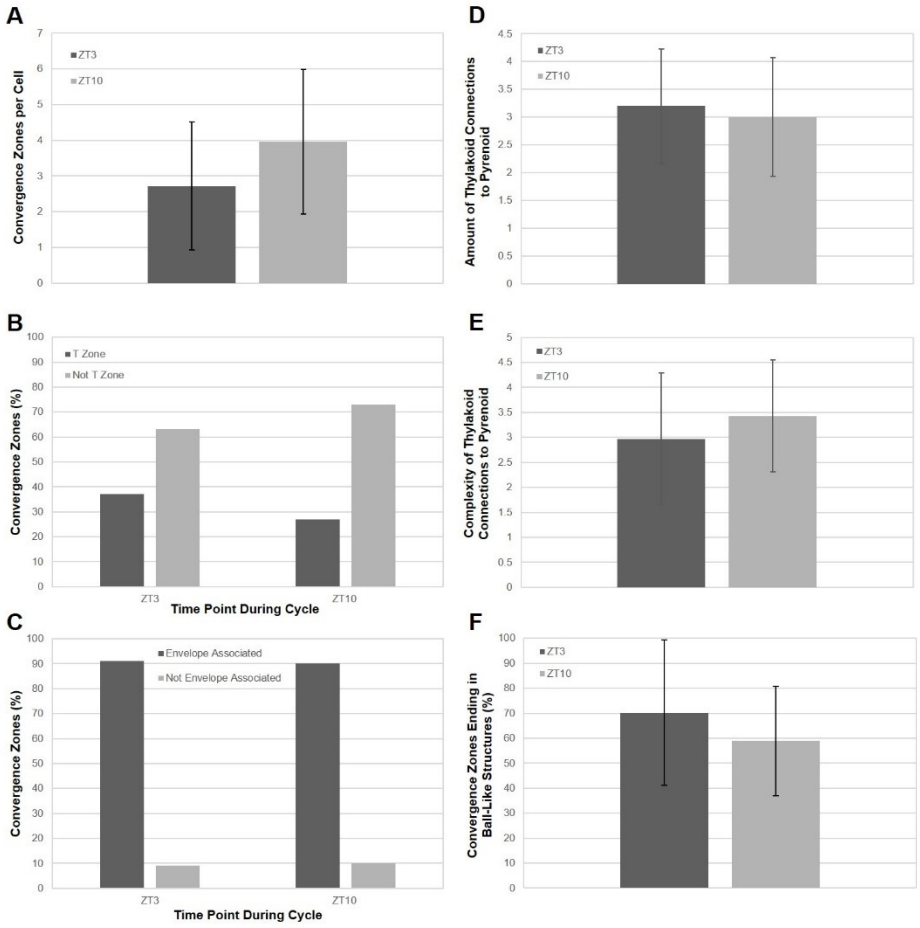

Figure 17. TEM ultrastructure analysis between ZT3 and ZT10 diurnally-entrained cells
(A) Number of convergence zones for both ZT3 and ZT10 cells.
Sample sizes of cells: ZT3 (n=32) and ZT10 (n=28).
(B) Percent of convergence zones found in T-zone (top of pyrenoid, lobe junctions, sides of pyrenoid) and percent of convergence zones found in non-T-zone areas (bottom of pyrenoid and lobes) for both ZT3 and ZT10 cells. Sample sizes of convergence zones: ZT3 (n=87) and ZT10 (n=111).
(C) Percent of convergence zones associated with the chloroplast envelope or not associated with the chloroplast envelope for both ZT3 and ZT10 cells.
Sample sizes of convergence zones: ZT3 (n=87) and ZT10 (n=111).
(D) Number of thylakoids that connect with the pyrenoid tubules for both ZT3 and ZT10 cells.
Sample sizes of cells: ZT3 (n=56) and ZT10 (n=31).
(E) Complexity (number of lipid bilayers) for the pyrenoid-thylakoid connections for both ZT3 and ZT10 cells. Sample sizes of connections: ZT3 (n=69), ZT10 (n=21).
(F) Percent of convergence zones ending in a ball like structure for both ZT3 and ZT10 cells.
Sample sizes of cells: ZT3 (n=32), ZT10 (n=28).
*All work conducted by Melissa V.P.

highly located within the lobe-junctions of the T-zone containing time point (ZT3) when compared to the non-localized time point (ZT10).

When tallied, the number of convergence zones did not correlate with the diurnal ZT3 time point displaying T-zone localized biogenesis (Figure 17A). The number of convergence zones per cell was variable, causing a high standard deviation but demonstrating that on average ZT10 diurnally-entrained cells contained more convergence zones (Figure 17A). Therefore, the presence of T-zone localization within ZT3 diurnally-entrained cells does not correlate with a higher occurrence of convergence zones indicating that convergence zone frequency probably does not play a prominent role within T-zone thylakoid biogenesis. Instead, the higher quantity of convergence zones was related to the greater amount of thylakoid membranes present within the larger ZT10 diurnally-entrained cells.

Similarly, characterization for the location of convergence zones also yielded a conflicting result displaying that most convergence zones occurred within chloroplastic areas not associated with the T-zone (Figure 17B, 18 and Supplemental Figure 10 A/B). The most frequent spatial localization of convergence zones regardless of the time point was along the chloroplast lobes or within the region posterior to the pyrenoid. However, the minority of convergences zones localized within the T-zone displayed a temporal shift where 35% of ZT3 convergence zones were found either anterior to the pyrenoid, positioned lateral to the pyrenoid, or within the lobe-junctions, versus the subsequent 25% of ZT10 convergence zones (Figure 17B). This 10% shift in localization appeared as a re-distribution of convergence zones from the basal chloroplast regions, the T-zone areas and posterior to the pyrenoid, specifically into the chloroplast lobes (Supplemental Figure 10A vs. 10B). A posterior-to-apical chloroplastic spatial shift coincides with the general concept of the T-zone model localized photosystem biogenesis and migration (Figure 1B) [2], [40]. The functional difference between T-zone and lobe localized convergence zones has recently been hypothesized to be a source-to-sink channeling of thylakoid membranes where new thylakoids originate from the T-zone localized convergence zones, move outwards into the chloroplast lobes becoming photodamaged upon extended light exposure, and eventually get removed through the lobe-tip convergence zones [16]. Therefore, despite most convergence zones not being found within the T-zone, there could be a minor role for the localization of convergence

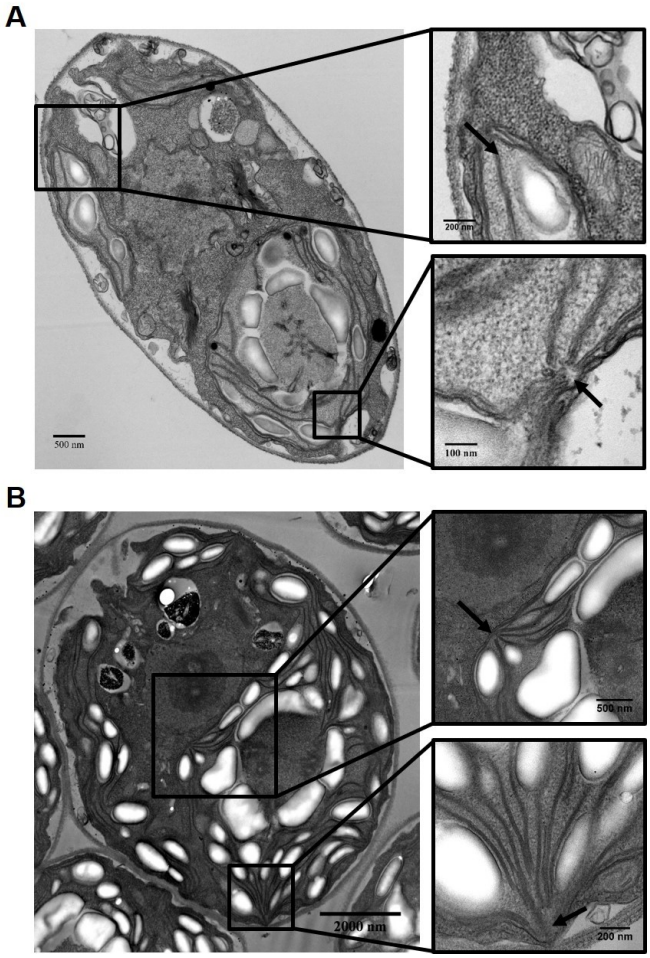

Figure 18. TEM ultrastructure images of Convergence Zones between ZT3 and ZT10 diurnally-entrained cells

(A) Left hand side; example image of a ZT3 cell containing convergence zones seen within anterior and posterior regions of the cell. Right hand side; magnification of ZT3 convergence zones.

(B) Left hand side; example image of a ZT10 cell containing convergence zones seen within anterior and posterior regions of the cell. Right hand side; magnification of ZT10 convergence zones.

*All work conducted by Melissa V.P.

zones within the proposed model of organized photosystem biogenesis as supported by the posterior-to-apical convergence zone shift within the ZT3 versus ZT10 diurnally-entrained cells.

To discern any structural differences and inferred functions between T-zone localized convergence zones and lobe localized convergence zones, we closely analyzed the endings of these thylakoid meeting points. Recent advances in cyanobacterial chloroplast organization have revealed the presence of biogenesis centers formed with the ends of converging thylakoids joined by a circular membrane structure [35], [43], [46]. Furthermore, greening of the *y-1* eukaryotic algal mutant has also displayed electron dense globular structures located specifically within the endings

of growing and curved thylakoid membranes [38]. Given the occurrence of circular ball-like structures at the ends of growing thylakoids and the existence of convergence zone-like thylakoid biogenesis centers within cyanobacterial chloroplasts, we attributed closer attention to the ending structures of convergence zones between the previously chosen diurnal light phase time points.

Characterization of convergence zone endings displayed a higher occurrence of ball-like structures within the ZT3 cells and the slight increase of ball-like convergence zone endings within the chloroplast lobes of ZT10 cells (Figure 17F and 18). Although variable, the frequency of convergence zones ending in a ball-like structure displayed on average a 10% increase within the ZT3 diurnal cell time point (Figure 17F). ZT3 convergence zones terminated upon a clearly curved membrane structure or with dense globular spots, conversely ZT10 convergence zones exhibited no dense globular spots and terminated upon a less defined straighter membrane or no curved

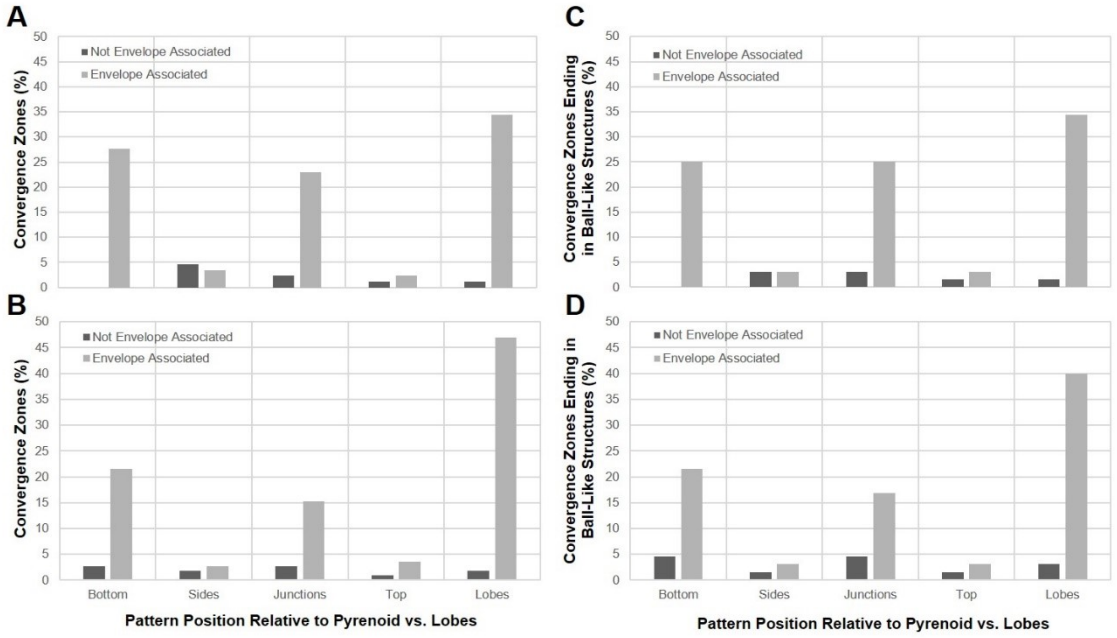

Supplemental Figure 10. TEM ultrastructure analysis of convergence zone locations and ending ball-like structures for ZT3 and ZT10 diurnally-entrained cells

(A) Percent of convergence zones classified into the chloroplast sub locations and their envelope association for ZT3 cells. Sample sizes of convergence zones: (n=87)

(B) Percent of convergence zones classified into the chloroplast sub locations and their envelope association for ZT10 cells. Sample sizes of convergence zones: (n=111)

(C) Percent of convergence zones ending in a ball-like structure classified into the chloroplast sub locations and their envelope association for ZT3 cells. Sample sizes of convergence zones: (n=64)

(D) Percent of convergence zones ending in a ball-like structure classified into the chloroplast sub locations and their envelope association for ZT10 cells. Sample sizes of convergence zones: (n=65)

*All work conducted by Melissa V.P.

membrane structure at all (Figure 18A vs 18B). This increased ZT3 occurrence and clarity of ball-like convergence zone endings was not spatially enriched where the sum of T-zone associated areas roughly displayed a similar percentage of ball-like endings when compared to the chloroplast lobes and the posterior region of the pyrenoid displayed the lowest percentage (Figure 18A and Supplemental Figure 10C). However, the ZT10 spatial localization of ball-like convergence zone endings denoted a decrease among all basally localized sites, while the chloroplast lobes displayed a 5% increase in ball-like ending structures (Supplemental Figure 10D). Therefore, this temporal basally targeted decrease of ball-like endings coupled with the apical increase, mirrors the previous shift seen for the overall convergence zone localization and subsequently supports the source-to-sink model explained above. This repeatedly observed posterior-to-anterior shift of convergence zones and their associated structures provides further evidence substantiating the T-zone model of organized photosystem biogenesis and subsequent migration within the chloroplast (Figure 1B).

Given this potential link between convergence zone quantity, their ball-like ending structure, and the theoretical source-to-sink model, we wondered if these diurnally-entrained convergence zones also were associated with the chloroplast envelope. Chloroplast thylakoid biogenesis necessitates many different chloroplast and nuclear genome-encoded components in addition to specialized lipid membranes, hence nuclear import through the chloroplast envelope is required [16], [26], [73], [74]. Additionally, past evidence supports the localization of chlorophyll and lipid synthesis nearby the chloroplast envelope further supporting the need for chloroplast envelope-to-thylakoid conduits which can be organized in a spatial-temporal manner to help facilitate these required exchanges [47], [73]–[75]. Convergence zones could serve as these chloroplast envelope-to-thylakoid conduits because they were located less then 100 nm away from the chloroplast envelope and demonstrated direct and indirect connections as well as invaginations with the chloroplast envelope [16], [22]. Therefore, we investigated if the convergence zones located within our chosen diurnally-entrained cell time points exhibited any spatial-temporal trends regarding chloroplast envelope association.

Spatial-temporal analysis revealed that most convergence zones displayed chloroplast envelope association regardless of the time point, reflecting the source-to-sink spatial shift (Figure 17C and Supplemental Figure 10). Both ZT3 and ZT10 cells exhibited a 90% frequency of convergence zone placement along the chloroplast envelope. As most convergence zones are

chloroplast envelope associated, their spatial localization is identical to the previously explained localization for all convergence zones (Supplemental Figure 10A vs. 10B). This posterior-to-anterior shift in convergence zones coincided with the proposed source-to-sink model used to remove photodamaged proteins through the lobe localized convergence zones [16]. Interestingly, the *in situ* localization of PSII subunit translation markers and D1 protein marker accumulation within green *y-1* cells supported this proposed thylakoid protein maintenance through the presence of distinct lobe-tip maxima which coincided spatially with the frequently seen convergence zones within the chloroplast lobes (Figure 4B red arrows, 7B red arrows and Supplemental Figure 10) [16]. These lobe-tip maxima were uniquely observed for the translation and accumulation of the core PSII protein D1 which is known to be the most frequently ROS damaged and repaired photosynthetic protein (Figure 7B vs. 7C) [65], [66]. Therefore, these chloroplast envelope-associated convergence zone findings support the proposed basal chloroplastic role of convergence zones as envelope-to-thylakoid conduits for the transfer of nuclear and lipid components and their hypothesized apical chloroplastic role as removal or repair zones for frequently damaged proteins such as the PSII core protein D1. This indirect evidence provides additional support for the T-zone model of organized photosystem biogenesis and migration within the chloroplast (Figure 1B).

The final chloroplast ultrastructure analyzed was the change in quantity and complexity of thylakoid-pyrenoid tubule connections when comparing ZT3 and ZT10 diurnal time points. The detailed layout of pyrenoid tubules and their encased min-tubules displayed uninterrupted connections with both the chloroplast stroma and thylakoid lumen which are hypothesized to serve as a biological highway to shuttle various molecules [16]. Furthermore, the amount of pyrenoid tubules has been shown to change when exposed to differing environmental conditions [29]. Given the biological significance and environmental responsiveness of pyrenoid tubules in relation to photosynthesis, we characterized their thylakoid connections.

The analysis of thylakoid-to-pyrenoid tubule connections displayed no obvious temporal differences in both quantity and complexity (Figure 17D and 17E). On average, ZT3 and ZT10 cells contained three thylakoid connections with the pyrenoid tubules. Similarly, the complexity of these connections also did not show any significant temporal changes. Therefore, these results indicated that thylakoid-to-pyrenoid tubule connections do not change temporally in accordance with T-zone localized biogenesis, despite their proximity to it.

In summary, these more prominent ultrastructural findings suggest a minor role of convergence zones within the T-zone model. The amount of convergence zones displayed a 10% temporal decrease among T-zone localized and basal chloroplastic regions while simultaneously exhibiting a temporal increase in convergence zones within the lobes. Furthermore, a larger quantity of convergence zones terminating upon a ball-like structure were found within the T-zone containing time point ZT3 where these circular structures have been associated with thylakoid biogenesis. Similarly, these ball-like endings also displayed this posterior-to-anterior temporal shift when compared to the non-localized ZT10 time point. Lastly, a majority of all convergence zones were found to be envelope-associated which supports the possibly that they are correlated with nuclear genome-encoded protein import and lipid provisions emanating from chloroplast envelope invaginations [16]. Therefore, parallels between these convergence zone findings and the proposed source-to-sink migration of thylakoids supports the previously presented T-zone model (Figure 1B). Other subtler TEM ultrastructures were seen but not quantified. However, given that these subtle ultrastructures resemble the previously observed electron dense thylakoid regions, the algal PLB-like structures, and could have a role within T-zone organized photosystem biogenesis, they are important enough to explore [22], [25], [38].

Upon examination, ZT3 cells displayed electron dense thylakoid membranes within the immediate vicinity of the pyrenoid and rare instances of PLB-like structures where these observed structures were temporally regulated because of their absence within ZT10 cells (Figure 19). The presence of electron dense thylakoids within a temporally increased context of thylakoid biogenesis is reminiscent of the previously documented electron dense thylakoid disc thickenings observed only among the elongating membranes of greening *y-1* cells [38]. These ZT3 large and irregular electron dense patches were localized to the thylakoid membranes near the pyrenoid which were connected to the pyrenoid tubules and convergence zones but were no longer observable among similarly positioned ZT10 thylakoids (Figure 19A white asterisks vs 19B). The other subtle ultrastructure formations resembled the previously documented algal PLB-like structures which are hypothesized to act as thylakoid biogenesis centers as documented within plant etioplast PLBs [22]–[25]. Algal PLB-like structures were observed inconsistently thus their characterization is incomplete and variable, however their potential association with convergence zones and their roles in algal thylakoid membrane biogenesis have been proposed [26]. Although the placement of these PLB-like structures was unfortunately never recorded their proposed role

within thylakoid biogenesis favors their spatial enrichment within the T-zone. The early ZT3 diurnal light phase time point displayed infrequent PLB-like structures occasionally associated with a plastoglobule and found only within the previously defined T-zone areas (Figure 19A white arrow and C black arrow). Although infrequent among ZT3 cells, these PLB-like structures are noteworthy because they were never seen among the non-localized ZT10 diurnal light phase time point. Despite the potential difficulty in quantification within the current data set, these electron dense thylakoid patches and these PLB-like structures warrant further investigation because of their spatial-temporal localization which correlates with the *in situ* T-zone biogenesis findings displayed above, and because of their hypothesized biological functions which coincide well with organized thylakoid biogenesis.

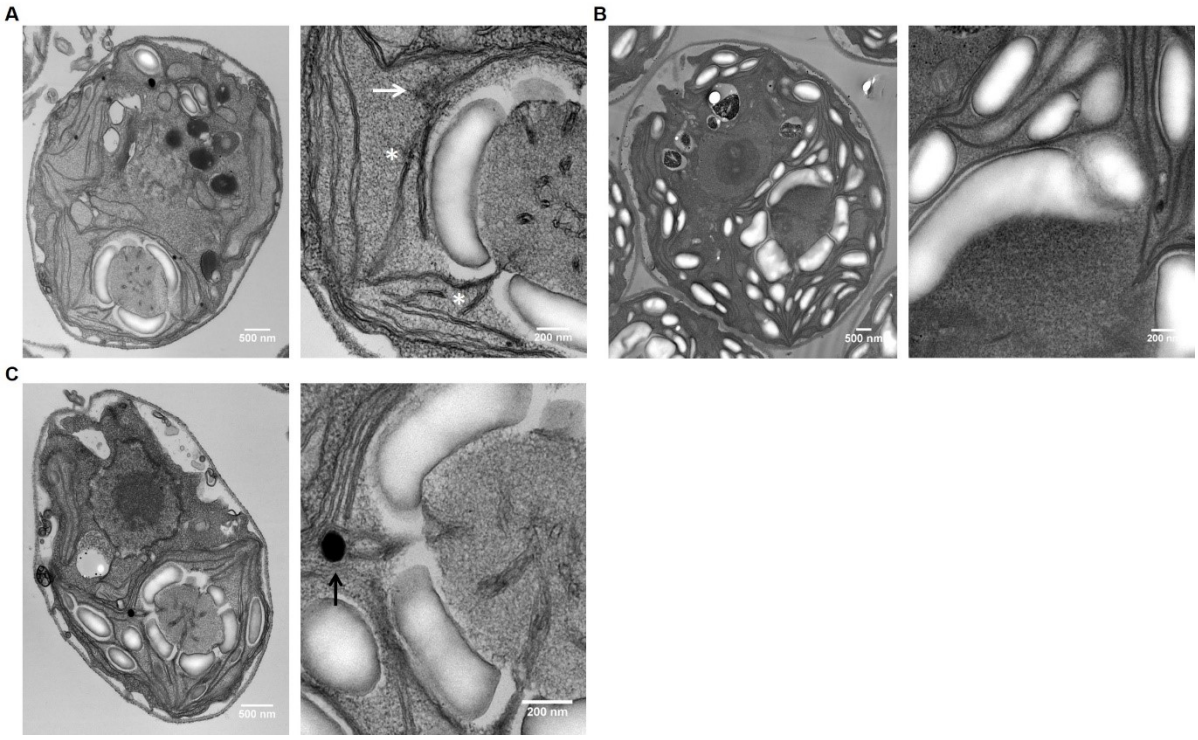

Figure 19. TEM ultrastructure images of electron dense thylakoids and prolamellar body-like structures between ZT3 and ZT10 diurnally-entrained cells

(A) Left hand side; example image of a ZT3 cell. Right hand side; magnification of T-zone denoting electron dense thylakoids = white asterisks and PLB-like structure = white arrow.
Scale bar sizes are indicated.

(B) Left hand side; example image of a ZT10 cell. Right hand side; magnification of T-zone denoting no electron dense thylakoids or PLB-like structures. Scale bar sizes are indicated.

(C) Left hand side; example image of a ZT3 cell. Right hand side; magnification of T-zone denoting an electron dense plastoglobule associated with a PLB-like structure = black arrow.
Scale bar sizes are indicated.

*Characteristics noticed by Dr. Zerges, figure creation conducted by Melissa V.P.

3.3 Concluding Remarks

Overall, the results presented above further elucidate the proposed T-zone model by showing its use within both differentiating chloroplasts and growing chloroplasts, as well as the additional spatial-temporal organization of PSI and chlorophyll biogenesis within the T-zone. This thesis provides the necessary foundation to continue expanding the T-zone model by localizing other PET chain complexes, components, translation factors, assembly factors, required enzymes, and related proteins or organelles. Currently, this expansion is underway and promising results are seen for several markers within both algal model systems used (Supplemental Figure 1).

Within the field of photosynthesis research, there is a growing need for the spatial-temporal organization of PET chain complex biogenesis and thylakoid biogenesis. Recently, this chloroplastic organization has been emphasized as an essential strategy to ensure the correct assembly of thylakoid membrane complexes and to avoid deleterious side-reactions [3], [37], [76], [77]. Furthermore, this proposed sub-organellar chloroplastic organization is reflected within land plants because of their evolutionary relationship with eukaryotic green alga and the similarity between their photosynthetic complexes. Recently the specific spatial organization of PSII repair, and the temporal organization of PET chain complex accumulation has been demonstrated within the chloroplasts of higher land plants [78], [79]. These findings indicate the plausibility of a similar organized model for PET chain complex synthesis and assembly during the thylakoid biogenesis of plant chloroplasts. Through our two plant-analogous algal model systems, the novel T-zone findings presented above may help uncover related or comparable organizational strategies within higher plants thus providing fundamental knowledge about this complex biological process and potentially impacting the agricultural industry.

3.4 Other Avenues of Investigation

Throughout our investigation of the *C. reinhardtii* chloroplastic spatial-temporal organization, we encountered several interesting adjacent avenues of investigation.

Firstly, the role of a ‘master clock’ in regulating photosystem biogenesis was suggested by the anticipatory T-zone localization during the dark phase, by the oscillations of PET chain protein quantities during the diurnal cycle, and by the apparent disassembly of the pyrenoid tubule network during the light phase (Supplemental Figure 11, 12, 13, 14). The diurnal dark phase *in situ* and CH

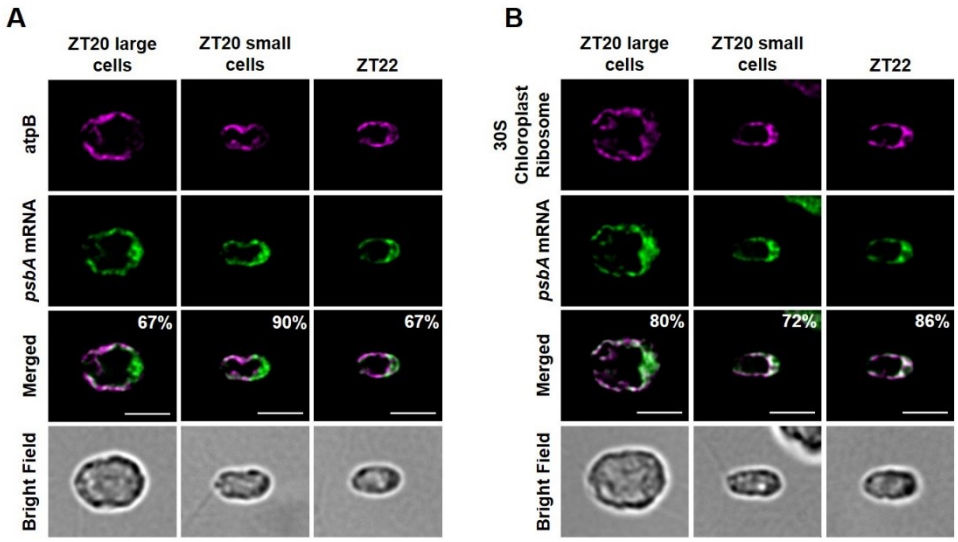

Supplemental Figure 11. *In situ* localization of PSII subunit translation markers and a thylakoid marker during the late dark phase of diurnally-entrained cells

(A) Immunofluorescence staining of the ATP synthase β subunit coupled with fluorescence *in situ* hybridization of the PSII-specific *psbA* message. Merged channels indicate lack of overlapping white areas between both markers. Bright field provides the cellular orientation. Percentages of the given pattern are displayed. The scale bar is 5 μm.

Sample sizes of cells: ZT20 large cells (n=9), ZT20 small cells (n=39), ZT22 (n=103).

(B) Immunofluorescence staining of the chloroplastic small (30S) ribosomal subunit coupled with fluorescence *in situ* hybridization of the PSII-specific *psbA* message. Merged channels indicate overlapping white areas between both markers. Bright field provides the cellular orientation. Percentages of the given pattern are displayed. The scale bar is 5 μm.

Sample sizes of cells: ZT20 large cells (n=15), ZT20 small cells (n=39), ZT22 (n=72).

* Dr. Yi Sun contributed 50% towards making the slides. Other 50% of making the slides, imaging, analysis, deconvolution, and figure making conducted by Melissa V.P.

analysis of PSII subunit translation revealed the presence of T-zone localization in most cells up to four hours before the subsequent light phase (Supplemental Figure 11 and 12). Moreover, the extensive pyrenoid tubule network disassembled and the pyrenoid matrix dissipated out of the pyrenoid, 1-2 hours before the dark phase (Supplemental Figure 13). Furthermore, many PET chain protein accumulation trends throughout the 24-hour diurnal cycle display oscillations which are independent of light energy because they occurred during the end of the light phase before the lights are removed and during the end of the dark phase (Figure 10A and Supplemental Figure 14). However, the control this circadian rhythm has over other cellular and chloroplastic events is a controversial subject, with indications of both circadian regulated and not regulated processes in all photosynthetic organisms [52]. Thus, these findings indicate the potential control of the circadian rhythm, given that their timing seems to be in anticipation of the next phase and

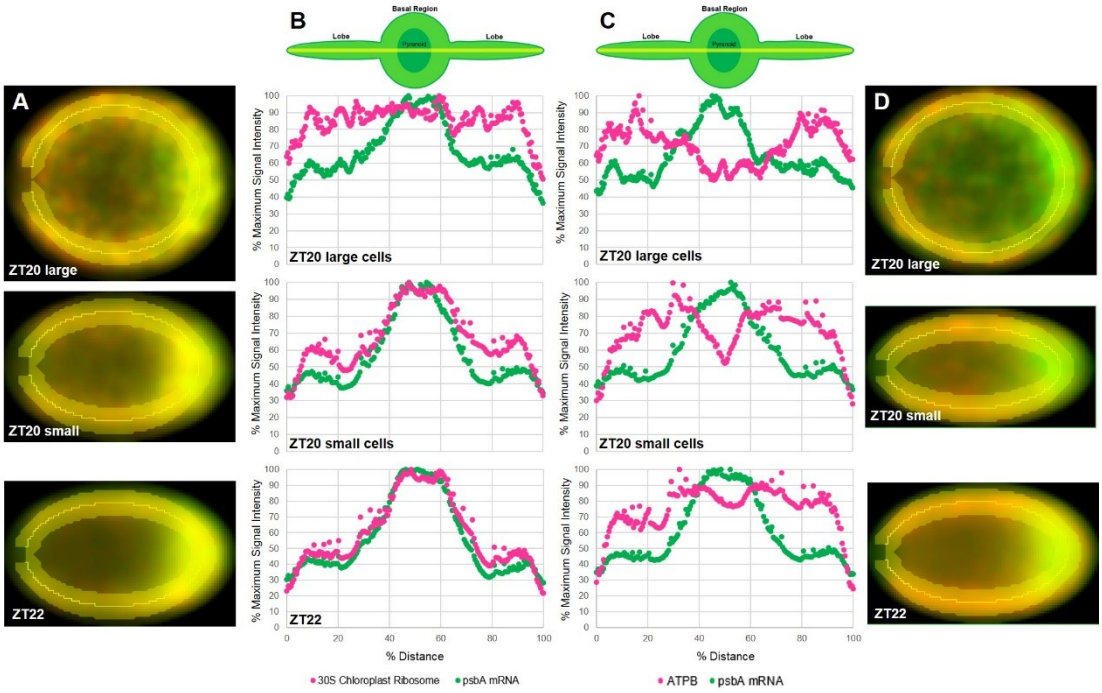

Supplemental Figure 12. Cell harvester analysis for PSII subunit translation markers and the thylakoid marking ATP synthase complex during the dark phase of diurnally-entrained cells
(A) Average compiled cells for the chloroplastic small (30S) ribosomal subunit and PSII-specific *psbA* message. Sample sizes of cells: ZT20 large cells (n=15), ZT20 small cells (n=48), ZT22 (n=64)
(B) Percent of Maximum Intensity vs Percent of Distance graphs for the images displayed in panel A. Straightened chloroplast denoted above graphs for positioning reference (pyrenoid center = 50%)
(C) Average compiled cells for the ATP Synthase β subunit and PSII-specific *psbA* message. Sample sizes of cells: ZT20 large cells (n=9), ZT20 small cells (n=54), ZT22 (n=112)
(D) Percent of Maximum Intensity vs Percent of Distance graphs for the images displayed in panel C Straightened chloroplast denoted above graphs for positioning reference (pyrenoid center = 50%)
*All work conducted by Melissa V.P.

independent of light energy or photosynthesis. Therefore, a future topic of research should be to investigate the potential circadian cycle regulation of the spatial-temporal T-zone localized PET chain complex biogenesis, the disassembly of the pyrenoid tubule network, and the temporal ordering or oscillations among the differing PET chain complex protein markers.

Secondly, the antibody against the cytochrome f protein of the cytochrome b_6f complex displayed strongly fluorescent foci which were not as evident in the Δ Cytf mutant and responded to growth conditions (Supplemental Figure 4). If these foci were an artifact they should not respond to the process of *y-1* chloroplast differentiation nor to growth in nitrogen deficient media, demonstrating that they represent a biologically relevant protein which is affected by chloroplast thylakoid biogenesis. Nitrogen starvation is known to specifically affect the cytochrome b_6f

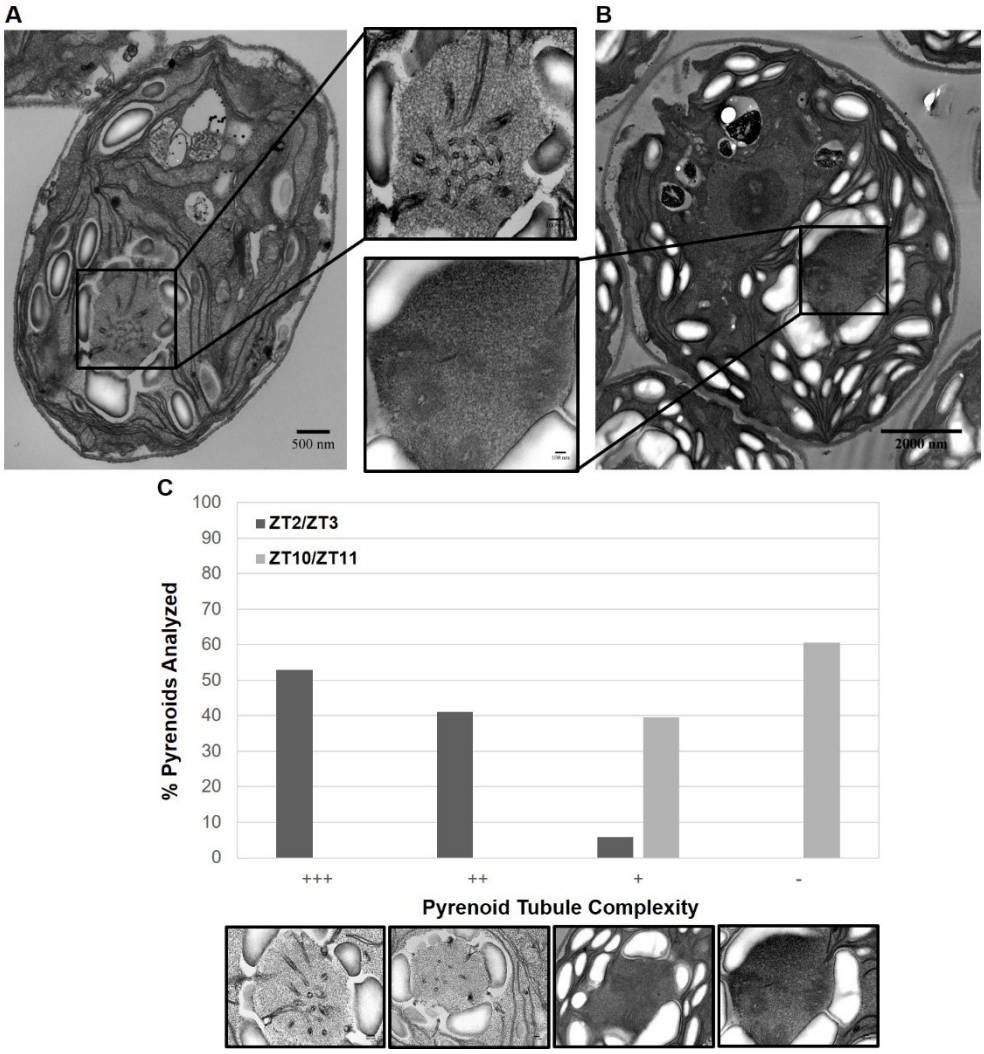

Supplemental Figure 13. TEM ultrastructure analysis of pyrenoid tubule dis-assembly during the light phase of diurnally-entrained cells

(A) Left hand side; Example image of a ZT3 cell. Upper central panel; magnification of pyrenoid tubules. Scale bar sizes are indicated.

(B) Left hand side; Example image of a ZT10 cell. Lower central panel; magnification of pyrenoid tubules. Scale bar sizes are indicated.

(C) Percentage of ZT2/3 and ZT10/11 pyrenoids qualitatively classified into categories, TEM category images below graph. Sample sizes of pyrenoids analyzed: ZT2/3 (n=68), ZT10/11 (n=38).

*All work conducted by Melissa V.P.

complex, furthermore this complex is also known to be CES regulated and is present in relatively high protein quantities during growth in the dark where it has a non-functional proton pump ability [42], [80]–[82]. Thus, investigation into the nature of these foci and which protein is being detected by this antibody would be of interest because of their relatedness to *y-1* greening and their response to nitrogen starvation.

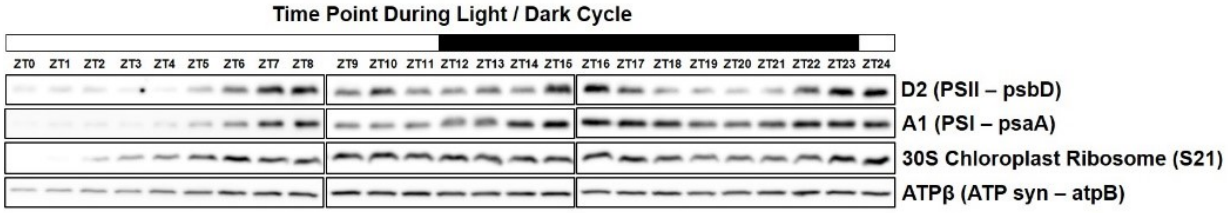

Supplemental Figure 14. Immunoblot characterization of diurnally-entrained cells for 24-hours
Marker proteins detected for: the PSI complex (D2), the PSII complex (A1 or PsaA) and the ATP synthase complex.
*Dr. Yi Sun contributed the most to this work. Contribution of samples and figure polishing provided by Melissa V.P.

Thirdly, diurnally-entrained cells displayed a rapid and dramatic cell death when not diluted for two days (Supplemental Figure 15). This cell death phenomenon was intriguing because the culture appears to die in a synchronized manner using a predictable series of events and at a relatively low cell density. These cultures reach a cell density of $1x10^7$ cells/ml, then begin to de-synchronized, followed by acidification of the media, then cell death, and eventually become a discolored yellow-brown in less than 12 hours. Normally, algal cultures can reach a higher cell density and not display this mode of cell death, thus nutrient deprivation should not be to blame. It is for this reason that investigation into a programmed cell death response is currently underway.

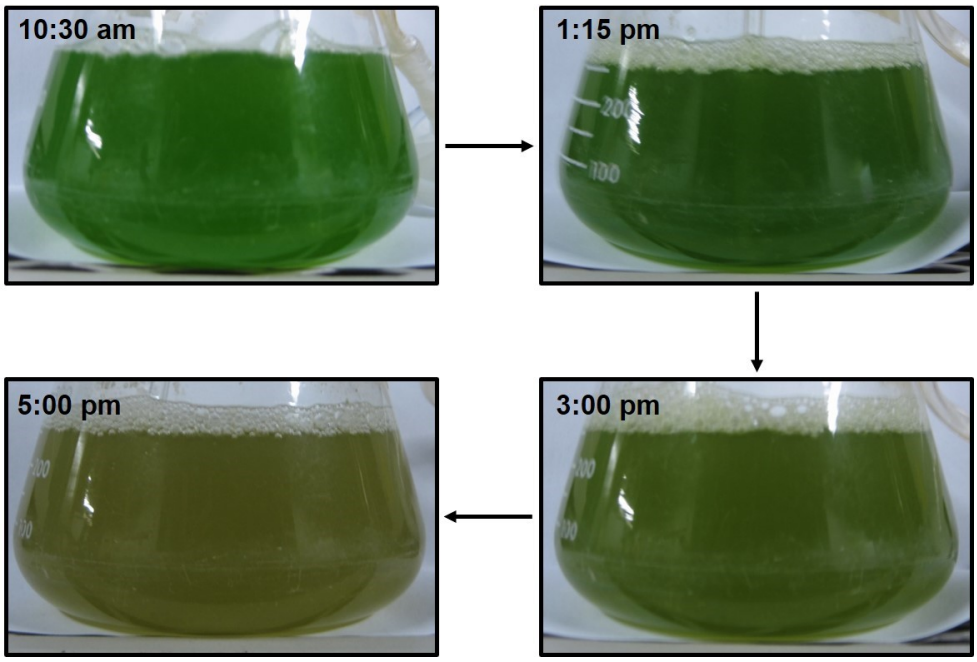

Supplemental Figure 15. Color change and cell death of diurnally-entrained cultures
Digital images of the same diurnally-entrained culture diluted daily for three 24-hour cycles and left undiluted for one full 24-hour cycle. On the second undiluted 24-hour cycle the culture displayed the above imaged color change which was accompanied by cell death.
*All work conducted by Melissa V.P.

Lastly, it was observed that the late light phase non-localized distribution of PSII subunit translation markers become re-localized at the ZT12 time point (Figure 11 and 13). However, this chloroplastic ribosomal marker and the *psbA* message form a differing pattern, resembling a discontinuous ring around the pyrenoid and pyrenoid infiltrating strings within ZT12 cells. This temporal ZT12 overlapping of the PSII subunit translation markers is likely not used for translation and is probably related to cpSG formation (Chapter 3 pp. 68-69). Later *in situ* analysis at ZT13 reveals the progressive movement of these markers into the pyrenoid, the same spatial location as the large rubisco subunit (results not shown). These findings require repetition, but the presence of the stress target *psbA* message within the same spatial location as the large rubisco subunit indicates the potential elucidation of a spatial-temporal organization for oxidized RNA management [48], [71].

Therefore, the research of this thesis achieved not only the expected objectives but also new information which fits into current Ph.D. investigations and revealed novel avenues of investigation for future M.Sc. students.

References

[1] J. Losos, K. A. Mason, and S. R. Singer, *Biology*, 8th ed. McGraw-Hill, 2008.

[2] J. Uniacke and W. Zerges, "Photosystem II Assembly and Repair Are Differentially Localized in Chlamydomonas," *Plant Cell*, vol. 19, no. 11, pp. 3640–3654, Nov. 2007.

[3] J. M. Zones, I. K. Blaby, S. S. Merchant, and J. G. Umen, "High-Resolution Profiling of a Synchronized Diurnal Transcriptome from *Chlamydomonas reinhardtii* Reveals Continuous Cell and Metabolic Differentiation" *Plant Cell*, vol. 27, no. 10, pp. 2743–2769, Oct. 2015.

[4] S. Gruschke *et al.*, "The Cbp3–Cbp6 complex coordinates cytochrome b synthesis with bc1 complex assembly in yeast mitochondria," *J Cell Biol*, vol. 199, no. 1, pp. 137–150, Oct. 2012.

[5] K. Kehrein *et al.*, "Organization of Mitochondrial Gene Expression in Two Distinct Ribosome-Containing Assemblies," *Cell Rep.*, vol. 10, no. 6, pp. 843–853, Feb. 2015.

[6] R. Sager and G. E. Palade, "Structure and Development of the Chloroplast in Chlamydomonas: I. the Normal Green Cell," *J. Cell Biol.*, vol. 3, no. 3, pp. 463–488, May 1957.

[7] I. K. Blaby *et al.*, "The Chlamydomonas genome project: a decade on," *Trends Plant Sci.*, vol. 19, no. 10, pp. 672–680, Oct. 2014.

[8] A. R. Grossman, "*Chlamydomonas reinhardtii* and photosynthesis: genetics to genomics," *Curr. Opin. Plant Biol.*, vol. 3, no. 2, pp. 132–137, Apr. 2000.

[9] S.-E. Shin *et al.*, "CRISPR/Cas9-induced knockout and knock-in mutations in *Chlamydomonas reinhardtii*," *Sci. Rep.*, vol. 6, p. 27810, Jun. 2016.

[10] E. H. Harris, D. B. Stern, and G. B. Witman, *The Chlamydomonas Sourcebook*, 2nd ed., 3 vols. Academic Press, 2009.

[11] E. Hummel *et al.*, "3D Ultrastructural Organization of Whole *Chlamydomonas reinhardtii* Cells Studied by Nanoscale Soft X-Ray Tomography," *PLOS ONE*, vol. 7, no. 12, p. e53293, Dec. 2012.

[12] W. Zerges, "Translation in chloroplasts," *Biochimie*, vol. 82, no. 6–7, pp. 583–601, Jul. 2000.

[13] J. E. Maul *et al.*, "The *Chlamydomonas reinhardtii* Plastid Chromosome," *Plant Cell*, vol. 14, no. 11, pp. 2659–2679, Nov. 2002.

[14] A. L. Manuell, J. Quispe, and S. P. Mayfield, "Structure of the Chloroplast Ribosome: Novel Domains for Translation Regulation," *PLOS Biol.*, vol. 5, no. 8, p. e209, Aug. 2007.

[15] J. Uniacke, W. Zerges, J. Uniacke, and W. Zerges, “Chloroplast protein targeting involves localized translation in Chlamydomonas,” *Proc. Natl. Acad. Sci.*, vol. 106, no. 5, pp. 1439–1444, Feb. 2009.

[16] B. D. Engel, M. Schaffer, L. K. Cuellar, E. Villa, J. M. Plitzko, and W. Baumeister, “Native architecture of the Chlamydomonas chloroplast revealed by in situ cryo-electron tomography,” *eLife*, vol. 4, p. e04889, Jan. 2015.

[17] G. Kreimer, “The green algal eyespot apparatus: a primordial visual system and more?,” *Curr. Genet.*, vol. 55, no. 1, pp. 19–43, Feb. 2009.

[18] I. Ohad, P. Siekevitz, and G. E. Palade, “Biogenesis of Chloroplast Membranes I. Plastid Dedifferentiation in a Dark-Grown Algal Mutant (*Chlamydomonas reinhardtii*),” *J. Cell Biol.*, vol. 35, no. 3, pp. 521–552, Dec. 1967.

[19] I. Polukhina, R. Fristedt, E. Dinc, P. Cardol, and R. Croce, “Carbon Supply and Photoacclimation Cross Talk in the Green Alga *Chlamydomonas reinhardtii*,” *Plant Physiol.*, vol. 172, no. 3, pp. 1494–1505, Nov. 2016.

[20] U. Klein, “Intracellular Carbon Partitioning in *Chlamydomonas reinhardtii*,” *Plant Physiol.*, vol. 85, no. 4, pp. 892–897, Dec. 1987.

[21] J. Jüppner *et al.*, “Dynamics of lipids and metabolites during the cell cycle of *Chlamydomonas reinhardtii*,” *Plant J. Cell Mol. Biol.*, vol. 92, no. 2, pp. 331–343, Oct. 2017.

[22] J. K. Hoober, C. O. Boyd, and L. G. Paavola, “Origin of Thylakoid Membranes in *Chlamydomonas reinhardtii y-1* at 38°C,” *Plant Physiol.*, vol. 96, no. 4, pp. 1321–1328, Aug. 1991.

[23] B. E. S. Gunning, “The greening process in plastids,” *Protoplasma*, vol. 60, no. 1, pp. 111–130, Mar. 1965.

[24] L. Kowalewska, R. Mazur, S. Suski, M. Garstka, and A. Mostowska, “Three-Dimensional Visualization of the Tubular-Lamellar Transformation of the Internal Plastid Membrane Network during Runner Bean Chloroplast Biogenesis,” *Plant Cell*, vol. 28, no. 4, pp. 875–891, Apr. 2016.

[25] I. Friedberg, I. Goldberg, and I. Ohad, “A Prolamellar Body-Like Structure in *Chlamydomonas reinhardtii*,” *J. Cell Biol.*, vol. 50, no. 1, pp. 268–275, Jul. 1971.

[26] A. Nordhues *et al.*, “Evidence for a role of VIPP1 in the structural organization of the photosynthetic apparatus in Chlamydomonas,” *Plant Cell*, vol. 24, no. 2, pp. 637–659, Feb. 2012.

[27] M. Meyer and H. Griffiths, “The internal plumbing of algal chloroplasts,” *eLife*, vol. 4, p. e05983, Jan. 2015.

[28] M. Meyer and H. Griffiths, “Origins and diversity of eukaryotic CO2-concentrating mechanisms: lessons for the future,” *J. Exp. Bot.*, vol. 64, no. 3, pp. 769–786, Jan. 2013.

[29] M. Rawat, M. C. Henk, L. L. Lavigne, and J. V. Moroney, “*Chlamydomonas reinhardtii* mutants without ribulose-1,5-bisphosphate carboxylase-oxygenase lack a detectable pyrenoid,” *Planta*, vol. 198, no. 2, pp. 263–270, 1996.

[30] D. Bhattacharya and and L. Medlin, “Algal Phylogeny and the Origin of Land Plants,” *Plant Physiol.*, vol. 116, no. 1, pp. 9–15, Jan. 1998.

[31] M. A. Ruggiero *et al.*, “A Higher Level Classification of All Living Organisms,” *PLOS ONE*, vol. 10, no. 4, Apr. 2015.

[32] R. M. Dent, M. Han, and K. K. Niyogi, “Functional genomics of plant photosynthesis in the fast lane using *Chlamydomonas reinhardtii*,” *Trends Plant Sci.*, vol. 6, no. 8, pp. 364–371, Aug. 2001.

[33] J. Rochaix, “Assembly, Function, and Dynamics of the Photosynthetic Machinery in *Chlamydomonas reinhardtii*,” *Plant Physiol.*, vol. 127, no. 4, pp. 1394–1398, Dec. 2001.

[34] Y. Sun and W. Zerges, “Translational regulation in chloroplasts for development and homeostasis,” *Biochim. Biophys. Acta BBA - Bioenerg.*, vol. 1847, no. 9, pp. 809–820, Sep. 2015.

[35] S. Heinz *et al.*, “Thylakoid Membrane Architecture in Synechocystis Depends on CurT, a Homolog of the Granal CURVATURE THYLAKOID1 Proteins,” *Plant Cell*, p. tpc.00491.2016, Aug. 2016.

[36] J. K. Hoober, D. B. Marks, J. L. Gabriel, and L. G. Paavola, “Role of the Chloroplast Envelope in Thylakoid Biogenesis,” in *Regulation of Chloroplast Biogenesis*, Springer, Boston, MA, 1992, pp. 323–330.

[37] J. K. Hoober, R. White, D. Marks, and G. Jerome, “Biogenesis of thylakoid membranes with emphasis on the process in Chlamydomonas,” vol. 39, pp. 15–31, 1994.

[38] I. Ohad, P. Siekevitz, and G. E. Palade, “Biogenesis of Chloroplast membranes ; II Plastid Differentiation during Greening,” *J. Cell Biol.*, vol. 35, no. 3, pp. 553–584, Dec. 1967.

[39] U. C. Vothknecht and P. Westhoff, “Biogenesis and origin of thylakoid membranes,” *Biochim. Biophys. Acta BBA - Mol. Cell Res.*, vol. 1541, no. 1–2, pp. 91–101, Dec. 2001.

[40] M. Schottkowski, M. Peters, Y. Zhan, O. Rifai, Y. Zhang, and W. Zerges, “Biogenic membranes of the chloroplast in *Chlamydomonas reinhardtii*,” *Proc. Natl. Acad. Sci. U. S. A.*, vol. 109, no. 47, pp. 19286–19291, Nov. 2012.

[41] P. Malnoë, S. P. Mayfield, and J. D. Rochaix, "Comparative analysis of the biogenesis of photosystem II in the wild-type and Y-1 mutant of *Chlamydomonas reinhardtii*.," *J. Cell Biol.*, vol. 106, no. 3, pp. 609–616, Mar. 1988.

[42] S. Schuldiner and I. Ohad, "Biogenesis of chloroplast membranes. III. Light-dependent induction of proton pump activity in whole cells and its correlation to cytochrome f photo-oxidation during greening of a *Chlamydomonas reinhardtii* mutant (y-1)," *Biochim. Biophys. Acta BBA - Bioenerg.*, vol. 180, no. 1, pp. 165–177, May 1969.

[43] A. Stengel, I. L. Gügel, D. Hilger, B. Rengstl, H. Jung, and J. Nickelsen, "Initial Steps of Photosystem II de Novo Assembly and Preloading with Manganese Take Place in Biogenesis Centers in Synechocystis," *Plant Cell Online*, vol. 24, no. 2, pp. 660–675, Feb. 2012.

[44] A. Rast, S. Heinz, and J. Nickelsen, "Biogenesis of thylakoid membranes," *Biochim. Biophys. Acta BBA - Bioenerg.*, vol. 1847, no. 9, pp. 821–830, Sep. 2015.

[45] E. Zak, B. Norling, R. Maitra, F. Huang, B. Andersson, and H. B. Pakrasi, "The initial steps of biogenesis of cyanobacterial photosystems occur in plasma membranes," *Proc. Natl. Acad. Sci. U. S. A.*, vol. 98, no. 23, pp. 13443–13448, Nov. 2001.

[46] J. Nickelsen and W. Zerges, "Thylakoid biogenesis has joined the new era of bacterial cell biology," *Front. Plant Sci.*, vol. 4, 2013.

[47] P. Wang and B. Grimm, "Organization of chlorophyll biosynthesis and insertion of chlorophyll into the chlorophyll-binding proteins in chloroplasts," *Photosynth. Res.*, vol. 126, no. 2–3, pp. 189–202, Dec. 2015.

[48] Y. Zhan, J. S. Dhaliwal, P. Adjibade, J. Uniacke, R. Mazroui, and W. Zerges, "Localized control of oxidized RNA," *J Cell Sci*, vol. 128, no. 22, pp. 4210–4219, Nov. 2015.

[49] R. Zoschke and R. Bock, "Chloroplast Translation: Structural and Functional Organization, Operational Control and Regulation," *Plant Cell*, p. tpc.00016.2018, Jan. 2018.

[50] A. B. Cahoon and M. P. Timko, "yellow-in-the-dark Mutants of Chlamydomonas Lack the CHLL Subunit of Light-Independent Protochlorophyllide Reductase," *Plant Cell*, vol. 12, no. 4, pp. 559–569, Apr. 2000.

[51] M. Mittag, S. Kiaulehn, and C. H. Johnson, "The Circadian Clock in *Chlamydomonas reinhardti*i. What Is It For? What Is It Similar To?," *Plant Physiol.*, vol. 137, no. 2, pp. 399–409, Feb. 2005.

[52] F. R. Cross and J. G. Umen, "The Chlamydomonas cell cycle," *Plant J.*, vol. 82, no. 3, pp. 370–392, May 2015.

[53] J. L. Spudich and R. Sager, “Regulation of the Chlamydomonas cell cycle by light and dark.,” *J. Cell Biol.*, vol. 85, no. 1, pp. 136–145, Apr. 1980.

[54] D. E. Shelton, M. P. Leslie, and R. E. Michod, “Models of cell division initiation in Chlamydomonas: A challenge to the consensus view,” *J. Theor. Biol.*, vol. 412, pp. 186–197, Jan. 2017.

[55] S. Mihara and E. Hase, “Studies on the vegetative life cycle of *Chlamydomonas reinhardtii* Dangeard in synchronous culture V. The transition point for the effect of 6-methyl purine in the cell cycle,” *Plant Cell Physiol.*, vol. 19, no. 1, pp. 83–89, Feb. 1978.

[56] A. D. Idoine, A. Boulouis, J. Rupprecht, and R. Bock, “The Diurnal Logic of the Expression of the Chloroplast Genome in *Chlamydomonas reinhardtii*,” *PLOS ONE*, vol. 9, no. 10, p. e108760, Oct. 2014.

[57] R. J. Porra, “The chequered history of the development and use of simultaneous equations for the accurate determination of chlorophylls a and b,” in *Discoveries in Photosynthesis*, vol. 20, Govindjee, J. T. Beatty, H. Gest, and J. F. Allen, Eds. Berlin/Heidelberg: Springer-Verlag, 2005, pp. 633–640.

[58] Q. Li *et al.*, “Young Leaf Chlorosis 2 encodes the stroma-localized heme oxygenase 2 which is required for normal tetrapyrrole biosynthesis in rice,” *Planta*, vol. 240, no. 4, pp. 701–712, Oct. 2014.

[59] J. Uniacke, D. Colón-Ramos, and W. Zerges, “FISH and immunofluorescence staining in Chlamydomonas,” *Methods Mol. Biol. Clifton NJ*, vol. 714, pp. 15–29, 2011.

[60] M. Gad and A. Ikai, “Method for immobilizing microbial cells on gel surface for dynamic AFM studies,” *Biophys. J.*, vol. 69, no. 6, pp. 2226–2233, Dec. 1995.

[61] H. Elimam *et al.*, “Genetic Ablation of Calcium-independent Phospholipase A $_2$ γ Induces Glomerular Injury in Mice,” *J. Biol. Chem.*, vol. 291, no. 28, pp. 14468–14482, Jul. 2016.

[62] C. Lemaire and F. A. Wollman, “The chloroplast ATP synthase in *Chlamydomonas reinhardtii*. II. Biochemical studies on its biogenesis using mutants defective in photophosphorylation.,” *J. Biol. Chem.*, vol. 264, no. 17, pp. 10235–10242, Jun. 1989.

[63] C. de Vitry, J. Olive, D. Drapier, M. Recouvreur, and F. A. Wollman, “Posttranslational events leading to the assembly of photosystem II protein complex: a study using photosynthesis mutants from *Chlamydomonas reinhardtii*,” *J. Cell Biol.*, vol. 109, no. 3, pp. 991–1006, Sep. 1989.

[64] E. Baena-González and E.-M. Aro, “Biogenesis, assembly and turnover of photosystem II units.,” *Philos. Trans. R. Soc. B Biol. Sci.*, vol. 357, no. 1426, pp. 1451–1460, Oct. 2002.

[65] K. J. van Wijk, L. O. Nilsson, and S. Styring, “Synthesis of reaction center proteins and reactivation of redox components during repair of photosystem II after light-induced inactivation.,” *J. Biol. Chem.*, vol. 269, no. 45, pp. 28382–28392, Nov. 1994.

[66] A. K. Mattoo, H. Hoffman-Falk, J. B. Marder, and M. Edelman, “Regulation of protein metabolism: Coupling of photosynthetic electron transport to in vivo degradation of the rapidly metabolized 32-kilodalton protein of the chloroplast membranes,” *Proc. Natl. Acad. Sci. U. S. A.*, vol. 81, no. 5, pp. 1380–1384, Mar. 1984.

[67] J. G. Umen, “Synchronizing Chlamydomonas reinhardtii,” 2015.

[68] N. H. Chua, G. Blobel, P. Siekevitz, and G. E. Palade, “Periodic variations in the ratio of free to thylakoid-bound chloroplast ribosomes during the cell cycle of *Chlamydomonas reinhardtii*.,” *J. Cell Biol.*, vol. 71, no. 2, pp. 497–514, Nov. 1976.

[69] Y. Choquet and O. Vallon, “Synthesis, assembly and degradation of thylakoid membrane proteins,” *Biochimie*, vol. 82, no. 6–7, pp. 615–634, Jun. 2000.

[70] M. Lohr, C.-S. Im, and A. R. Grossman, “Genome-Based Examination of Chlorophyll and Carotenoid Biosynthesis in *Chlamydomonas reinhardtii*,” *Plant Physiol.*, vol. 138, no. 1, pp. 490–515, May 2005.

[71] J. Uniacke and W. Zerges, “Stress induces the assembly of RNA granules in the chloroplast of *Chlamydomonas reinhardtii*,” *J. Cell Biol.*, vol. 182, no. 4, pp. 641–646, Aug. 2008.

[72] N. Murata, S. Takahashi, Y. Nishiyama, and S. I. Allakhverdiev, “Photoinhibition of photosystem II under environmental stress,” *Biochim. Biophys. Acta BBA - Bioenerg.*, vol. 1767, no. 6, pp. 414–421, Jun. 2007.

[73] C. Benning, “Mechanisms of Lipid Transport Involved in Organelle Biogenesis in Plant Cells,” *Annu. Rev. Cell Dev. Biol.*, vol. 25, no. 1, pp. 71–91, 2009.

[74] C. Benning, “A role for lipid trafficking in chloroplast biogenesis,” *Prog. Lipid Res.*, vol. 47, no. 5, pp. 381–389, Sep. 2008.

[75] J. Joyard and R. Douce, “Import receptor in chloroplast envelope,” *Nature*, vol. 333, no. 6171, pp. 306–307, May 1988.

[76] S. Caffarri, T. Tibiletti, R. C. Jennings, and S. Santabarbara, “A Comparison Between Plant Photosystem I and Photosystem II Architecture and Functioning,” *Curr. Protein Pept. Sci.*, vol. 15, no. 4, pp. 296–331, Jun. 2014.

[77] S. Järvi, M. Suorsa, and E.-M. Aro, “Photosystem II repair in plant chloroplasts — Regulation, assisting proteins and shared components with photosystem II biogenesis,” *Biochim. Biophys. Acta BBA - Bioenerg.*, vol. 1847, no. 9, pp. 900–909, Sep. 2015.

[78] Z. Liang *et al.*, “Thylakoid-Bound Polysomes and a Dynamin-Related Protein, FZL, Mediate Critical Stages of the Linear Chloroplast Biogenesis Program in Greening Arabidopsis Cotyledons,” *Plant Cell*, p. tpc.00972.2017, Jan. 2018.

[79] S. Puthiyaveetil *et al.*, “Compartmentalization of the protein repair machinery in photosynthetic membranes,” *Proc. Natl. Acad. Sci.*, vol. 111, no. 44, pp. 15839–15844, Nov. 2014.

[80] Y. Choquet, F. Zito, K. Wostrikoff, and F.-A. Wollman, “Cytochrome f Translation in Chlamydomonas Chloroplast Is Autoregulated by its Carboxyl-Terminal Domain,” *Plant Cell*, vol. 15, no. 6, pp. 1443–1454, Jun. 2003.

[81] I. Goldberg and I. Ohad, “Biogenesis of Chloroplast Membranes: V. A Radioautographic Study of Membrane Growth in a Mutant of *Chlamydomonas reinhardtii* y-1,” *J. Cell Biol.*, vol. 44, no. 3, pp. 572–591, Mar. 1970.

[82] L. Wei *et al.*, “Nitric Oxide–Triggered Remodeling of Chloroplast Bioenergetics and Thylakoid Proteins upon Nitrogen Starvation in *Chlamydomonas reinhardtii*,” *Plant Cell*, vol. 26, no. 1, pp. 353–372, Jan. 2014.

Appendix I : Technical Guide to Synchronized Culture Set up

Table of Contents

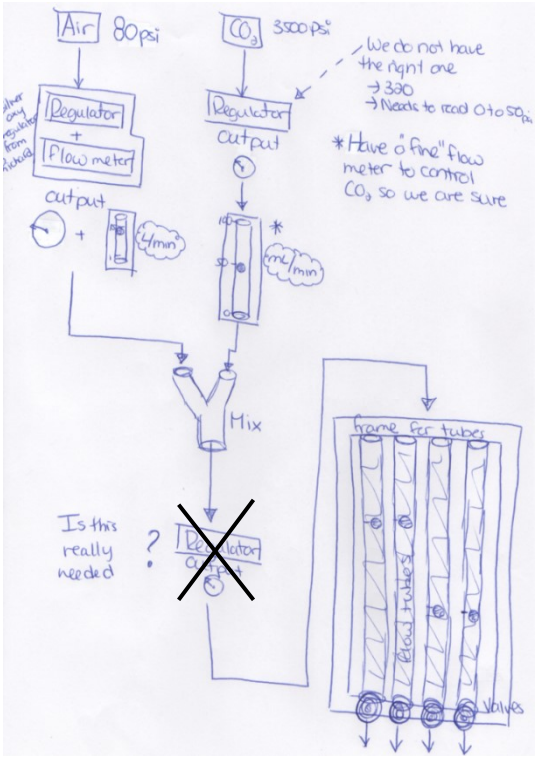

CO_2 system layout

The layout of the system is as drawn on the left. In parallel, air and CO_2 are being sent through various regulators and flow meters until it arrives at a mixing chamber.

The air is pumped into a pressure gage (which registers the PSI) then the air is fed through a flow meter to determine the coarse flow rate in L/min. Meanwhile, the CO_2 is being emptied from a tank into a regulator (which controls the PSI of the tank and registers the PSI being fed out from the tank) then into a fine flow meter showing the flow rate in ml/min.

Once in the mixing chamber, the gas is now 0.5% carbon dioxide/air mixture, this gas is then sent to the partitioning system. This system is held in a frame which has four flow meters; two of which are in ml/min (for 250ml cultures) and the other two are in L/min (for large 1L cultures). These flow meters register the flow rate and feed it, through long tubing, into the cultures.

Air to CO_2 ratio

The air flow meter is coarse (L/min) thus to determine the percentage in relation to the CO_2 you have to convert it to ml/min (like the fine CO_2 flow meter).

For cell synchronization a percentage of 0.5% is recommended by Dr. Umen's Lab. As an example, 0.5% of 1000 ml/min is 5 ml/min. Therefore, depending on what your air flow meter is registering as a flow rate you have to then set your CO_2 flow meter accordingly. This chart was designed to help with the quick set up of the CO_2 flow meter according to what the air flow meter is measuring.

Air		Co2
ml/min	***l/min***	***ml/min***
1000	1	5
2000	2	10
3000	3	15
4000	4	20
5000	5	25
6000	6	30
7000	7	35
8000	8	40
9000	9	45
10000	10	50
11000	11	55

Actual system setup

This is the setup of the CO_2 system hook up described in the page above.

All of the components are present and will be pointed out one by one later on in this document.

This is the CO_2 gas tank, must be replaced when the PSI reaches zero. A full tank is approximately 800-900 PSI.

CO_2 delivery system

CO_2 tank is joined to an appropriate regulator.

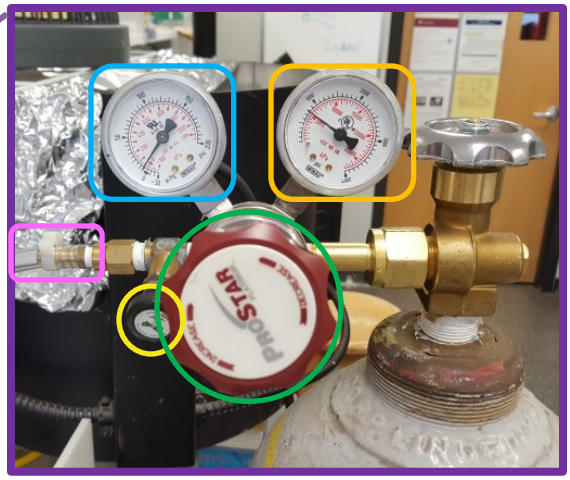

This regulator has a PSI range appropriate for the tank input and the regulator output on its respective gauges. Lastly, the regulator controls the output via two knobs. The large one needs a strong enough output so that it won't shut itself, but it also cannot be to high. Meanwhile, the small knob is for finer refinement, and it needs to have an output with enough strength to generate a low hissing noise.

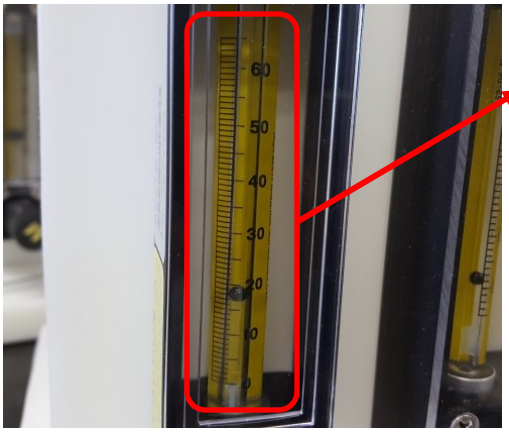

The CO_2 tank regulator is attached, via tubbing, to the fine CO_2 flow meter.

It must be set appropriately according to the coarse flow rate of air measured by another flow meter set in parallel. The percent of CO_2 must be 0.5% (Table pg.1). This fine CO_2 flow meter is mounted on the same frame as the partitioning system.

The flow rate of CO_2, exiting the fine CO_2 flow meter, is then sent to the mixing chamber via tubbing.

The mixing chamber, as shown in the picture on the right, has 2 inputs and 1 output.

One input feeds CO_2 into the chamber, while the other input feeds the air (being sent in parallel to the CO_2).

Air/Mixed gas delivery system

Meanwhile, the air is being pumped into the setup by 2 simultaneously running fish pumps.

These 2 fish pumps are linked together, by tubing and a 'Y' junction, to feed into the same downstream pressure regulator and thus the same flow meter.

Fish pumps need to be plugged into an outlet in order to function. They also take the air in the environment and pump that into the system; so the air around the pumps needs to be chemical/vapor/contaminant free.

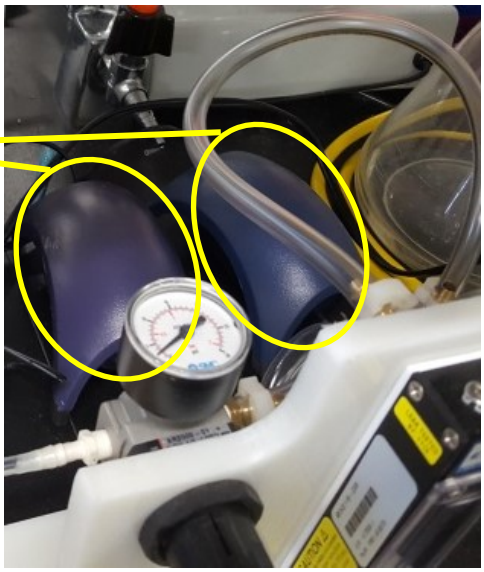

N.B. Warning!!! House air (or air delivered by the air pipes in the lab, located on the benches) cannot be used in this system! Long term use of house air is discouraged since it is contaminated with oil. This oil will fill up the tubing and flow meters, then everything needs to be replaced!!! If house air must be used, please contact 2400 to set up an oil trap filter outside our lab in the external air duct.

To the left is an example of a flow meter ruined by house air. As you can see the oil from the air, is coating the inside of the flow meter. Once dirtied, it cannot be cleaned and the oil WILL disrupt the floatation of the ball by the pumped air.

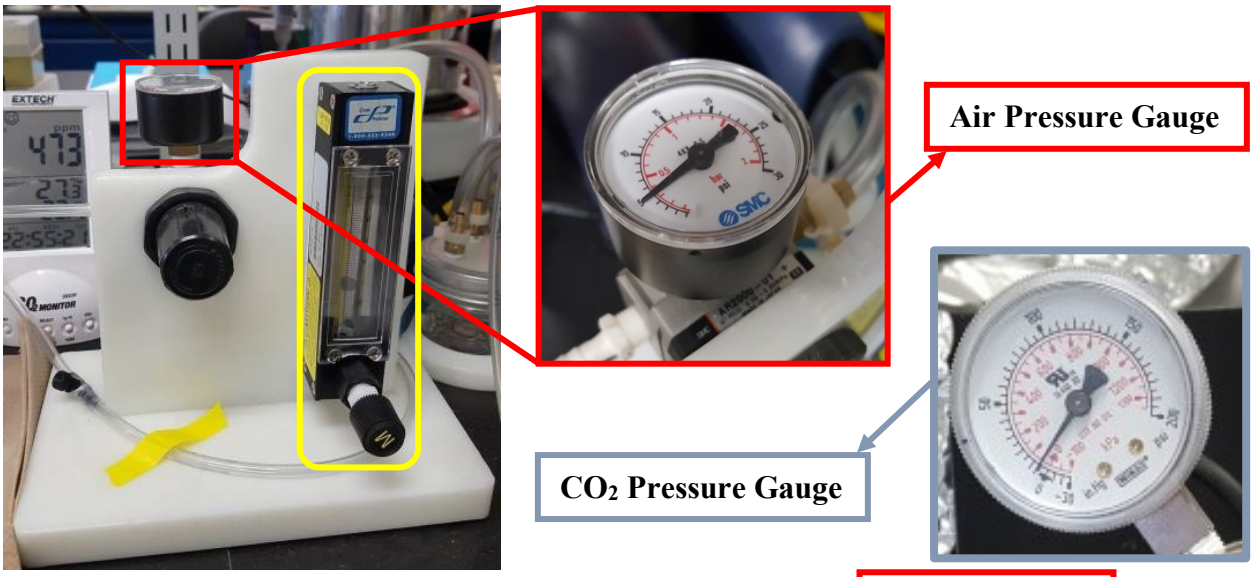

The pumped air (by the fish pumps) is combined and fed into the Air pressure gauge. This pressure gauge will only show the PSI going through it if the output side is blocked (for example if you bend the tube on the output side so the air is blocked for a couple of seconds).

It is important to recall that the air PSI (on the air pressure gauge) must match the PSI pressure on the CO_2 output gauge (located on the CO_2 tank regulator).

This is a precaution to avoid back pressure, or outcompeting of one gas with the other!

The air is then fed from the Air pressure gauge to the back of the coarse air flow meter which reads and adjusts the flow rate of the pumped air.

This given flow rate of air (which corresponds to an appropriate flow rate of the CO_2) will then get fed from the coarse air flow meter into the mixing chamber.

As explained previously, air will be mixed with the CO_2 to create 0.5% CO_2 mixed with air.

This mixed air is then pushed out of the mixing chamber and fed into the bottom of the partitioning system.

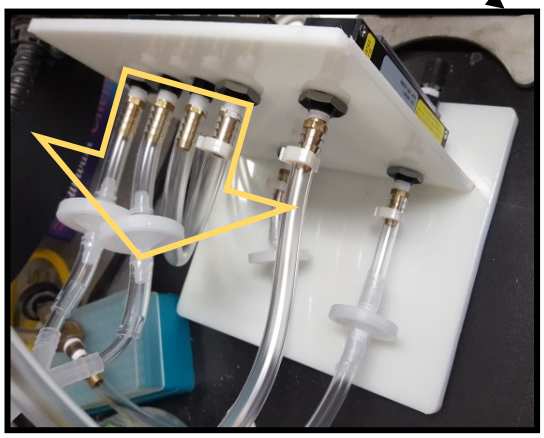

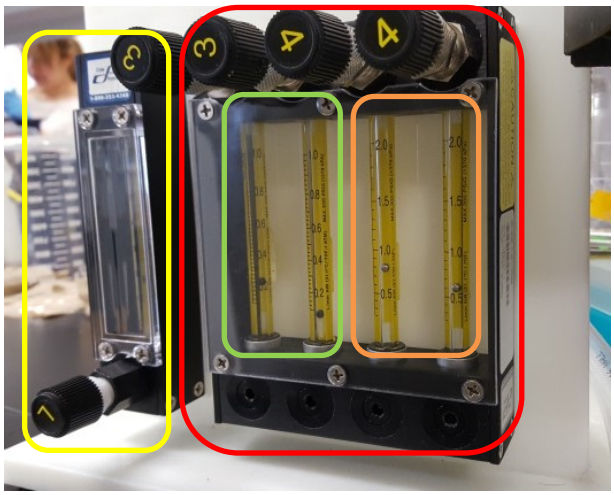

The partitioning system is mounted on the same frame as the fine CO_2 flow meter. This system splits the incoming air into 4 flow meters. Two of which are extra fine and can measure a max flow rate of 1000 ml/min (or 1 L/min). The other two are fine and can measure a maximum of 2 L/min. This partitioned air is then fed to the respective cultures connected to it (as depicted above).

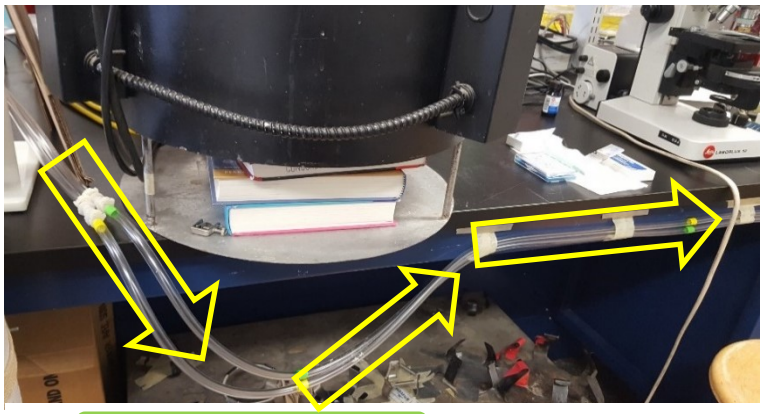

The two extra fine flow meters are connected to an incubator outside of the lab using 50-foot tubbing. Meanwhile, the two fine flow meters are slightly open and connected to a buffering flask to help with the back pressure of the system.

Lastly, the whole in lab system is monitored for potentially dangerous leaks by the usage of a CO_2 detector. This system has the potential to be dangerous if the CO_2 tank/CO_2 regulator malfunctions and the 100% CO_2 (normally contained safely in the tank) escapes into the closed lab rapidly.

Some concentrated CO_2 inhalation can cause headaches, dizziness, and sleepiness. While excess concentrated CO_2 can cause death by suffocation.

External incubator setup

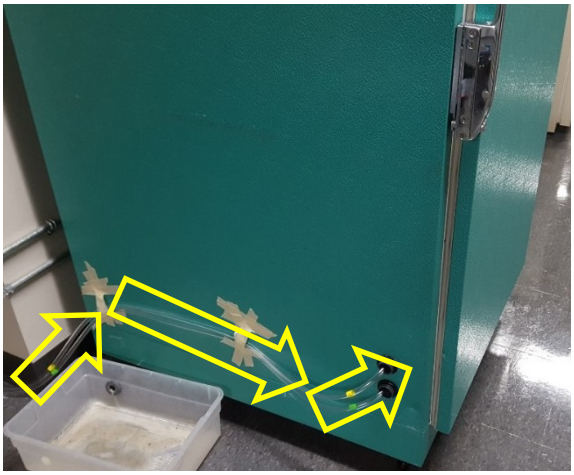

The CO_2 system in the lab is connected to an incubator outside the lab via 50-foot tubing. This tubing leads to the interior of the incubator and then connects to the cultures. As you can see there are 2 tubes, one for each of the extra fine flow meters in the partitioning system. Each one connects to a different culture and can be identified using the colored tape (green/yellow). The bottom of the incubator has been modified by; the removal of a rack, the closure of the open holes with panels, and the addition of 'grow lights' to the sides at the bottom. Also, the incubator itself has been programed specifically for synchronized cells ("Programing Growth Chamber Version #2). This incubator model has internal electrical plugs; allowing electricity to be provided to additional modules. A power bar was connected to the incubator power source and timers for the light box and fan were connected to it appropriately. The fan is connected directly into its analogue timer (instructions for it are stuck to the timer itself). Similarly, the light box is also plugged into its digital timer directly; this timer allows the user to program and ON/OFF cycle with **specific time and days** (if all days are not set then the program will only last for one day!). Lastly, this photo shows a removable black garbage bag cover. This cover is useful for time points taken during the dark cycle. Since the sensitivity of the cells to light is unknown, all precautions were taken including the covering of the bottom of the trolley (covering aliquoted samples); used to block the emergency light in the corridor.

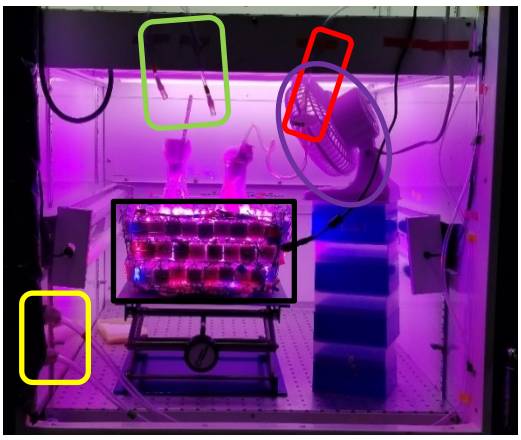

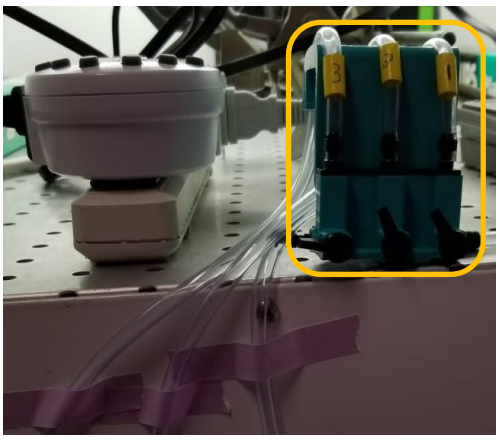

These pictures depict the bottom interior of the incubator; what was previously covered with the garbage bag. There are the two sets of tubing (from the before mentioned CO_2 system) on the right hand side. The tubing enters from an aeration hole in the incubator (on the right), then turns around the perimeter of this bottom section of the incubator. Finally, they are separated, and tapped on the top panel corresponding to the culture they aerate. Color coding facilitates the 'tracking back' of which culture is bubbled by which flow meter from the partitioning system. The two main tubes can be further separated (on the left hand picture) by a splitter, if 3-4 cultures are needed at one time. The light box is composed of LED's that are arranged in a rectangle; LED lights were purchased at Addison Electronics, and are several separate sets of lights; half of which are blue and the other half are red. Sets were connected using electrical junctions to avoid a short circuiting (more lights can still be added on) and arranged on barbeque racks in an alternating Blue-Red-Blue-Red pattern within the box. This light box can accommodate four 500mL flasks which receive light intensities ranging from of 230-280 µE. Alternatively, one 1000mL flask can be placed in the center, which will receive 230 µE. The **temperature** of the incubator is primarily controlled by the chamber itself (the programming cycle), but the incubator needs help to avoid overheating and killing the cultures! This help comes in two ways; by a fan and by an open aeration hole on the side of the incubator. The fan is used to circulate the air in the light box because the box is closed off and has poor circulation (it is not the same temperature as the whole incubator). Meanwhile, the open aeration hole (not visible above) located on the outside left hand side of the incubator; it is taped open and clearly labelled "Do NOT close this valve". Lastly, the light box is **supported** by a "Lab Jack" that can be lowered or elevated to the required height giving easier access (according to the size of flask being used for the experiment).

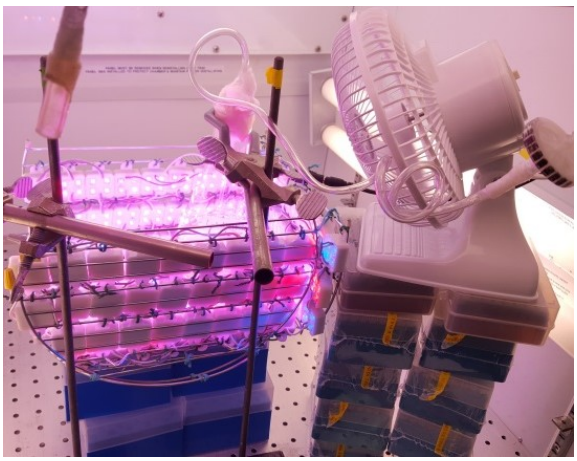

Alternate culture supports

Synchronized cultures in the light box can be suspended in the light box using two proven methods; a clamp + stand or a rack with a hole in it. Cultures need to be suspended in air, and cannot just sit on top of the light box directly; to avoid overheating and poor air circulation around the flask. The original method devised for suspension was by using a heavy stand and a strong clamp (as seen above), however it can also be inconvenient. Inconvenience, and loss of time, were observed when hourly time points needed to be taken quickly and the limiting factor was unscrewing and re-screwing the culture back to the clamp. That being said this method does provide better aeration (since the culture is not touching any surface) and also allows the most light to illuminate the bottom of the flask.

Alternatively, we have recently tried another method that is more convenient and still works in terms of cell synchronization (as seen below). This method involves the use of a shortened small rack with a hole in it (slightly smaller then the flask). It is more convenient because there is no time wasted by screwing the clamp (its simpler to just put the flask down on the rack). However, the rack does block some light and it also has the potential to cause some temperature issues if not monitored.

Flask assembly/layout

The flasks for synchronized cultures are assembled specifically and autoclaved after assembly. Assembly requires; a flask, HSM media, a tighter cotton plug, and an aeration glass pipette attached to a bacterial air filter with tubing. Care must be taken to wash the tubing and aeration pipettes after every use to avoid clogging. This aeration delivery system (pipette + tubbing and filter) must be joined prior to assembly of the flask itself; once joined, it can be tucked securely in the cotton plug meant for the flask. The cotton plug must contain the aeration system tucked inside it (not just on the side) and must be the right size for the flask. Furthermore, since these cultures are receiving aeration, their cotton plugs **need not** be to lose (asynchronous cultures have loose plugs to allow air exchange). Once all assembled, the flasks are filled with HSM media, covered appropriately with aluminum foil, and then sent to autoclave. Aluminum foil needs to cover the bacterial filter and its junction, as well the junction of the aeration pipette and the tubbing. Lastly, a large rectangle of aluminum foil covers the whole top of the flask to secure the aeration pipette in place. The pipette cannot be touching the media inside the flask, or it will suck the media out due to the pressure of the autoclave machine, so it must be lifted away from the liquid media. This can be secured by the final large piece of aluminum foil and by a piece of masking tape. Also, the tubbing and the bacterial filter need to be wrapped around the flask and secured with tape, to avoid the filter touching the water the autoclave bin and absorbing it!

Recently we have added another length of thin tubing extending from the inside of the flask to the outside. This tubing was added to facilitate frequent sampling (using a syringe) and has been proven successful. This tubing can be easily contaminated, so care must be taken to ensure it is properly autoclaved and remains as sterile as possible (ex: above we see the covered opening when it is not being used). Like the aeration pipette, this tubbing also cannot be touching the internal media when autoclaving!

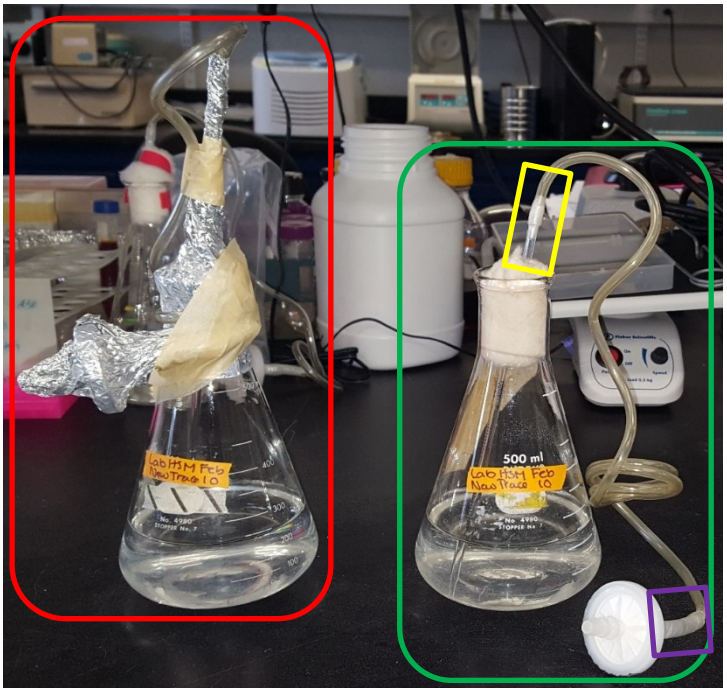

Culture dilution

After autoclaving an assembled synchronized culture flask, the media inside the flask needs to remain at room temperature for 24-48 hours. HSM media becomes cloudy after autoclaving; this cloudiness needs to go away or the culture will not grow as well. The flasks in this image have clear media ready for inoculation. The autoclaved flask needs to be prepared for inoculation by the removal of the aluminum foil and sealing of junctions with parafilm.

The junctions requiring parafilm are: between the aeration tube and plastic tubing, and between the plastic tubing and the bacterial air filter. Cultures are diluted daily to survive; if they are not diluted the cells will sediment, look yellow, smell terrible, and the cells will die.

The process of dilution requires the transfer of a volume of ‘old culture’ to a new prepared flask. To determine the volume you need to transfer, you must first count the ‘old culture’ to know the cell density. From that cell density, you can then calculate how much volume of the ‘old culture’ is needed to give a density of 1-2 x 10 ^5 cells/ml in the 250ml of new HSM media. Cultures should be diluted to 1-2 x 10^5 cells/ml in order to achieve proper synchronization; if it is diluted to much then the culture will not achieve the optimal 10 fold increase required, and if it is to dense then the culture will die or de-synchronize during division because they are to dense in number.

Dilution of the culture needs to be conducted aseptically, so prepare all materials you need in advance. The materials required are displayed in the picture above. Used falcon tubes must be re-washed, autoclaved and re-used. You should only get ready to dilute the culture once you know how much volume of the 'old culture' you need to add to the new flask. Avoid prolonged disturbance of the synchronized culture; in other words, do not keep it disconnected from the CO_2 and away from the light for to long!

The steps for diluting are as follows:

- disconnect the old culture and bring it to your prepared aseptic zone
- turn on flame and take out the securing tape on the old culture
- remove the autoclave tape from your falcon tube and unscrew the cap of your falcon tube but keep it covering the opening of the tube
- mix the old culture very well by swirling then carefully remove the cotton and tubing far enough from the opening of your old culture so you can flame it and do the following steps while keeping the opening clear (do not remove it completely!)
- flame the opening well, mix the old culture again and pour a little bit of the old culture into the waste beaker (this is needed to cool down the lip of the flask, which avoids killing cell as they get poured into the flacon tube later on)
- mix the old culture again, open the falcon tube and pour the needed volume of culture into the falcon tube
- close the culture and put aside quickly, then flame the falcon tube and close it quickly

At this point you can take a small breather and push aside any unneeded materials, then continue on to the following steps:

- unscrew the falcon tube but keep the cap on top to cover the aliquoted culture
- take the new flask, carefully remove the cotton and tubing far enough from the opening of the new flask so you can flame it and do the following steps while keeping the opening clear
- quickly remove the cap of the falcon tube and gently/aseptically pour in the aliquoted culture into the new flask
- put the falcon tube aside, flame the opening on the newly diluted culture and plug it closed with the cotton/aeration delivery system.

Note: Just to be sure you conducted the proper dilution, you should also remove an aliquot of newly diluted culture and count the culture density.

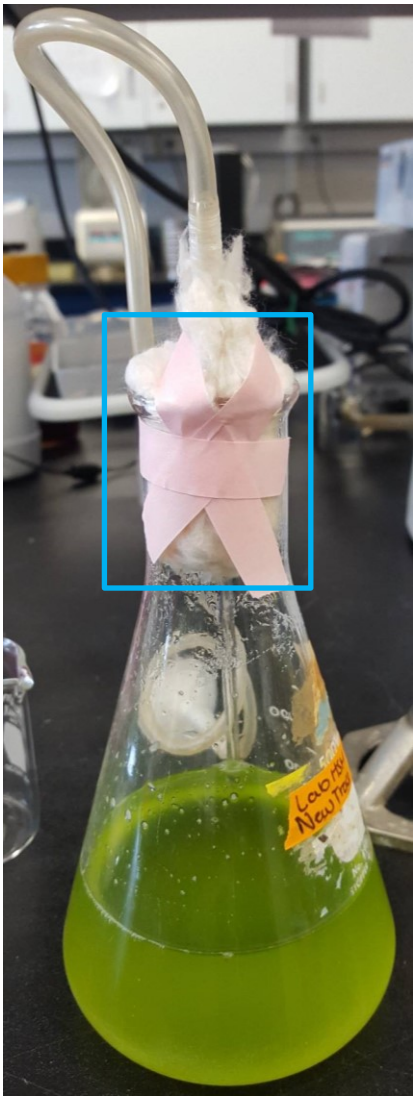

Once the dilution is complete, the culture is secured by adding key portions of tape.

The aeration delivery system is the aspect of the culture which requires anchoring with the tape. The glass pipette needs to be at a specific point within the depth of the culture; it must be low enough near the bottom to allow efficient mixing, aeration, and suspension of cells (to avoid cell sedimentation and death) but not low enough that the tube is blocked! Above we see an example of a pipette which is place correctly, not to low but not to high either.

When the tube is positioned correctly, it can then be secured using two pieces of tape. The fist long piece is placed in an X across the pipette and cotton to keep the glass pipette snug at its proper height against the wall of the flask. The last piece of tape is placed horizontally across the tapped X to secure it.

The aeration delivery system should also be spatially separated from the sampling tube when being secured with tape. If the aeration delivery system and the sampling tube are not spatially separated, then there is a risk of improper mixing/sampling. Like the aeration delivery system, the sampling tube should also be lowered (aseptically) into the culture when preparing them for inoculation. The sampling tube should not be lowered to far into the culture or placed to close to the surface; the ideal placement is in the middle of the culture's media.

System start up

When planning to use synchronized cells for experiments it is best to **turn on the gas system 1 day prior to when it is needed.**

Starter cultures are inoculated to grow, to a useable density under light/dark entrainment, on Friday afternoon until Monday morning at approximately 10am.

The autoclaved culture flask is prepared as indicated above on page 11, then they are inoculated with a sterile loop. The loop must be sterilized as much as possible, from the loop tip all the way until the start of the plastic handle, to ensure no contamination. Sterilization of the entire inoculating loop is not commonly done when inoculating smaller cultures; but in this case it is necessary since the entire loop needs to be inserted into the 250ml flask in order to re-suspend low enough on the wall of the flask so that it is touching the liquid media.

During this growth step, between Friday and Monday, the starter cultures are grown in the growth chamber programmed for synchronization under light/dark cycles (to undergo a training of sorts) with 0.5% CO_2/air bubbling; just as any other synchronized culture. However, this starter culture **does NOT** get diluted during this time period, the first dilution takes place on Monday morning at approximately 10am.

Therefore, the system **MUST be started** on Thursday morning allowing the researcher the ability to ensure its stability, in terms of gas flow rates, over the course of Thursday afternoon and overnight from Thursday to Friday.

To start the gas system a series of simple steps must be taken, these steps are as follows:

1 – Open the CO_2 gas tank. The tank is opened in the direction indicated by the arrow on its opening valve (on the right). The valve does not need to be opened all the way, it just needs to be opened enough to allow the CO_2 tank pressure (PSI) to register on the regulator as explained previously; this is usually about half of a full rotation for the valve.

2 – Adjust the regulator. Multiple knobs on the regulator need to be adjusted to achieve a decent flow rate that is not to little nor to much. If the flow rate is to high, the tubbing connecting the fine CO_2 flow meter and the regular risks exploding off due to backpressure.

Conversely, if the flow rate is to low the gas system will shut itself off over time. The attainment of an ideal flow rate is why the system is turned on one day before utilization.

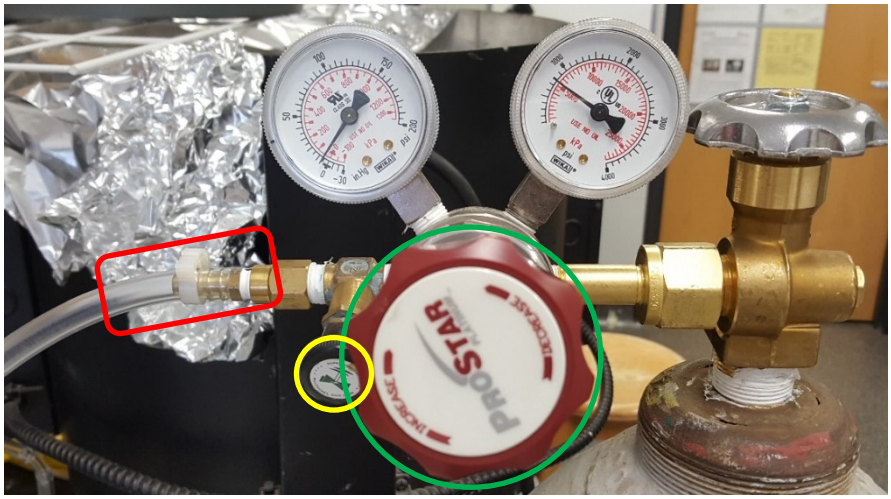

The first knob which requires adjusting is the large one; as mentioned earlier, this knob needs to be turned enough to allow a decent output so that the system won's shut itself off but it also does not need to be excessively high or else it can wear down the regulator over time.

The second smaller knob is for finer refinement of the CO_2 flow rate. In order to set an ideal output, the researcher must listen to the hissing intensity of the expelled CO_2 ; this can only be done if the tube connecting the regulator and the fine CO_2 flow meter is detached temporarily. An appropriate output can be characterized by an audible low hissing noise. Once everything is adjusted, the tube can be re-attached and secured tightly with the plastic clamp.

3 – Plug in the fish pumps (which provide the air). The fish pumps are unplugged during the shut down procedure, to ovoid overuse/burn out, therefore they must be re-plugged into the wall outlet as seen below.

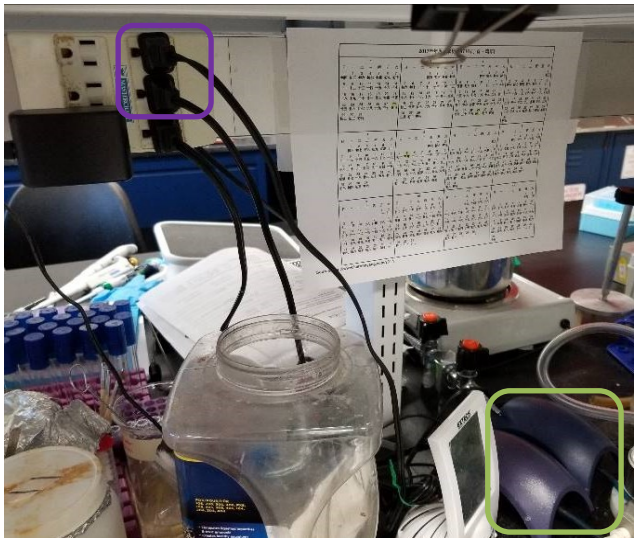

4 – Inspect/Adjust all flow meters. The first flow meter to inspect is the coarse air flow meter, which is the one being fed by the fish air pumps. This flow meter should read approximately 20 which corresponds to 2 L/min or 2000 ml/min; if this is not the case then one of the fish pumps is malfunctioning.

Then the next flow meter to check is the fine CO_2 flow meter, which is the one being fed by the tank/regulator. This should be adjusted to read between 15-20 ml/min which is between 0.5% to 1% CO_2. The flow rate is set slightly higher for two reasons; because the backpressure of the system can cause temporary fluctuation ± 5 ml/min, and because the float (the ball) seems to get stuck on dust particles at 10 ml/min and 20 ml/min (to avoid false flow rate readings we avoid those two areas).

Lastly, the flow rates of the partitioning system need to be inspected/adjusted through each of the four individual flow meters.

The two fine flow meters (with the silver floats on the far-right hand side) should be open enough to allow release of backpressure from the system, but not to much since it will drain flow rate from the extra fine flow meters being fed to the incubator. These two fine flowmeters can be used to feed another larger culture placed in the circular light box nearby OR they can be fed into a buffering flask to release any accumulated backpressure in the system. Another backpressure release valve is plugged into the system before the partitioning set up; this bleed valve is fed into the same buffering flask and can be adjusted as needed. Simultaneously, the two extra fine flow meters need to be monitored/adjusted so that enough vigorous bubbling is provided to the cultures in the incubator outside the lab. Adjustment of these flow meters depends on several aspects; if both flow meters are being used, the size of the cultures in the outside incubator, and if the output for each respective flow meter is being further partitioned downstream (using a splitter in the incubator). The ideal flow rate is determined when all downstream cultures being fed have a constant, reliable, vigorous bubbling; this bubbling should be strong enough to agitate/re-suspend cells in the culture, but it should also be slow enough to see rapidly ascending individual CO_2 /air bubbles.

5 – Plug in all un-plugged apparatuses in the outside incubator. During the shut down process the lights and fan are unplugged to ensure that they are not overworked and burn out. At this point these apparatuses should be plugged back into their respective timers.

6 – Re-set/adjust timers. Be sure to reset the timer for the lights and fan if you have changed the program timing of the incubator itself! Even if the timing has not been changed it is still a good idea to double check that the incubator and both timers still have the appropriate programming and that they have the **same clock time**. Clock time of the incubator and timers has to be identical, if not then you must re-set one or the other or both!

7 – Monitor the system for backpressure. At this point the system is fully set up and ready to be used the following day. However, the backpressure in the system can change over time (due to buildup) in accordance with all the adjusted parameters above. Therefore, it is important to monitor the flow rates of all flow meters several times a day (especially the day the system is started) and adjust them accordingly. Recall that it is important to relive backpressure or it will continue to cause issues in the subsequent days of your experiment. To relive backpressure you can increase the output of the bleed valve, or increase the flow rate of the two fine flow meters (with the silver floats) of the partitioning system.

System shut down

Shutting down the system is simpler then starting it; most steps taken during shut down are precautions which were developed to protect and prolong the life of our equipment.

The steps are as follows:

1 – Close the CO_2 tank! This is always the first step in the shut down process, since the CO_2 tank contains a dangerous gas (if emptied into the atmosphere of a small room such as a lab) and can become a projectile missile if the regulator malfunctions. Shutting down the tank is like opening it, it is done through the opening valve. The valve needs to be closed by turning the opposite way from when you first opened it; this is denoted on the valve using arrows.

2 – Empty out the regulator. To avoid/prevent ware and tear, the regulator must be emptied of all stored CO_2. This is accomplished by temporarily disconnecting the tube merging the regulator and the fine CO_2 meter, then turning the small black knob on the regulator to the fully open position. When doing this, you should hear a loud and intense hissing noise as the regulator is emptying, then it should stop within a couple of seconds. If it does not stop then you **did NOT close the tank!** So go back and close the tank, then try again.

3 – Unplug the fish air pumps. As mentioned earlier, to avoid eventual malfunction (decrease in pumping air capacity), the fish pumps are un-plugged from the wall outlet.

4 – Confirm that all gas is shut down. This can be accomplished by simply looking at the system carefully. If all gas (both air and CO_2) was shut down properly then there would no longer be any bubbling within the experimental cultures and the buffering flask. Another method to ensure this, is by looking to make sure ALL flow meters are now resting at zero as seen by the float being found at the bottom of the flow meter tube (seen below).

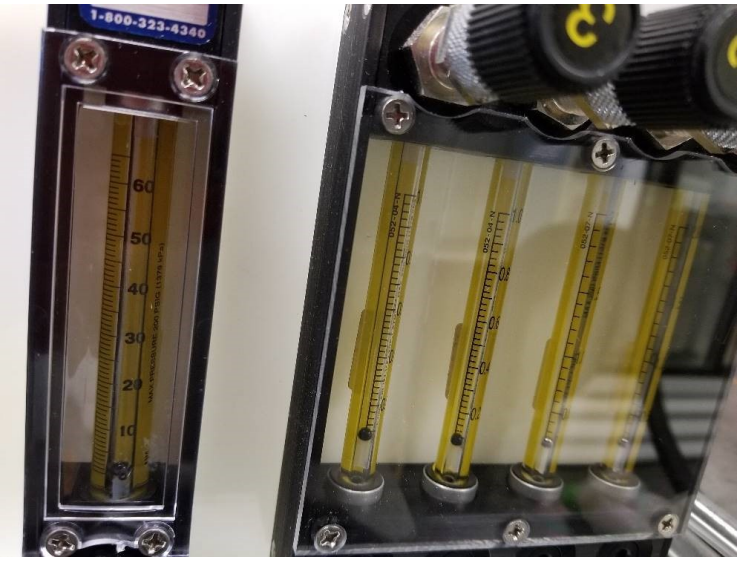

5 – Unplug all apparatuses in the outside incubator. Once again, to avoid over use and destruction of out lights and fan it is best to un-plug them when not in use.

Cleaning the system

<u>The cultures:</u>

Once used the culture set up needs to be washed so that we can re-use all parts.

The flasks should be disassembled by removing the cotton, aeration delivery system, sampling tubes, and all tape from them. Then the flask should be washed by hand with a test tube brush and scrubbed until all cell residue on the walls/bottom is removed. Once washed it should be rinsed 3 times with distilled water, and 3 times with millipore water; then it can be used to make new cultures to be autoclaved.

The cotton should be inspected closely once removed; if it has any mold on it, or smells bad then it is thrown away. If the cotton got partially wet, and most can be saved, then the wet part is removed and the rest is re-used. If the cotton is mostly wet, then it is thrown away.

The glass pipette is detached from the plastic delivery tubbing and set aside to wash. The tubbing is also detached from the bacterial air vents and set aside for inspection/wash.
The glass pipettes are washed using sparkleen, the exterior is scrubbed by hand and the interior is run through with sparkleen several times. Then these pipettes are rinsed multiple times with tap water, distilled water, once with 70% ethanol, and once with 99% ethanol. They are then dried with a kim wipe and place vertically to drain overnight (in tube rack).
The detached plastic tubbing is inspected for any growth/dirt inside, if the inside is clean then only the exterior of the tubes needs to be cleaned. Tubbing exterior can be wiped clean (of glue residue from the tape) by using 99% ethanol on a paper towel and some vigorous scrubbing. If the interior of the tube is dirty, then it is washed in the same way as the glass pipettes mentioned above.
The bacterial air vents are **NOT washed**! If the membrane inside these vents becomes wet, the whole vent is useless. These vents cost 15-20$ each, so they must be re-used for as long as possible. A vent becomes un-usable if the internal membrane is wet or if there is significant growth of bacteria/mold on the internal membrane; both scenarios block the air flow, causing backpressure issues for the system in addition to contamination of the experimental cultures.
The gas system:
This gas system does have some cleanable parts which should be regularly maintained.
The buffering flask should be washed with soap and rinsed with distilled water every couple of weeks to avoid mold/mildew buildup. Distilled water should be used to re-fill the flask because it is less likely to develop mold/mildew growth when compared to tap water.
The individual flow meter tubes can be cleaned if the floats keep getting repeatedly stuck in multiple positions (which leads to false flow rate readings!). This process should be avoided as much as possible since you can inadvertently: introduce more dust into the flow tubes, damage small malleable parts by removal, lose small parts of the system, and it is time consuming to dismantle each individual flow meter and the flow tube within the meter.
Once opened, the flow tubes can be washed with 99% ethanol and a pipe cleaner, followed by drying using compressed air (sold in a canister). Be attentive to all small removable parts such as the floats and stoppers; never touch said parts with your bare hands or dirty gloves (use clean gloves or avoid touching them all together and use paper funnels/tweezers respectively). Remember how the system was assembled so that re-assembly is easier once you are done.

Product List

The gas system:

- CO_2 Detector (or "Indoor Air Quality CO_2 Monitor")
  - Company → 'Extech Instruments'
  - Product number → C0220

- CO_2 Tank
  - Company → Praxair
  - Product number → CD50/UN1013
  - Connection → CGA320
  - Size → 22.7 kg or 50lbs
  - Price → 25.32 $

- Regulator/tank connector 'Nut' for CO_2
  - Company → Praxair
  - Product number → WES CO – 2
  - Connection → CGA320

- Regulator/tank connector 'Nipple'
  - Company → Praxair
  - Product number → WES CO – 3
  - Connection → CGA320

- Coarse air flow meter ('Aluminum 65mm correlated flowmeter with valve')
  - Company → Cole Parmer
  - Product number → 03216-28
  - Max flow rate → 6318 ml/min

- Fine CO_2 flow meter ('Aluminum 65mm correlated flowmeter with valve')
  - Company → Cole Parmer
  - Product number → 03216-08
  - Max flow rate → 104 ml/min

- Partitioning system fine flow meter x 2 ('Flowmeter system 65mm direct reading flow-tube air')
  - Company → Cole Parmer
  - Product number → 32047-11
  - Max flow rate → 2 L/min

- Partitioning system fine valve x 2 (‘16 turn valve cartridge range 4 for AI frame system’)
    - Company → Cole Parmer
    - Product number → 03218-62
    - Min/Max flow rate → 1 L/min to 2.5 L/min

- Partitioning system extra fine flow meter x 2 (‘Flowmeter system 65mm direct reading flow-tube air’)
    - Company → Cole Parmer
    - Product number → 32047-09
    - Max flow rate → 1 L/min

- Partitioning system extra fine valve x 2 (‘16 turn valve cartridge range 3 for AI frame system’)
    - Company → Cole Parmer
    - Product number → 03218-61
    - Min/Max flow rate → 200 ml/min to 1 L/min

- Metal Adaptors (for gas mixing system)
    - Company → Watts (bought at Addison Electronics)
    - Product Number → LFA-200A
    - Size → 5/16 in ID and 1/8 in MIP

- Fish air pumps (‘Whisper 40 Aquarium Air Pump’)
    - Company → Tetra

<u>The cultures:</u>

- Tygon tubbing (smaller for sampling tubes)
    - Company → Cole Parmer
    - Product number → 06407-76
    - Size → ID 1/8 by OD 1/4 by 1/16
    - Price → ~2.50$ per foot

- Tygon tubbing (larger for aeration deliver system)
    - Company → Cole Parmer
    - Product number → 06407-09
    - Size → ID 3/16 by OD 1/4 by 1/32
    - Price → ~1.50$ per foot

- Bacterial Air Vents (Pack of 24)
    - Company → Pall Corporation (bought form VWR)
    - Product number → PN 4210
    - Price → Greater then 300$

Incubator system:

- Aluminum "Lab Jack" (12 inch square plate, 50cm max height, max load 100lbs)
    - Company → Fisher Scientific
    - Product Number → 1467353
    - Price → 40$ (it was a deal, the actual price is 390$)

- LED Blue/Red lights ('Set of 20 encapsulated LED's)
    - Company → Addison Electronics
    - Product number → 172152 (Blue) and 172154 (Red)
    - Price → 24.99$

- Fan (' 6" desktop/clip combo fan')
    - Company → Facto
    - Model number → F-0600/F-0610

- Splitter ('Lok-tite non corrosive aquarium gang valve')
    - Company → Penn-Plax
    - Catalogue number → VN3

* N.B. to modify the incubator you need to get permission from the head technical officer Sonia Ruiz, she will then ask the mechanics to build/remove the requested parts and document the modification thoroughly.

Appendix II :

Programming ‘Conviron TC-16’ Growth Chamber for Synchronized Cells

1) Main Screen → Click Program button (flashing) to access current program

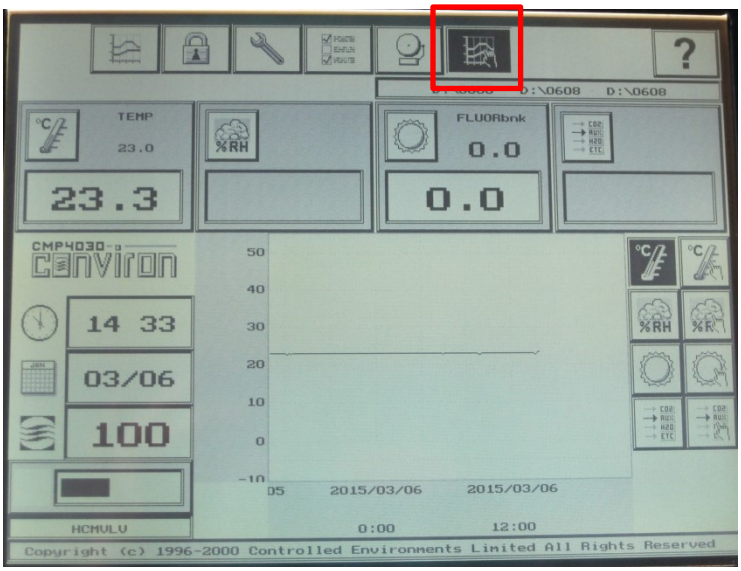

2) Program Screen → Stop old program by clicking STOP , the return to main widow

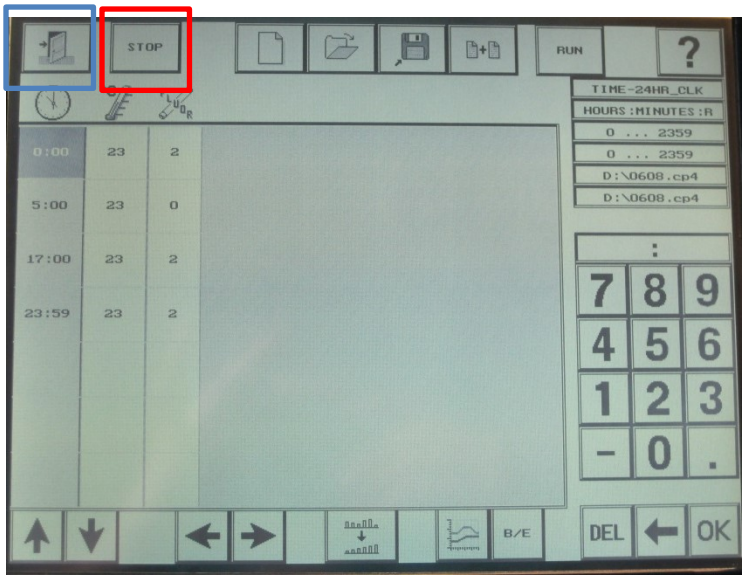

3) Main Screen → Access Options Screen if you want to change the internal time of the growth chamber and other parameters

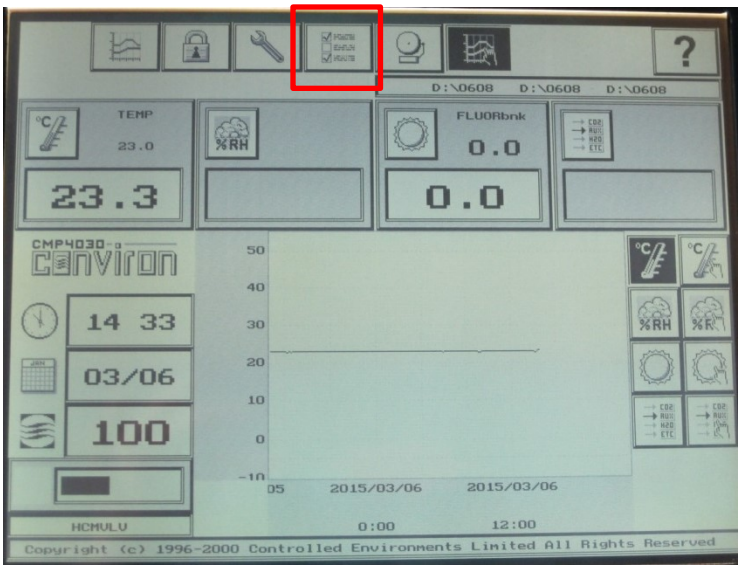

4) Options Screen → Change internal time/date and any other parameters you need then return to main screen

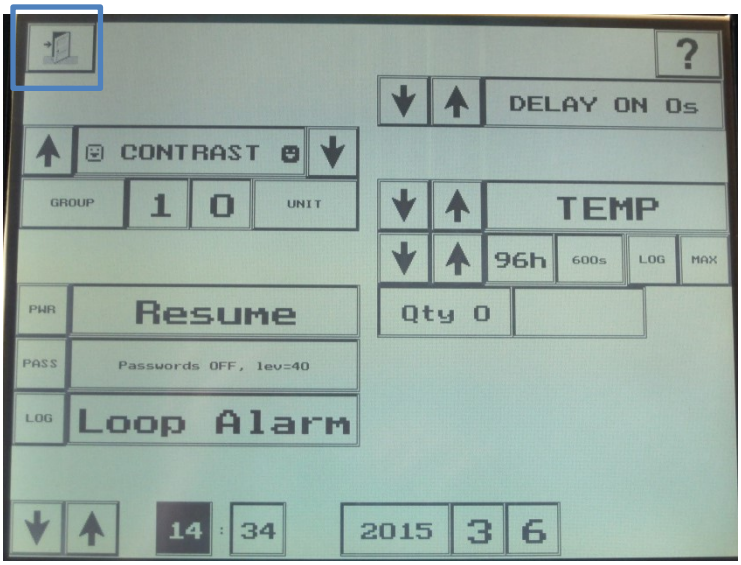

5) Main screen → Access program screen again (as in step one), then change the program values…

- Time when you want the setting to change; N.B. this unit must have a 0:00 time setting and a 23:59 time setting present in any program so as to run properly
- Temperature you wish to have at that specific time
- Light settings on (2) or off (0); N.B. lights cannot be put to half intensity (1) on this growth chamber unit

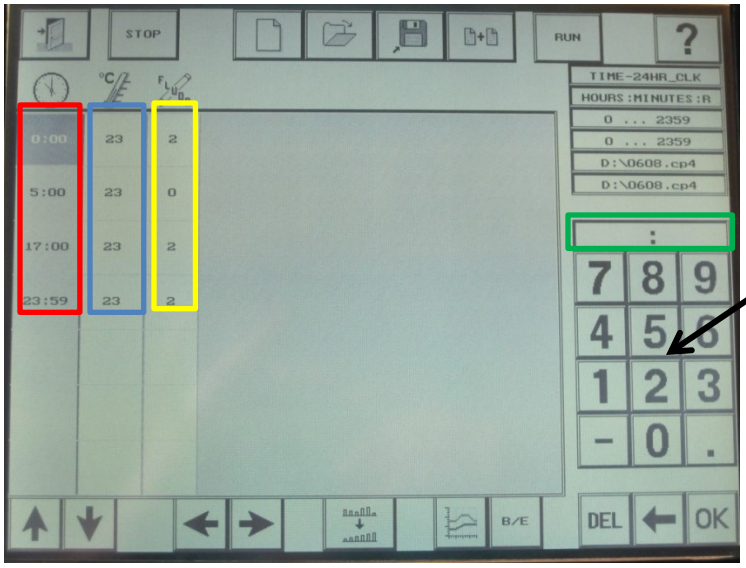

Values for all of the parameters stated above can be changed using the key pad indicated by the arrow. One correct value appears in green box, press ok to enter enter.

Note: if you change temperature between time points, then the machine will automatically deal with the temperature shift by "ramping". This ramping will take place over the <u>entire</u> given time period between the two time points.
Example, if you change the temperature from 23 ºC to 20 ºC for the 5:00 time point then the machine will slowly fo from 23 ºC to 20 ºC over the course of 5 hours.
There is a way to trick the machine into not ramping…

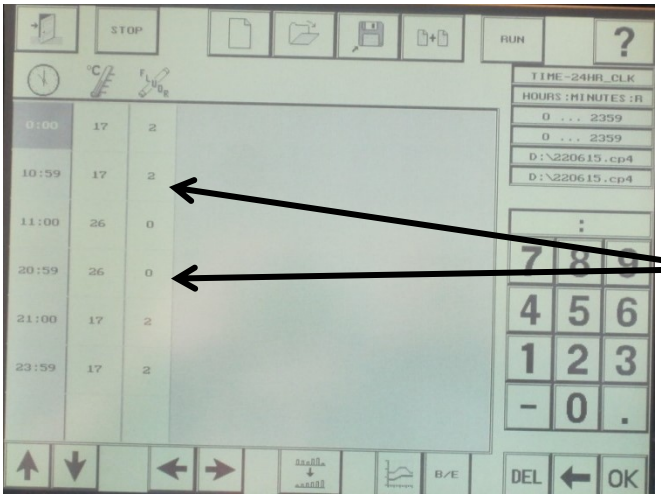

To trick the machine into not ramping you must insert time points one minute <u>before</u> your temperature shift indicating the previous temperature. Therefore, the machine will have to maintain your previous temperature until the added time point, but it will also have to change it before the next one (over the span of one minute instead of hours).
Ex: indicated by arrows

6) Program screen → once all changes are completed save program by pressing the floppy disk

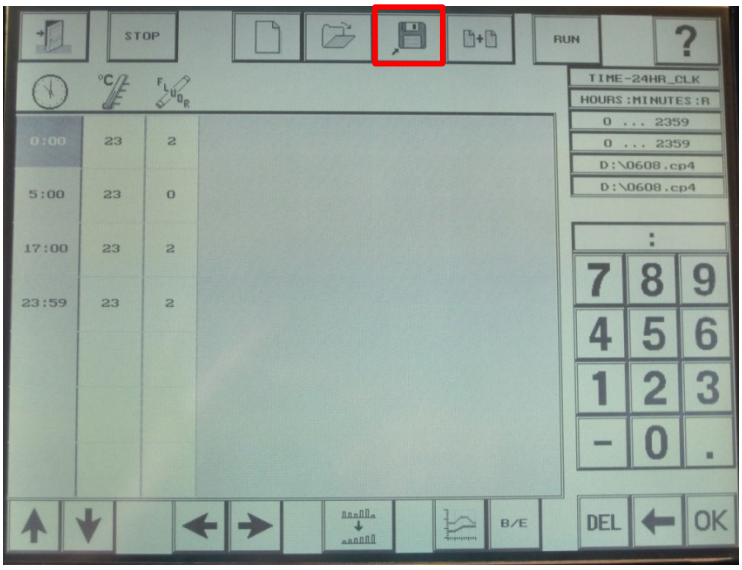

7) Save Screen → enter a number using the key pad and press ok to save the program into the growth chamber (note the number down)

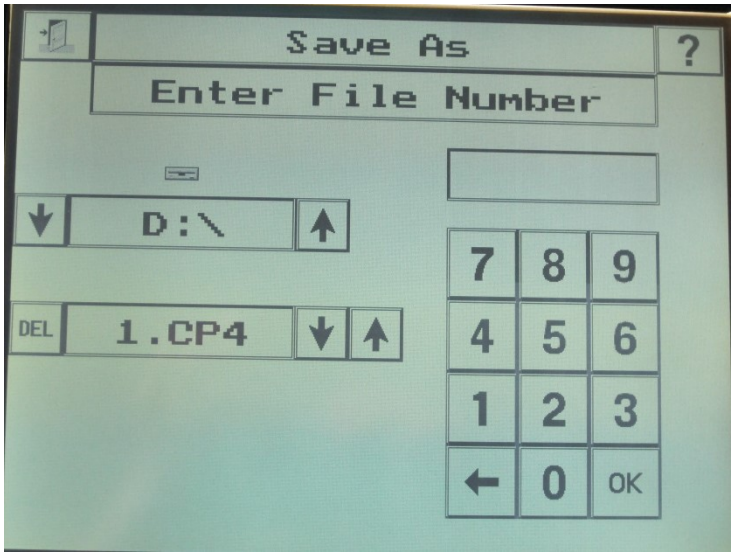

8) Program screen → once program is saved, chain the program to another (or to itself) to make the growth chamber continue to run past 24 hours; press copy button

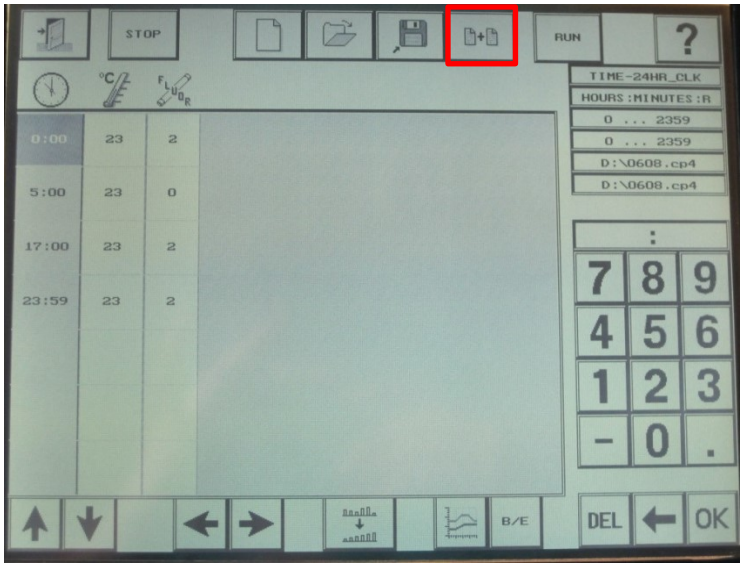

9) Chain Screen → enter the saved number of the program (using the key pad) you wish to chain your current program to, if you want to loop your current program onto itself just enter the number you previously saved and noted down; then press ok

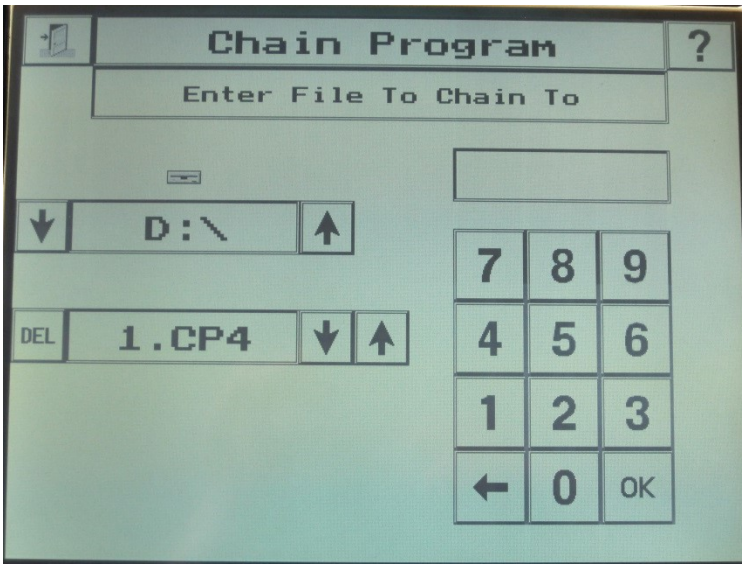

10) Program Screen → Once completed and ready, start the program by pressing RUN. Please allow proper cool down time (approximately 5-10 min) for the growth chamber between stopping/starting programs. Then return to main screen

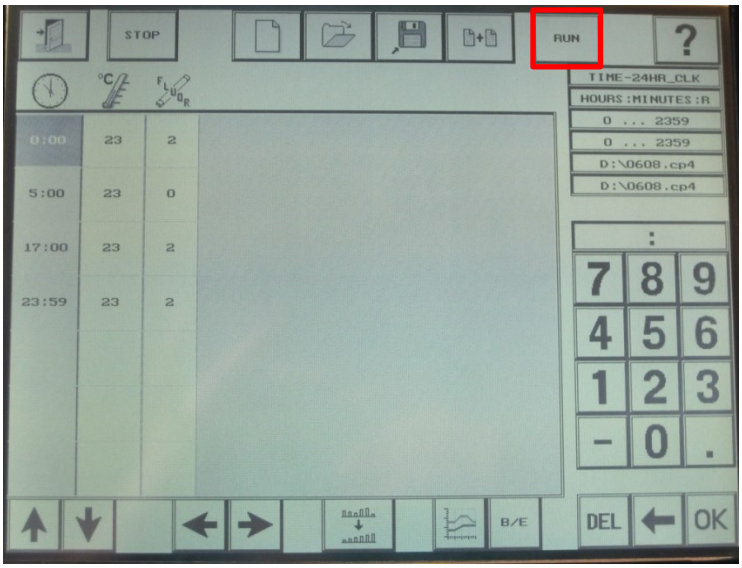

11) Verification that the program was entered correctly can be achieved by ensuring that the lights turn on and off at the appropriate times and by using the display buttons. EXAMPLE: the light display button (the sun) where the furthest light button to the right (the one containing a hand) has been chosen and is displaying what the programed cycle for lights *should be*. As you can see the lights are set to turn off at 5am and turn on at 5pm, as indicated in the program setting above (step 10). Note, the other variety of display buttons (without the hand) demonstrate what the growth chamber has been running previously.

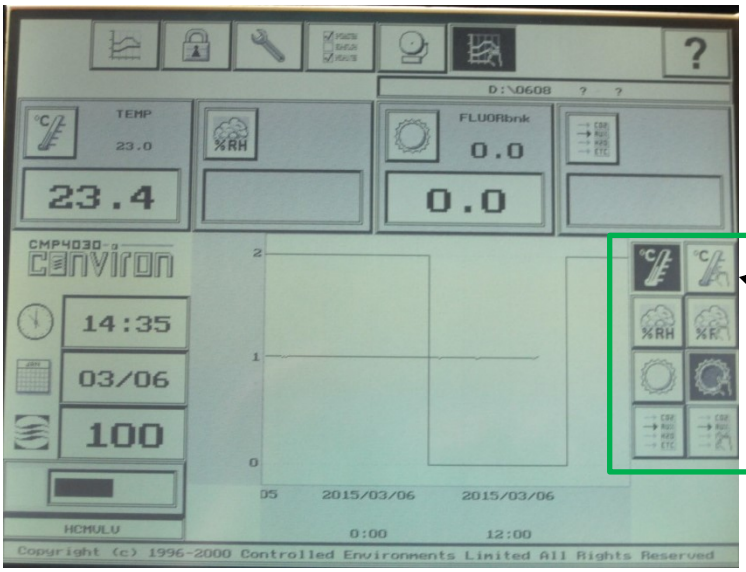

Note that you can also ensure that no ramping is taking place (if you are using temperature shifts between time points) using the temperature display button with the hand. Temperature shift should be indicated by straight vertical lines and not sloped ramping lines.

The Conviron TC-16 growth chamber has now been programed correctly

Example of diurnal 12 light:12hour dark synchronized cell growth chamber program (scheduled from 8am-8pm = light phase, and 8pm-8am = dark phase)